Analytical Comparability Strategies for Originators and Biosimilars

by

Jukyung Kang

A dissertation submitted in partial fulfillment
of the requirements for the degree of
Doctor of Philosophy
(Pharmaceutical Sciences)
in the University of Michigan
2019

Doctoral Committee:

Associate Professor Anna Schwendeman, Chair
Associate Professor Wei Cheng
Professor Brandon T. Ruotolo
Professor Steven P. Schwendeman

Jukyung Kang

jukyung@umich.edu

ORCID iD: 0000-0002-2592-9401

Dedication

To my love, Sechang and Evie.

To my family, Manseok, Myunghee, Yooncheol and Jieun

Shinhwan, Junghee, Eunsol and Gunhee.

Thank you for your love and support.

With love, always.

Acknowledgements

I would like to thank my advisor Dr. Anna Schwendeman for prescribing the appropriate amount of strictness and leniency and life advice as a mom and a scientist. I would also like to thank my dissertation committee for all support and guidance; Prof. Steven Schwendeman, Prof. Wei Cheng and Prof. Brandon Ruotolo.

I would also like to thank the College of Pharmacy, Promega, Amneal pharmaceuticals and Adello biologics for funding me over the course of my studies and providing me valuable samples and reagents. In addition, many of my works were done in collaboration with: Dr. Vivekanandan Subramanian, Dr. Yuwei Tian, Daniel Vallejo, Dr. Tyler Hageman, Derek White, Dr. Michael Ford, Dr, Sergei Saveliev, Dr. K. Ilker Sen, Dr. Eric Carlson, Prof. Tom Tolbert, Prof. David Weis and Prof. Brandon Ruotolo. Thank you for all your effort and helps.

I am so lucky to have been part of the Schwendeman Labs; Dr. Wenmin Yuan, Dr. Karthik Pisupati (My dear leader), Alexander Benet (Team Karthik), Jenna Walker (My love), Maria Fawaz (Chit-chat crew), Sang Kim, Dr. Jie Tang, Dr. Dan Li, Minzhi Yu, Lindsay Scheetz, Dr. Jia Zhou, Justin Hong, Jason Albert, Jenny Shenkar, Dr. Hiren Patel, Dr. Yayuan Liu, Dr. Ling Mei, Dr. Hongliang He, Dr, Lisha Liu, Dr. Gergely Lautner, Dr. Tina Li, Dr. Morgan Giles, Dr. Amy Doty, Dr. Max Mazzara, Dr. Rae Sung Chang, Dr. Brittany Bailey, Dr. Kari Nieto, Dr. Avital Beig, Troy Halseth and Jill Coghlan (the futures of Team Karthik), Kristen Hong, and Ziyun Xia. And, of course, to our lab managers, Rose Ackermann and Karl Olsen. I will miss our conversations, March madness bracket,

kayaking, picnic and Kroger trips. Thank you for your expertise, companionship and making my 5 years with a full of joy.

To my friends, Sang Kim, Yunsu Na, Kwangwoo Jeong, Huimin Ji, Seonghoon Hur, Jeonghyo Lee, and Youngmin Kang, thank you for sharing happiness and sorrow for 5 years. I will always cherish our times together. I am very lucky to have great friends, Jenny Nguyen and Alex Yu, thank you for your support.

Last, I would like to thank Sechang and Evie. Without your love and support this would not be possible. I would also like to thank my parents, brother, parents in law and sister in law. Thank you for always having my back.

Table of Contents

List of Figures

List of Tables

Abstract

Biologics are pharmaceuticals produced by living systems. Biosimilars, the follow-on counterparts to biologics are unlike small-molecule generics in the fact that they are large and complex and may contain minor variations from the originator product. The presence of these variations, derived from post-translational modifications (PTMs), necessitates a more rigorous approval procedure than that which is implemented for small-molecule generics. Extensive physicochemical characterization must be undertaken to confirm that the biosimilar's quality attributes closely match the originator in molecular and functional features. If high similarity is confirmed by these studies, the extent of preclinical and clinical trials may be reduced. Based on this, we performed extensive analytical comparability studies for filgrastim and several mAbs using various methods including several different liquid chromatography (LC) separations and mass spectrometry (MS) techniques.

In the first study, we compared Neupogen® and its proposed biosimilar filgrastim in terms of structural (primary and higher order) and chemical variants (size, oxidation, deamidation) using tandem MS, intact MS, 2D NMR and LC separations. Both molecules showed identical primary structure, comparable higher order structure and low levels of each variant except in deamidation levels, where originator filgrastim showed higher levels than that of the biosimilar.

In the second study, we combined the multi-attribute method (MAM) analysis with multiple orthogonal techniques to structurally compare Rituxan® and a proposed

rituximab biosimilar while focus specifically on glycosylation and resulting biological activity. We hypothesized that different glycosylation distributions between the originator and biosimilar rituximab could result in different biological activities, including differences in binding affinity to the FcγIIIA receptor and differences in antibody dependent cell cytotoxicity (ADCC). We show that both mAbs had identical primary structures by tandem MS and similar higher order structures by ion mobility (IM) MS and hydrogen deuterium exchange (HX) MS. We observed similar levels of deamidation and oxidation for both products, but significant differences in the levels of specific glycoforms. In particular, the biosimilar not only had a higher level of afucosylated glycans but also showed a higher FcγIIIA binding affinity and higher ADCC potency, thus suggesting a possible difference in clinical efficacy.

Finally, we identified initial structural differences/similarities and attempted to identify whether or not these differences could be amplified through the application of thermal stress through three originator-biosimilar pairs; rituximab, bevacizumab and trastuzumab. Initially, we detected highly similar secondary and tertiary structures and different levels of size and charge variants for each pair. After 4 weeks of incubation at 40 ºC, we measured differences in charge variant distributions and unfolding patterns. Taken together, our study shows the ability to establish comparability by creating a profile of initial differences for multiple mAb pairs and determining how those differences change when subject to thermal stress.

In conclusion, our studies provide an exemplary analytical exercise that can be implemented in the development of future biosimilar products.

Chapter 1: Introduction

1.1 Key characteristics of biologic products

Biologic product development is a growing field with a breadth of impact in cancer [1], and hematologic [2], autoimmune [3], and infectious diseases [4]. As of June 2017, approximately 2700 biologics are under development [5], fueled by their efficacy, safety, and the advancements in technology and regulatory pathways. [6–8] Biologic products are large complex molecules derived from living cells and can include therapeutic recombinant proteins, vaccines, or blood components. They are distinct from the relatively simple structure of small molecule drugs and have a more complicated manufacturing process. As shown in Figure 1-1, small molecules, such as acetaminophen at 151.2 da in size, can be thought of as a bicycle compared to the 30-150 kDa small and large biologics, erythropoietin and an IgG antibody, which would be considered the much more complicated, car or airplane. Biologics are not only more complex in structure, they also require a more elaborate and delicate manufacturing process than the chemical synthesis of small molecules, relying on the living cell system which is dynamic and highly sensitive to the external environment, leading to their heterogeneity and higher potential for immunogenicity. [9–11] For these reasons, development of biosimilars, is far more complex not only in manufacturing but in regulatory approval processes.

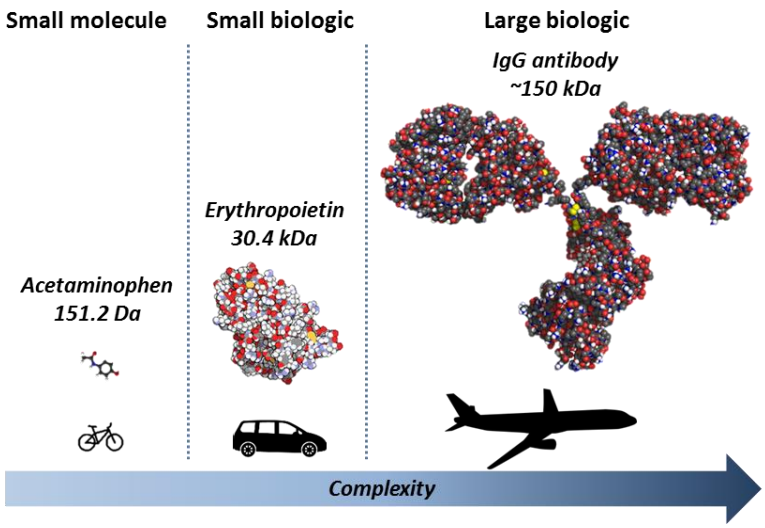

Figure 1-1 *Molecular weight and complexity differences between small molecules and biologics.*

1.2 **Biosimilars**

Biologic products are increasingly coming off patent, which has opened up the opportunity for biosimilar development and approvals. Notably, a biosimilar is not considered a generic version of a biologic since it is impossible to produce identical copies of biologic products. A biosimilar is a follow-on biologic which is highly similar in safety, purity and potency to an approved innovator biologic. [12,13] Since 2006, the European Medicines Agency (EMA) has led the approval of biosimilars with 54 approved products, and the U.S. Food and Drug Administration (FDA) has approved 23 biosimilars as of July 2019. [14,15]

1.2.1 Key differences between generics and biosimilars

The development process of a biosimilar is more complicated than generic drug product development due to the complexity of the innovator biologic, requiring a much more detailed approval process than the generic drug approval. As depicted in Figure 1-

2, innovator biologic, biosimilar, and generic drug developments differ in the extent of the process as well as where the bulk of the analysis lies. The abbreviated generic drug approval process only requires proof of matching between innovator and generic bioequivalence and bioavailability data in healthy subjects. [16,17] The innovator biologic development process places most emphasis on the clinical data, whereas the biosimilar development process requires a more extensive analytical development and characterization process due to the complexities of structure and manufacturing process. [18,19] Biologics, unlike generics, can have different indications than their innovator product due to differences in mechanisms of action (MoA) across indications, number or complexity of binding sites, or confound risk factors within different disease populations. [20,21] For example, the innovator of epoetin alfa (Epogen®) was initially approved for cancer treatment but the biosimilar, Binocrit, was approved for anemia and chronic kidney failure and not cancer. [22] In contrast to generics, innovator and biosimilar products cannot be interchangeably dispensed in the US. [23] The FDA requires the submission of an additional application in order to attain interchangeability status, allowing for the biosimilar product to be attained by patients without the need for a new prescription. As of July 2019, no US biosimilar has been granted interchangeability status. [24] The EMA does not have a policy in place for evaluating interchangeability, relying on individual member states to determine whether drugs are interchangeable. [25]

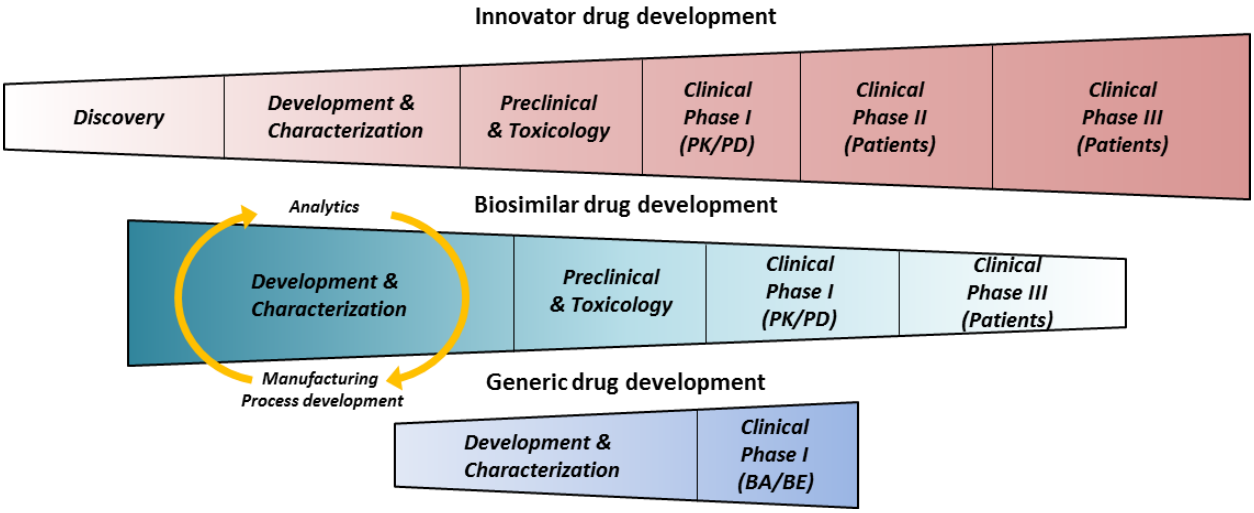

Figure 1-2 *Differences in drug development processes: innovator, biosimilar and generic. PK: pharmacokinetics; PD: pharmacodynamics; BA: bioavailability; BE: bioequivalence*

1.3 **Manufacturing process and consideration for biologic/biosimilar products**

The innovator biologic manufacturing processes is proprietary information, thus an exact replicate cannot be produced, resulting in alterations in the final biosimilar product. [26–28] The manufacturing process of biologics is depicted in Figure 1-3 and is discussed elsewhere. [29–33] Each manufacturing step is extremely sensitive to changes in the external environment and can influence the final biologic product, even impacting batch-to-batch variation within a strictly controlled facility. [33–35] Thus, the manufacturing processes and any changes made to it need to be approved by regulatory agencies, confirming no effect on the overall clinical efficacy or safety. [36–40] For example, manufacturing changes in rituximab (Rituxan®) caused a shift in basic variants and a higher antibody dependent cell cytotoxicity (ADCC) potency, which ultimately involves the mechanism of action, although it was not predicted to result in any changes in clinical outcome. [34]

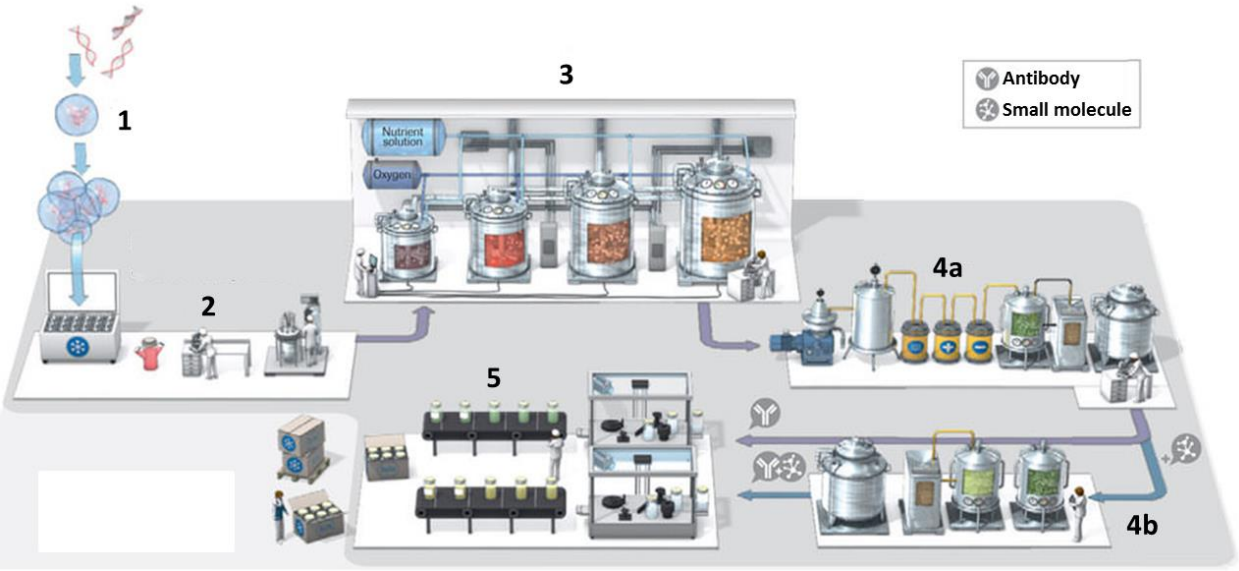

Figure 1-3 *Biologics manufacturing process; (1) production of cell line, (2) cell culture, (3) large scale cell culture – fermentation, (4a) purification, (4b) conjugation, and (5) formulation, filling and packaging. Images reproduced with permission from Roche.*

1.3.1 Critical quality attributes

Critical quality attributes (CQAs) are defined as a physical, chemical, biological, or microbiological property that should be within an appropriate limit, range, or distribution to ensure the desired product quality. [41] Establishing CQAs for biosimilar products start by selecting quality attributes (QAs) based on molecular structure, mechanism of action, safety and efficacy and defining analytical methods to test them. [42,43] Through various models, the risk and impact on clinical outcome (PK, PD, etc.) of each QA is assessed through quantitative and/or qualitative methods and criticality is assigned. In one example of criticality scoring, a score is assigned by multiplying two categories: impact x uncertainty, where a known (low uncertainty) clinical impact would rank higher than an unknown potential (high uncertainty) clinical impact. The drawback of using a quantitative method such as this is its sensitivity to changes in individual scores which can result in major shifts and inconsistency in criticality ranking of QAs. On the other hand, using a

qualitative approach involving more judgement and expert opinion can be used, but is less substantiated or standardized.[47] Examples of CQAs based on their criticality that are used for the analytical biosimilarity assessment of infliximab biosimilar (Inflectra®) and filgrastim biosimilar (Zarxio®) are shown in Table 1-1.

Table 1-1 *Examples of CQAs for the analytical biosimilarity assessment of a mAb drug – infliximab and a small protein drug – filgrastim. [49,50] **Relative criticality was assigned by each developer based on literature and experiments*

Example 1: Infliximab biosimilar – Inflectra®			**Example 2: Filgrastim biosimilar - Zarxio®**		
CQAs	**Criticality****	**Related to**	**CQAs**	**Criticality****	**Related to**
Primary structure	High	Efficacy, safety, immunogenicity	Primary structure	Very high	Efficacy, safety, immunogenicity
Protein content	High	Efficacy	Protein content	Very high	Efficacy
FcRn binding	High	PK	Potency	Very high	Efficacy, safety
Target binding to sTNF-α	High	Efficacy	Target binding	Very high	Efficacy, safety
Purity/impurity	High	Efficacy, Immunogenicity	Higher order structure	High	Efficacy, immunogenicity
Size variants /aggregation	High-moderate	Efficacy, immunogenicity	Size variants /aggregation	High	Immunogenicity
Excipient	Moderate	Efficacy, safety, immunogenicity	Oxidized species	High	Efficacy
Charge variants	Moderate-low	Efficacy	Sub-visible particles	High	Immunogenicity
Glycosylation	Moderate-low	Immunogenicity	N-terminal truncated species	Low	None
Target binding to tmTNF-α	Moderate-low	Efficacy	Norleucine species	Very low	None
C1q binding & CDC activity	Low	Immune system mediator	Deamidate species	Very low	None
Fc binding	Low	Immune system mediator			

Next, the FDA also requires a tier assignment, based on risk and potential clinical impact and uncertainty, of each of the specified methodologies used to analytically assess the CQAs. [42] An overview of the 3-tier system including examples of QAs for specific biologics (infliximab and filgrastim) and statistical methods is shown in Table 1-2. In tier 1, CQAs with a high criticality that affect biological activity, PK/PD, immunogenicity, and

safety, require statistical equivalence tests between innovator and biosimilar. In tier 2, CQAs with moderate criticality that have potential impact on biological activity, PK/PD, immunogenicity, and safety require a quality range approach where values must fall within a specified number of standard deviations from a mean value, depending on the assessment. In tier 3, CQAs with low criticality which have no impact on biological activity, PK/PD, immunogenicity and safety, are assigned and assessed more comparatively, this is also where qualitative and techniques binary in nature are categorized. [43,44] The FDA has not officially determined a preferred method for CQA or criticality determination and has recently withdrawn a draft guidance document on “statistical approaches to evaluate analytical similarity” due to the complexities involved with the number of product lots required and the possibility of false-negative equivalence results, ultimately affecting the efficiency and cost of biosimilar development. [45–48] In contrast, the EMA does not require tier assignment for analytical assessments nor a specific subsequent statistical analysis method, but is also currently discussing ways to improve and define the analytical assessment of biosimilarity through critical quality attributes along with the FDA. [49]

Examples of quality attributes of interest include amino acid sequence, disulfide bridges, carbohydrate attachment, molecular weight, extinction coefficient, and electrophoretic, liquid chromatographic, and spectroscopic patterns. [50,51] A multi-level comparison of biosimilars with their reference drugs must be conducted prior to approval in which any potential differences are detected and determined not to change immunogenicity, safety, or efficacy profiles outside the range of variation for the originator drug. Important quality attributes can be broken up into several categories: primary

structure, higher order structure, size, post-translational modifications, purity, and binding activity.

Table 1-2 *The 3-tiered approach for biosimilar statistical quality attribute evaluation. [49,50,57] EM: equivalence margin; QR: quality range; SD: standard deviation*

Tier	Tier assignment condition	Example 1: Infliximab	Example 2: Filgrastim	Recommended assessment method	EM/QR limit
1	Critical quality attributes most relevant to clinical outcomes	Target binding (e.g. TNF-α binding), protein concentration	Target binding, potency, protein concentration, amino acid sequence	Equivalency test with null hypothesis	1.5 sd
2	Less critical quality attributes moderately relevant to clinical outcomes	Peptide mapping, Glycosylation	Subvisible particle, aggregates	Quality range approach: mean ± xδ	3 sd
3	Least critical quality attributes least relevant to clinical outcomes	High-order structure	Truncated variants, deamidation	Raw data and graphical comparison	-

1.4 **Physicochemical assessment of biosimilarity**

1.4.1 Primary structure

Alterations in protein amino acid sequence composition can alter the hydrogen bonding patterns of α-helixes and β-sheets, which can influence protein folding and binding with protein ligands, potentially resulting in changes to its functionality. [52] Hence, biosimilars must have 100 percent primary sequence similarity to the reference product, no variability of primary structure is permitted. [25,26]

Currently, the most widely used method to elucidate the primary sequence is through reverse phase liquid chromatography (RP-LC), coupled with mass spectrometry (MS) based techniques. These include a variety of applications ranging from intact mass to peptide mapping. [53–57] As a top-down method, intact mass can be used to confirm the primary structure in a macroscopic manner, where data can provide rapid and precise profiling through matrix-assisted laser desorption/ionization (MALDI) or electrospray ionization (ESI) coupled to a time-of-flight (TOF), quadrupole (Q), ion trap (IT) or LTQ-

Orbitrap. [50] Differences of intact mass measurements indicate the presence of primary structural variation, which may occur as a result of an altered amino acid sequence. As a bottom-up method, peptide mapping involves the chemical or enzymatic digestion of protein into its constituent peptide fragments, which are subsequently separated by LC and analyzed by MS^n. A crucial consideration for peptide mapping is to maximize peptide sequence coverage, which can be achieved through protein digestion with different enzymes such as trypsin, Lys-C, Asp-N, and Glu-C (Figure 1-4). [58] Recently, -sheathless capillary electrophoresis has been introduced for coupling to electrospray ionization tandem MS (CESI-MS/MS) to assess biosimilarity of mAbs as a replacement for LC.[59,60] In addition, amino acid analysis coupled with LC or capillary electrophoresis-electrospray ionization-tandem mass spectrometry (CESI-MS) can be used to determine amino acid composition and protein content and to detect atypical amino acids such as norleucine and hydroxyproline. [61–63]

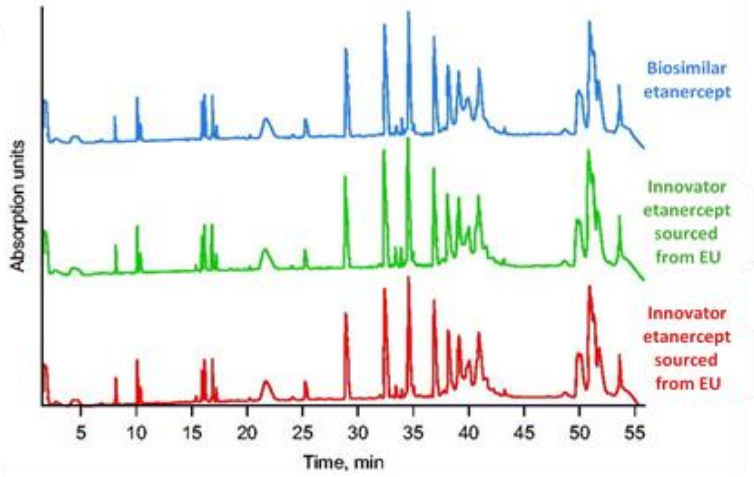

Figure 1-4 *Overlay of HPLC chromatograms from Lys-C digest peptide map digestion of innovator (EU and US) and biosimilar etanercept products. Images reproduced with permission from Ref. [73].*

1.4.2 Higher-order structure

Proteins undergo folding in cells, forming higher order structures (HOS), which refer to the secondary, tertiary and quaternary structure of proteins. Proprietary manufacturing systems can result in HOS differences of biosimilars and any differences in HOS between the biosimilar and the innovator should be addressed by applying orthogonal and state-of-the-art methods to set the basis for biosimilarity. [64]

For the determination of secondary structure, fourier transform infrared spectroscopy (FTIR), far-UV circular dichroism (CD), x-ray crystallography and nuclear magnetic resonance (NMR) are typically used. Among them, FTIR and CD are most commonly used to compare the innovator and biosimilar structural content of α-helix, β-sheet and random coils. [54,55,65–70] FTIR spectroscopy can be used regardless of the physical state of the samples (solid/liquid, crystalline/non-crystalline, aqueous/organic solution and film/dispersion), with no limitation on protein size and requiring a relatively small amount of sample (10-100 µg) while providing a high signal to noise ratio, allowing data collection in as little as 10 ms. [71,72] CD provides data in a short time period (few hours) and with small amounts of sample (<20 µg),but requires that samples be in aqueous solution. Particularly for far-UV CD spectrum, absorption is derived from the peptide bond region (<240 nm) [73], therefore allowing conformational information, such as α-helix, β-sheet and random coil structures, to be obtained from characteristic CD spectra as well as secondary structural estimation using various algorithms (Figure 1-5A). [74] X-ray crystallography can be used for secondary structural analysis with high sensitivity and specificity, but is not optimal for routine analysis due to its time consuming nature and because samples must be crystallized, which is not always achievable. [75,76]

Similarly, NMR generates useful protein secondary structural data but requires high sample concentration due to the lack of active isotopes present in the protein drug molecule and is time consuming. Due to the complex structure of large molecule protein drugs, 1-D NMR is typically used more for smaller biopharmaceuticals and can be used as a fingerprint comparison to show the structural similarity between innovator and biosimilar products. [77–79] These techniques can provide useful information on the entire folded structure, but lack sensitivity in relation to specific residues when compared to other HOS analysis methods. [80]

Tertiary structure can be determined through near-UV CD, differential scanning calorimetry (DSC), 2D-NMR, antibody array, and intact mass spectrometry, such as hydrogen deuterium exchange MS (HDX-MS) and ion mobility MS (IM-MS). Near-UV CD (250-320 nm) can detect differences in the tertiary structural environment of disulfide bonds and aromatic residues, which are highly sensitive to their environment. [73,81,82] DSC is widely used to evaluate thermal and conformation stability of proteins during processing and manufacturing. [83–85] Highly similar DSC thermograms and T_m denote the similarity of tertiary structures as a result of thermal stability (Figure 1-5B). Recently, 2D-heteronuclear single quantum coherence (HSQC) NMR, which measures the coupling of two different nuclei present on one bond, has been utilized to provide sensitive, robust and precise structural assessment of biologics. This technique has not yet been widely applied to mAb biosimilars due to their large size, although several biochemical strategies have been investigated in order to overcome this limitation. [86] ^{1}H-^{15}N HSQC was used to show the correlation of nitrogen and amide protons within the conformation along the polypeptide chains of innovator and biosimilar filgrastim (Figure 1-5C). [78,87–90]

However, 2D-NMR requires highly concentrated samples and a long acquisition time to attain a large enough signal from the naturally low abundant levels of ^{15}N and ^{13}C present in the protein's native state. [91] Antibody array utilizes binding of polyclonal antibodies against peptide fragments of a target mAb and is a highly sensitive and specific tool to detect regional changes in HOS at the molecular level and has a similar setup to sandwich ELISA. [54,91–96] HDX-MS can monitor conformational protein dynamics, relying on the deuteration of labile hydrogen in amide bonds along the polypeptide backbone followed by online pepsin digestion, LC separation and MS analysis. [76] Subtle differences in HOS can be detected, depending on the degree and rate of deuterium exchange of the same fragments between innovator and biosimilar products (Figure 1-5D and E). [54,55,97] The advantages of HDX-MS are its analytical capacities of complex buffer systems, large proteins, and its minimal sample requirement (5-100 pmol). [98] IM-MS is a rapid (msec) and sensitive (nmol) emerging technique for generating HOS fingerprints for biologics. [56,99–101] In addition to IM-MS, collision induced unfolding (CIU) has been applied for structural analysis, which is subsequently analyzed by IM-MS. CIU fingerprints yield distinct gas-phase unfolding patterns of proteins as a function of collisional heat so that small variations in protein structure can be easily resolved, something that is hard to achieve by IM alone. [99,102–104] Recently, CIU was utilized for a comparative study of innovator and biosimilar infliximab and showed highly comparable gas-phase unfolding between the innovator and the biosimilar in a quantitative manner (Figure 1-5F). [53]

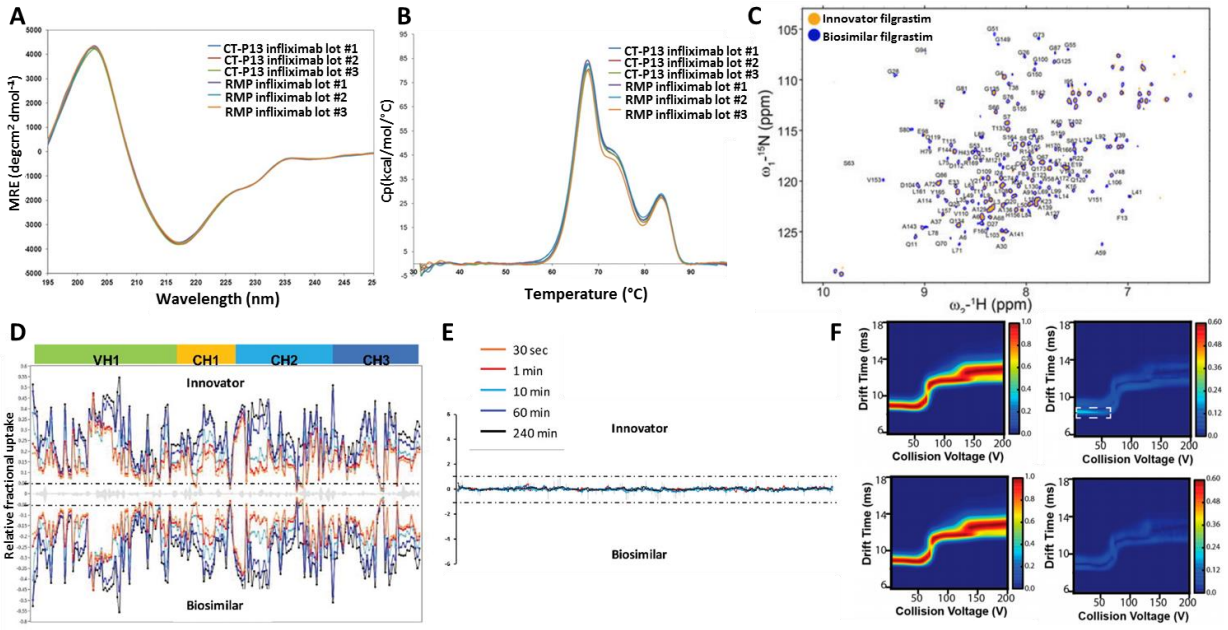

Figure 1-5 *Examples of methods that compare higher order structure. A) CD overlay spectrum of innovator and biosimilar infliximab in the far-UV region (190-250 nm). Adapted with permission from Ref.* [55]*. MRE: Molar Residue Ellipticity, RMP: Reference Medicinal Product B) DSC thermal stability overlay plot of innovator and biosimilar infliximab products. Adapted with permission from Ref.* [55]*. C) 2D NMR overlay plot of innovator and biosimilar filgrastim. Adapted with permission from Ref.* [86]*. D) HDX-MS generated butterfly plot of deuterium incorporation profiles and E) deuterium uptake difference plot of a heavy chain of innovator and biosimilar infliximab. Adapted with permission from Ref.* [97]*. F) IM-MS generated collision induced unfolding (CIU) fingerprints showing the averages [left] and standard deviations [right] of innovator [top] and biosimilar [bottom] infliximab products. Adapted with permission from Ref.* [53]*.*

1.4.3 Product variants

While sequencing predicts the primary amino acid sequence of biologics, the precise structure of an active form cannot be determined until it is isolated and purified due to post translational modifications (PTMs) generated during *in vivo* [76,105] and *in vitro* manufacturing steps leading to inherent variability. [106–108] The most abundant and common modifications regarding biologics are glycosylation, amino acid modifications, and charge variants. [108,109] PTMs can directly and indirectly alter

activity and immunogenicity of biologics, thus investigation of any PTM is necessary. [105,110]

Glycosylation, the addition of sugar moieties (oligosaccharides/glycans) to proteins in endoplasmic reticulum and golgi apparatus, is one of the most prevalent PTMs in eukaryotic cells, such as mammalian cell lines, and induces significant heterogeneity. Differences in glycoform profiles depend on both the expression system and manufacturing process, and can affect various biologic functions such as PK, PD, immunogenicity and biological activity depending on their composition (Table 1-3). [111] For example, the scale-up of adalimumab manufacturing processes led to differences in galactose and mannose glycoforms. [112] Glycan analysis for biologics can be performed at three levels: intact glycoprotein, glycopeptide and released glycan analysis.

Table 1-3 *Impact of glycoforms on the PK/PD of mAb biologics. [167]*

Glycan	Impact on PK	Impact on PD
Afucosylated glycan	-	Enhanced FcγRIIIa binding/ADCC [113–121]
Bisecting GlcNAc glycan	Accelerated clearance of Fc-fusion protein from the blood [122,123]	Enhanced FcγRIIIa binding/ADCC[124]
Galactosylated glycan	-	Enhanced CDC[125,126] Anti-inflammatory[127]
High mannosylated glycan	Accelerated mAb blood clearance[128,129] → lower mAb exposure	Enhanced FcγRIIIa binding/ADCC[130,131] Decreased C1q binding/CDC [130–132]
Sialylated glycan	Decreased clearance of Fc fusion proteins. → higher exposure (high Cmax, high AUClast)[133]	Anti-inflammatory[132,134–138]

Intact glycoprotein and subunit analysis (for mAbs) by top-down approaches, such as a high-resolution MS system, can provide a quick estimation on the glycoform heterogeneity of biologics (Figure 1-6A-C). In the same manner, subunit analysis, with the usage of enzymes, such as IdeS to get Fc and $F(ab')_2$, can provide information on

subunit specific glycosylation. These are useful to evaluate and control manufacturing processes and batch-to-batch consistency with minimal sample preparation and short analysis times. [139–141] However, these analyses cannot provide information on the presence of minor glycoforms. [141] Glycopeptide analysis provides information of glycoform micro-heterogeneity and site-specific protein glycosylation sites (Figure 5D-F). [142] Similar to bottom-up approaches, glycoproteins are digested into glycopeptides and then analyzed, typically by LC-MS or MS/MS systems. RP and hydrophilic interaction liquid chromatography (HILIC) columns are commonly used for LC separation. To overcome the low abundance of glycopeptides in a complex digest mixture, glycopeptide enrichment is employed to increase abundance and specificity prior to MS analysis. [143,144] Then, various glycan databases and search engines are applied to screen and identify glycopeptides from complex sample data. [145–149] To generate the quantitative glycan profiles[141], endoglycosidases (e.g., PNGaseF, reductive alkaline) are commonly used to release glycans that are then analyzed with or without derivatization. [54,79,96,150–153] The most widely used platform is the labelled glycan workflow, glycans are fluorescently labeled, purified and then injected on an HILIC column and detected by a fluorescence detector and further confirmed by MS (Figure 1-6G). [154] Nowadays, there are several kits and also automated systems available for the released glycan analysis that provide faster and simpler steps for sample preparation at high levels of sensitivity. [155,156] To avoid concern about minor sialic acid loss during fluorescent-labeling [157], label-free glycan workflow is available using a high-performance anion exchange chromatography coupled with pulsed amperometric detection (HPAEC-PAD). [96] PAD is highly specific for glycan analysis with separation by charge and size, requires

only pmol of sample and is available for the analysis of monosaccharide composition. [158–160] However, the lack of commercial standards for highly branched glycans can be a limiting factor for complete glycan mapping. [161]

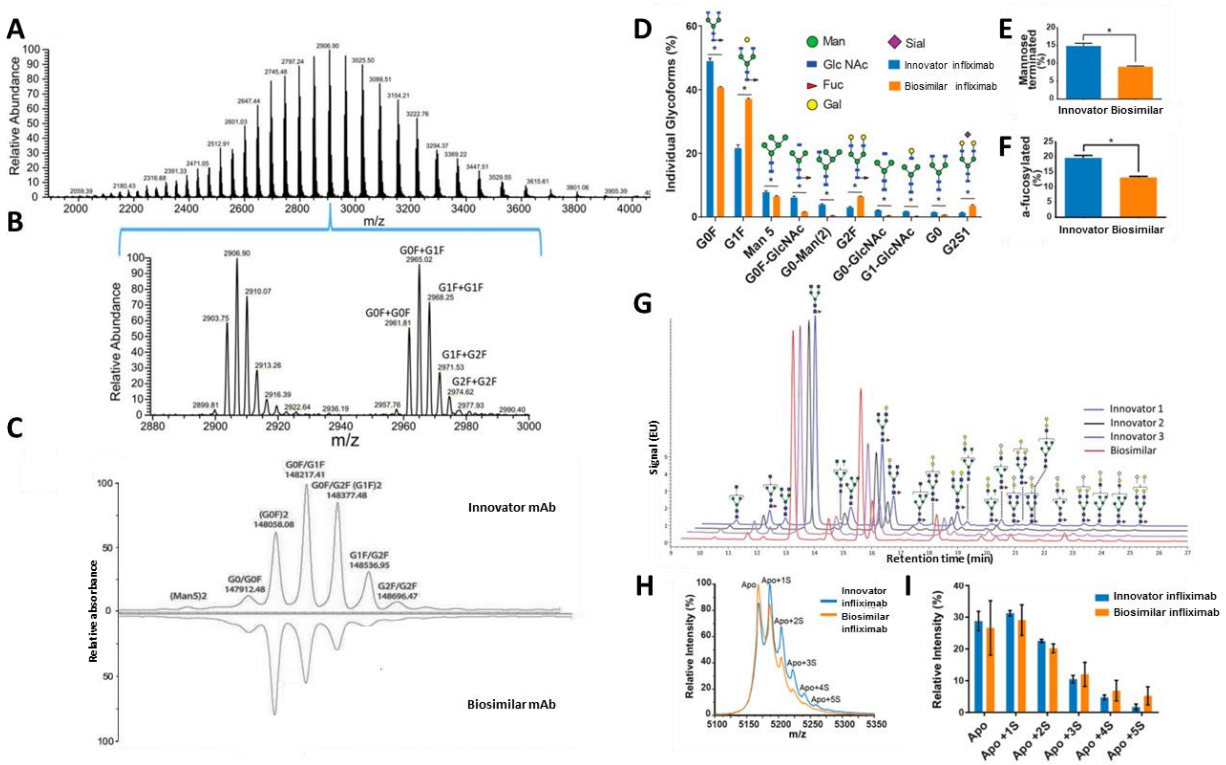

Figure 1-6 *Examples of methods that compare innovator and biosimilar glycosylation profiles. A) Full MS mAb spectrum B) Enlarged inset of two continuing charge states from A. Adapted with permission from Ref.* [162]*. C) Mirror plot comparing deconvoluted masses between innovator and biosimilar mAb. Images reproduced with permission from Ref.* [163]*. D) LC-MS/MS N-glycan quantification of infliximab innovator infliximab. Calculated % of E) mannose terminated and F) afucosylated species from D. Images reproduced with permission from Ref.* [53]*. G) HILIC chromatograms comparing released N-linked glycans of innovator and biosimilar infliximab. Adapted with permission from Ref.* [97]*. H) Mass spectra comparison of the 19^{+} charged Fab regions of innovator and biosimilar infliximab (Apo+1S to Apo+5S corresponded number of glycations) I) Relative intensity comparison of Fab glycation between innovator and biosimilar infliximab. Adapted with permission from Ref.* [53]*.*

During cell fermentation, purification, formulation and storage, biologics can be modified via PTMs (enzymatic reaction) or chemical modifications (non-enzymatic reaction) resulting in amino acid modifications such as oxidation, deamidation,

pyroglutamate (pGlu) formation and charge variants. [164,165] Both enzymatic and non-enzymatic modifications may result in a significant effect on biologics' quality, safety and efficacy. Oxidation is correlated with the propensity of aggregate formation [166–170], and the loss of function of various proteins. [171,172] For IgG1 and IgG2, several studies have reported that methionine (Met) oxidation in the Fc domain is related to decreased neonatal Fc receptor (FcRn) binding, which is related to IgG recycling and transcytosis. [173] Due to the proximity of Met residues to the FcRn binding interface, Met oxidation disrupts antibody conformation and IgG oligomerization, both of which are necessary for C1q binding and CDC activity, resulting in reduced binding and activity. [174–177] For example, filgrastim has 4 Met residues at positions 1,122,127 and 138, where oxidized variants at positions 122,127 and 138 showed reduced potency by an in vitro proliferation assay, likely due to the proximity of these positions to the binding sites in the granulocyte colony stimulating factor (G-CSF) receptor. [78]

Deamidation, the cyclization of asparagine (Asn) residues to form either aspartic acid (Asp)/isoaspartic acid (Iso-Asp), frequently occurs depending on the primary structure of nearby amino acid residues, tertiary structure, storage temperature, and properties of formulation solution such as pH, buffer and ionic strength. [178,179] Glutamine (Gln) can also be deamidated but is hardly detected in recombinant biologic products due to the 100-fold slower reaction rate. [180] Deamidation is a main cause of chemical degradation and may introduce negative charge and potential local charge structure distortion. [181,182] It has been reported that deamidation at Asn 30 in the light chains of the trastuzumab innovator (Herceptin®) showed a potency reduction of 70% [183], with Asn 55 deamidation showing a 14-fold decrease in antigen binding affinity.

[182] Furthermore, Iso-Asp is a non-natural amino acid residue, and therefore potentially immunogenic. [184] To characterize amino acid modifications, the most widely used method is digestion followed by peptide mapping by LC-MS or MS/MS, similar to primary structure characterization (Figure 1-7A, B). [182,185–188] Many amino acid variants can also be classified as charge variants and are commonly observed in biologic products, especially mAbs. For example, succinimide formation and C-terminal Lys generate basic variants due to an addition of the positive charged amine, while deamidation and N-terminal terminal pGlu formation generates acidic variants due to a loss of the positively charged primary amine. [189,190] It has been shown that these changes in pGlu and charge variants do not have significant clinical impact, but these modifications need to be monitored and identified because the introduction of heterogeneous species reflects a lack of manufacturing process control. [55,191–193] Characterization of charge variants for biosimilar approval is generally performed by ion exchange chromatography (IEX) and CE-based methods such as isoelectric focusing (cIEF), imaged cIEF (icIEF) and capillary zone electrophoresis (CZE). [96,150,151,194] IEX separates proteins according to their overall net surface charge and even differentiates isoforms with single charge residue differences. [195–198] To further identify the nature of each peak separated by IEX, subsequent MS analysis is necessary. Proteins with high isoelectric points (pI), such as mAbs, are generally separated by cation exchange chromatogram (CEX) (Figure 1-7D). [196,199–201] CE-based methods in combination with MS can provide a more rapid analyses than IEX, while utilizing only small amounts of samples and reagents. [202] Recently, several technical challenges on CE-MS have been solved such as automation and ESI compatibility. [203–205] cIEF separates proteins based on their isoelectric points

(pIs) in a capillary, but requires a mobilization step that can cause peak broadening, resulting in increased run time, reduced resolution and poor reproducibility. [206,207] icIEF attempts to overcome this issue by scanning the entire capillary without the need of the mobilization step. [208–210] CZE separates proteins based on electrophoretic mobility (mass-to-charge ratio) with the application of an electric field between a cathode and an anode. However, charge variants can have highly similar molecular masses, thus, separation mainly occurs based on their charge. [211–213] Unlike cIEF, in CEZ, peaks are detected at 200-220 nm which can provide higher sensitivity while preventing over/under estimation of charge variants with different UV absorption profiles at 280 nm. [214,215]

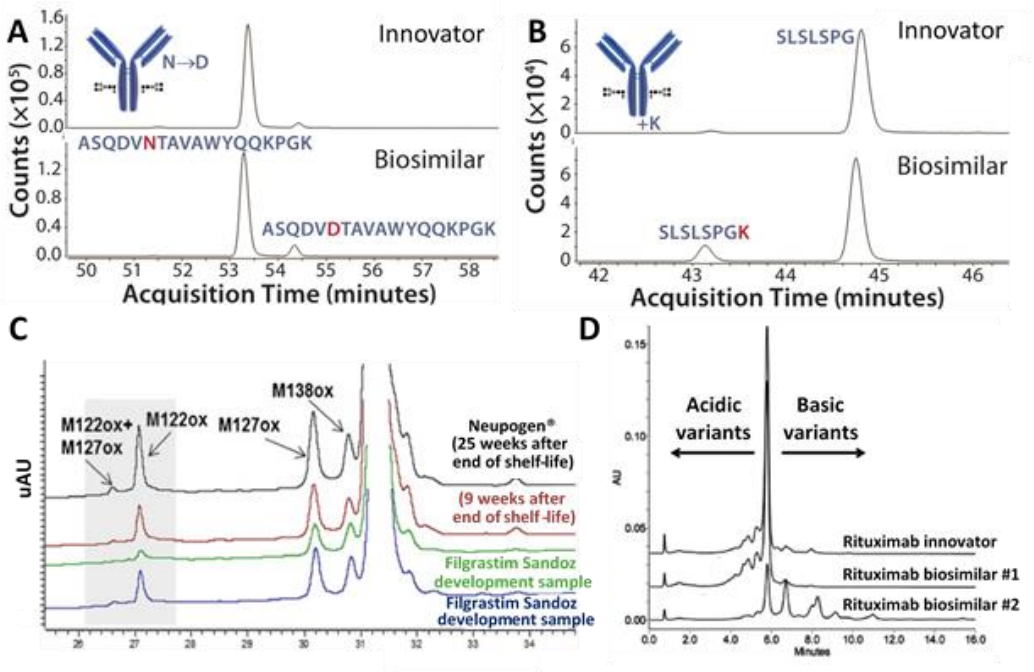

Figure 1-7 *Methods to detect amino acid modification. A) Extracted ion chromatograms of innovator and biosimilar trastuzumab of asparagine deamidation after tryptic digestion and LC-MS analysis. B) Extracted ion chromatograms of innovator and biosimilar trastuzumab of c-terminal lysine truncation after tryptic digestion and LC-MS analysis. Adapted with permission from Ref.* [216]*. C) Reverse phase HPLC chromatogram of innovator (after/before expiry) and biosimilar filgrastim oxidation, with each oxidized peak confirmed by fragment ion analysis. Images reproduced with permission from Ref.* [188]*. D) Charge variants analysis of innovator and biosimilar rituximab by CEX-HPLC. Images reproduced with permission from Ref.* [201]*.*

1.4.4 Impurities

In the course of manufacturing and during storage, biologics may obtain impurities, product and process related, which can affect the final products' stability safety and efficacy. Product-related impurities are undesired modifications such as disulfide bond variants, glycation and aggregation while process-related impurities correspond to materials used in the production process such as cell culture, extraction and purification steps. [217] These impurities differ from product variants which are considered comparable to the biologic product. [218]

Disulfide bonds are product-related impurities that play a critical role in biologics both structurally and functionally, facilitating protein HOS folding and stabilization. [219,220] Disulfide bonds link the light and heavy chains via inter-chain bonding and stabilize subdomain folding via intra-chain bonds. [221] The heterogeneity of recombinant mAb disulfide bonding has been previously reported. [189,222,223] Incorrect disulfide bonding, such as breakage and scrambling can occur when biologics are exposed to environmental stresses during downstream processing steps. [224,225] Thus, it is essential to evaluate the presence of expected and unexpected disulfide bonds, which reflects protein misfolding or aggregation and can lead to changes in potency and safety. For example, etanercept, and its biosimilar have complex disulfide patterns with 29 disulfide bridges throughout their structures and are known to have incorrect disulfide variants between specific cysteines in the receptor domain, leading to changes in their potency (Figure 1-8A, B). [79,226,227] To characterize disulfide bonding, non-reducing peptide mapping using a RP-LC-MS or MS/MS system is regarded as the standard method. Peptide fragments retaining a single disulfide bond are generated using

enzymatic digestion and separated by RP-LC and subsequently confirmed by MS or MS/MS. [228–230] Indirectly, the presence of cleaved disulfide bonds can be further quantified by free cysteine (thiol) analysis using Ellman's reagent as a colorimetric method. [151,231]

Glycation is the attachment of reducing sugars to the primary amine of proteins, which are typically Lys residues. [232,233] For biologics, glycation mainly occurs on mAb products during cell fermentation and storage, where sugars are a source of energy and a main ingredient. [234–236] It is known that glycation can reduce biologic activity and stability of recombinant proteins depending on their binding site and cause the loss of the positively charged Lys residue, resulting in charge variants. [237–241] The two main methods to analyze protein glycation are boronate affinity chromatography (BAC) and LC-MS. [53,69,79,96,151] In BAC, boronate groups in the column retain glycated proteins at high pH conditions, which are then eluted out by either decreasing the pH, or by adding a competing sugar agent, such as sorbitol. [234] However, glycosylated proteins can be retained on BAC columns, which may lead to non-specific binding [242,243] and quantitative data is not provided since it cannot differentiate between proteins with single and multiple glycations. [240] Various top-down and bottom-up LC-MS based methods can be used for glycation analysis, which are highly similar to the approaches used for glycan analysis. Top-down approaches provide a quick characterization of glycation levels after deglycosylation and the removal of C-terminal Lys by detecting +162Da mass shifts (Figure 1-6H, I). [53,96,244] Bottom-up approaches can provide information on glycation sites by detecting missed tryptic cleavage sites that have +162Da mass shifts since the glycation of Lys residues blocks tryptic digestion. [236,245] Each method has

different sensitivities and therefore comparisons cannot be made across methods. Most analyses are being done with MS technologies.

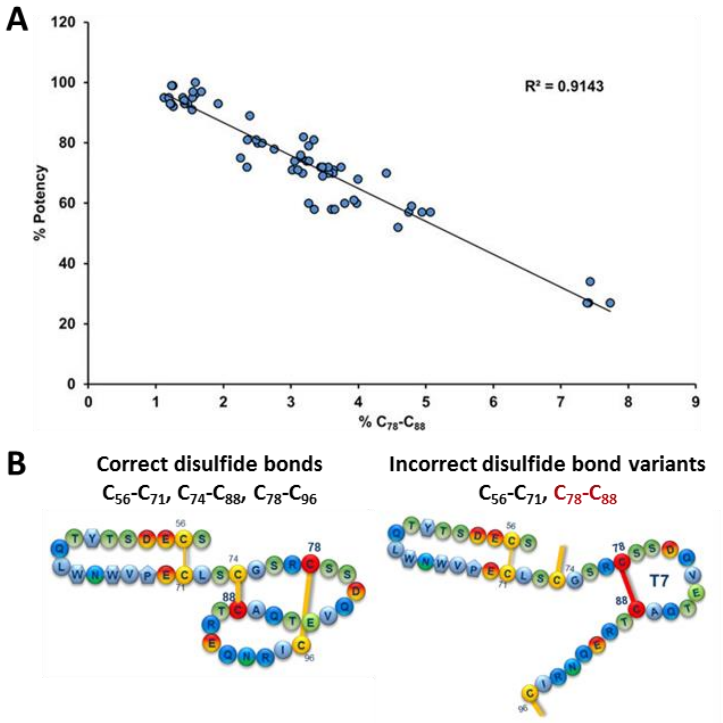

Figure 1-8 *A) Correlation of % potency (TNF-α neutralizing activity) with % incorrect disulfide bonding at C78-C88 for etanercept. B) Structure of etanercept with correct and incorrect disulfide bonding. Images reproduced with permission from Ref.* [246].

Another major challenge in producing biologics is their natural propensity to aggregate.[76] These aggregates vary in size (nm-μm), structure (native/non-native), morphology (spherical/fibrillar/amorphous), and their reversibility. [247] Not only does the presence of protein aggregates compromise therapeutic efficacy and bioavailability, but they may elicit immune responses to the protein drug, even generating anti-drug antibodies (ADA). [248–252] The elicited immune response results from the combination of one or more changes of solubility [249], viscosity [253] and exposure of neo-epitopes, induced by conformation alteration, considered as foreign by the immune system (Figure

1-9A). [254] In the case of the infliximab biosimilar, there have been reports that aggregates might affect TNF-α binding which is a critical mechanism of action and potential for immunogenicity. [96] However, there is no single method that can assess a wide size range of aggregates (Figure 1-9B). Therefore, biosimilar developers should analyze aggregates by employing several orthogonal methods for cross-validation to ensure the presence of comparable or lower levels of aggregates with the reference throughout the product's life-cycle, manufacturing, storage and delivery. Among the diverse methods of aggregate determination, size exclusion chromatography (SEC) is the most commonly used analytical method for quantification and size estimation of aggregates (Figure 1-9C). SEC is based on molecular sieving, which separates from larger to smaller molecules depending on their molecular size in solution. [247] In addition, SEC can be combined with UV, fluorescence, multi-angle laser light scattering (MALS) and other detectors. SEC-MALS provides increased accuracy by acquiring absolute molar mass for each eluted fraction over SEC or MALS alone. [255] However, it has been reported that SEC can incorrectly detect aggregates due to either unwanted secondary interaction with the stationary phase (adsorption) [256], removal of large insoluble aggregates during sample preparation, or dissociation of reversible aggregates during dilution. [257,258] Asymmetric flow field-flow fraction (AF4) determines particle size by laminar and perpendicular cross-flows through a liquid across two different plates, separating particles depending on the particle diffusion coefficient. [259] AF4 can be combined with various detection methods such as UV, MALS and refractive-index. [260] However, method validation can be difficult and possible dissociation of aggregates can also occur during dilution. [257] Analytical ultracentrifugation (AUC) is another commonly

used method for size detection and can be utilized in two different ways, sedimentation velocity (SV), a hydrodynamic approach, and sedimentation equilibrium (SE), a thermodynamic approach. In general, AUC separates particles of various shape and sizes by centrifugal force and by detection with attached optical systems (absorbance/interference/fluorescence) (Figure 1-9D). The biggest advantage of AUC is the ability to directly measure aggregates in various native solutions and over a wide range of sample concentrations. [261] While useful for absolute size measurements, AUC is low-throughput, requires high quality instrumentation and complicated data analysis. [247,262] Dynamic light scattering (DLS) and nanoparticle tracking analysis (NTA) measure particle diffusion coefficients based on Brownian motion and light scattering. DLS is a useful tool for fast size assessment, providing a wider range of particle size and sample concentrations than NTA. DLS requires low sample volume (μL) and samples can be easily collected for further analyses. DLS generates an intensity distribution of particle sizes (Figure 8E), which is sensitive to the presence of larger particles like contaminants and aggregates that may dominate light scattering signals, resulting in misrepresented particle size distributions. [247,263,264] NTA tracks and visualizes movement of particles using a microscope coupled with a camera system providing size distribution representative of number distribution. Compared to DLS, NTA generates information on particle concentration in solution with a better resolution on samples with polydisperse size distribution. However, NTA often requires sample dilution to analyze, which will in turn reduce the particle number and reproducibility when compared to DLS. [263,265,266]

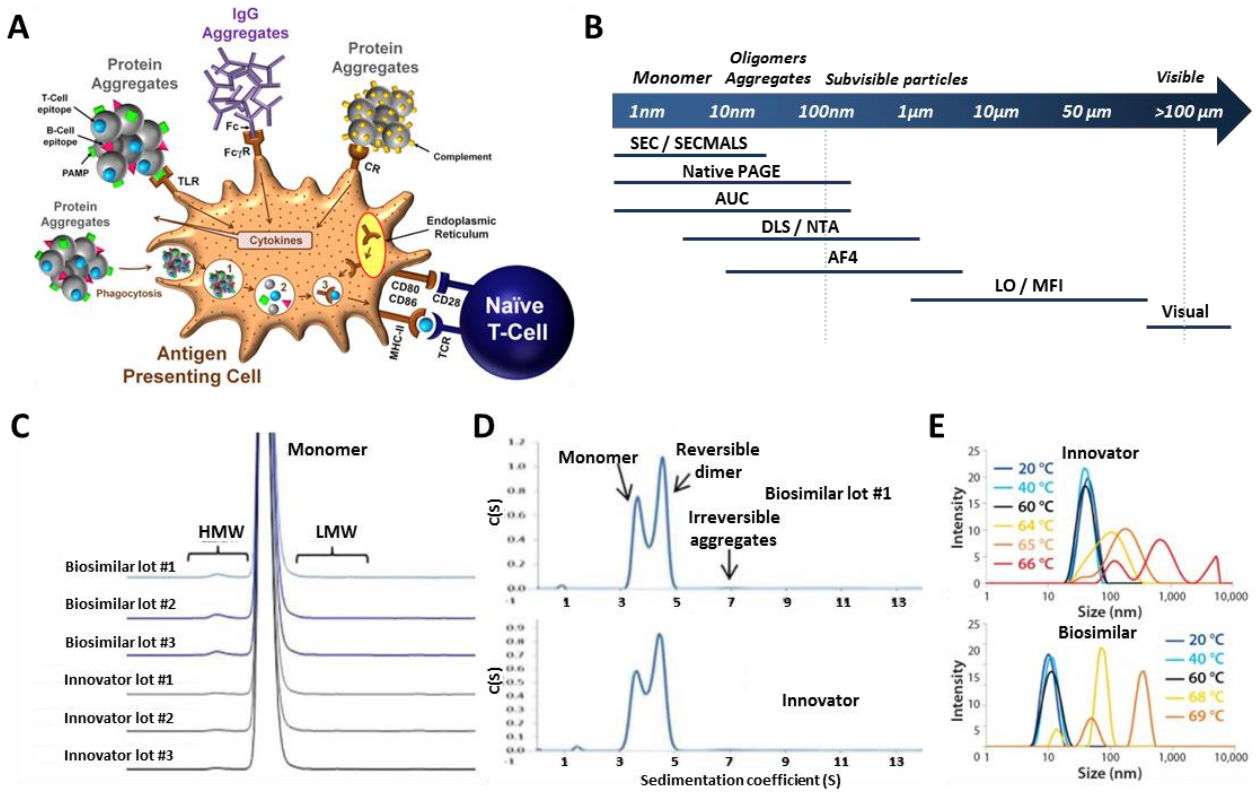

Figure 1-9 *A) In vitro interactions of protein aggregates with antigen presenting cells (APCs) that can potentially trigger an immune response through different kinds of receptors - FcγRs, TLRs and/or CRs. In addition, following the receptor mediated phagocytosis of aggregates, lysosome digested peptides are presented on the cell surface that stimulates naïve T-cells. Adapted with permission from Ref.* [254]*. B) Size-dependent analysis methods of various aggregates and particle sizes. C) Comparison of SEC chromatograms and D) sedimentation coefficient distribution plots between innovator and biosimilar infliximab. Images reproduced with permission from Ref.* [54]*. E) DLS particle size distribution plots of innovator and biosimilar mAbs that have undergone thermal stress (20°C to 90°C). Images reproduced with permission from Ref.* [267]*.*

1.5 **Functional assays for biosimilarity assessment**

The functionality assessment of a biosimilar product is as important as physicochemical property assessment. Physicochemical assessment does not provide information on the functional capabilities, but rather, provides only structural and physical information for molecules. It is critical to validate that no structural differences may lead to meaningful clinical efficacy and safety implications. To demonstrate this, multiple functional assays such as, but not limited to, ligand-binding assays (LBA) and cell-based assays (CBA) must be developed to adequately assess biosimilarity. For this reason, the FDA and EMA have been developing a regulatory guidance recommending multifactorial and stepwise approaches to demonstrate and assess biosimilarity. [26,64,268] The goal of functional assessment is to verify that any structural differences identified from physicochemical assessment do not result in differences in pre-clinical/clinical testing.

1.5.1 Ligand binding assay

The large portion of biosimilars under development and innovator products that are close to off-patent are mAbs whose therapeutic effect relies on binding to specific target sites. Hence, LBAs become more critical in biosimilar development to validate whether specific binding sites correspond to those of the innovator product. LBAs provide the measurement of interactions between antibody and antigen such as strength of binding affinity. [269] Although LBAs do not provide as comprehensive information on biosimilarity as CBA and in-vivo assessments do, they are useful as an early evaluation during development.

There are two general methods for assessing ligand-binding analysis: ELISA, a solid phase assay, and surface plasmon resonance (SPR), a kinetic binding assay.

Generally, ELISA uses a sandwich approach where coated capture antibody binds to target analyte which can later be detected by detection antibody conjugated with HRP. [270] ELISA is not only used to demonstrate the binding between mAb and analytes, it is also commonly used to measure other bindings such as binding of C1q and the Fc-domain which plays a key role in activation of complement-dependent cytotoxicity (CDC). [271] ELISA has been a preferred method due to the use of standard instrumentation and materials in addition to a broad familiarity with the technology while still providing high sensitivity and specificity. However, ELISA can be labor-intense, time-consuming, and provokes intra- and inter-assay variation through multiple pipetting and washing steps making them potentially unreliable as standardized assays. [272]

AlphaScreen and AlphaLISA are newer forms of immunoassays where biotinylated antibody and antibody-conjugate AlphaLISA acceptor beads are used to capture the target analyte (Figure 1-10A, B). Donor beads coated with streptavidin capture an analyte-specific biotinylated antibody while acceptor beads that are conjugated with a secondary antibody can readily recognize the different epitope of the analyte. This binding recruits donor beads and acceptor beads within 200 nm proximity of each other, allowing excited donor beads to release singlet oxygen that can excite a fluorescent signal in the acceptor beads. [273,274] Currently, few studies have used the AlphaLISA assay to measure relative bindings to Fc domain including FcγRIa, FcγRIIIa (158V), and FcγRIIIa (158F). [270,275] Compared to ELISA, AlphaScreen/AlphaLISA is more high-throughput, requires a lower sample volume while offering a wider analytical range and is more sensitive than other preceding immunoassays. [274] AlphaScreen technologies also do not require a wash step which can preserve biological interaction. [274] However,

AlphaScreen/AlphaLISA is sensitive to long exposure to ambient light, donor beads can photo bleach which limits it to a single reading, singlet oxygen can be sequestered by compounds that could scavenge radical oxygen, and it is not adaptable to all plate readers like ELISA. [274] The assay to assess the binding of FcRn to mAb was developed on the AlphaScreen platform which was found to be more accurate, precise, specific, and simple compared to ELISA, fluorescent-activated cell scan, and SPR.[276] Similar to AlphaLISA, FcRn-loaded donor beads and IgG1-loaded acceptor beads are incubated with mAb and dose-dependent decreases in emissions are monitored (Figure 1-10A, B).

SPR is a real-time, label-free (RT-LF) platform that is widely used for ligand binding analysis along with ELISA. However, unlike ELISA, SPR monitors the association and dissociation of binding complexes in real-time to measure the binding kinetics, affinity, and binding specificity of Fc-receptors with their targets, including FcRn, FcγRIIa, FcγRIIb, FcγRIIIa, and FcγRIIIb. [68,96,275] In SPR, sample is flowed over the surface of a sensor chip that is coated with analytes such as target molecules or Fc receptors and changes in refractive index are used to determine the association rate constant (k_a), dissociation constant (k_d), and dissociation equilibrium binding constant (K_D) of antibody-antigen interactions. [277,278] SPR collects kinetics of binding data whereas ELISA collects end-point binding data. Therefore, SPR can provide more comprehensive data collection than ELISA. SPR does not require any labeled reagents or wash steps and it does not require standards like ELISA, where assay results are dependent on the functional quality of the standards. [279] SPR uses calibration-free concentration analysis (CFCA) which does not require a standard curve while relying on changes in binding rate

with varying flow rates, when the rate is limited by analyte diffusion on the sensor surface (Figure 1-10C, D). [280–282]

Bio-Layer Interferometry (BLI) is relatively newer RT-LF platform that has more potential to support high-throughput demands in current pharmaceuticals. [283,284] BLI is an optical analytical technique that uses dip and read biosensors to measure the interference patterns of light caused by a binding between molecules in solution and molecules immobilized on the biosensor tip surface (Figure 1-10E). Compared to SPR, BLI is relatively robust to fluctuations in the refractive index, is free of microfluidics, and is capable of high-throughput analysis. [285]

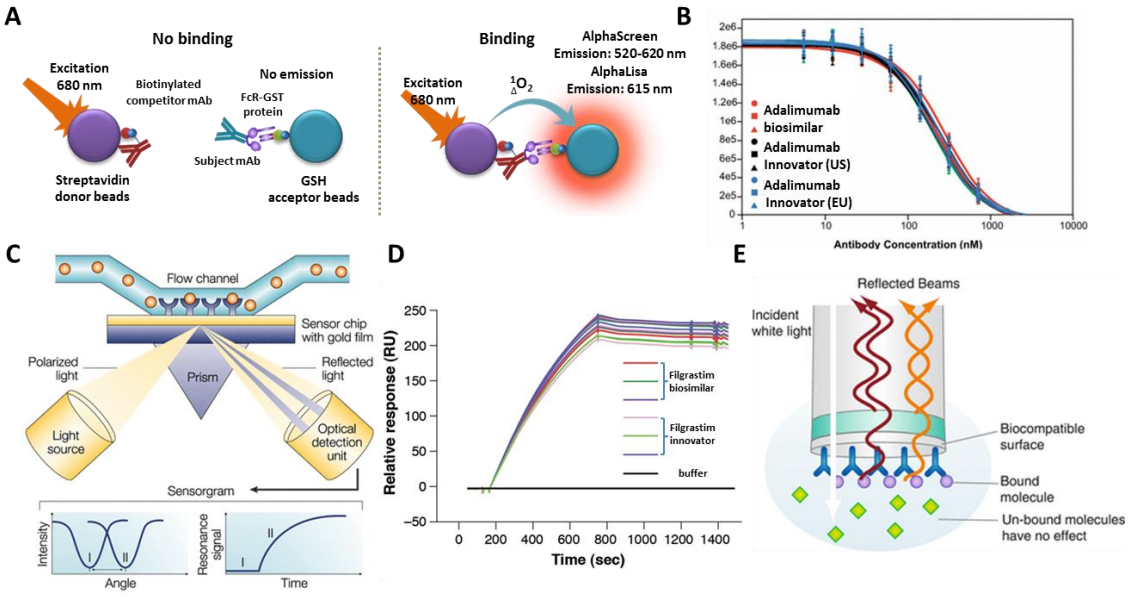

Figure 1-10 *Methods for the determination of ligand binding. A) Comparing FcγRIIIa binding affinity competition of mAbs A) in the presence of (left) or not in the presence of biotinylated competitor mAb (right) using AlphaScreen or AlphaLisa. B) Comparison of dose response curves of innovator and biosimilar adalimumab showing FcγRIIIa (158V) binding (in the presence of TNF-α) using AlphaScreen. Adapted with permission from Ref.* [270]. *C) Principle of SPR analysis for target binding. Adapted with permission from Ref.* [286]. *D) Comparison of target binding between innovator and biosimilar filgrastim by SPR. Images reproduced with permission from Ref.* [77]. *E) Principle of BLI to measure target binding affinity of mAbs As more molecules bind to the biosensor surface, the wavelength shift of the reflected light will be shown on a sensorgram. Adapted with permission from Ref.* [287].

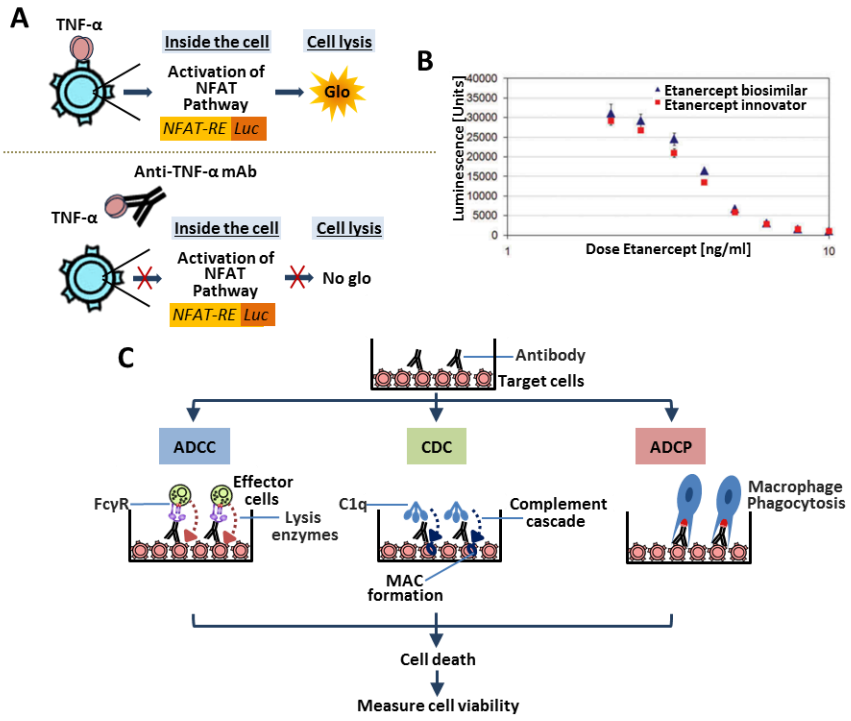

Figure 1-11 *Cell based bioactivity assays. Mechanism of NFκB-dependent luciferase reporter gene assay for measuring Fab mediated TNF-α neutralization A) with (upper) or without (bottom) anti-TNF-α mAb. B) Comparison of dose-dependent TNF-α neutralization activities between innovator and biosimilar etanercept. Images reproduced with permission from Ref.* [288]*. C) The assessment of effector functions induced by Fc domain – ADCC, CDC and ADCP. ADCC is mediated by FcγRIIIa, CDC is mediated by C1q, and ADCP is mediated by FcγRIIa with antibody to induce cell death. MAC: Membrane Attack Complex.*

1.6 **Cell-based bioactivity assay**

The mechanism of actions (MoA) and stimulation of downstream signaling events of each therapeutic mAb varies. Therefore, a bioactivity assay is required to evaluate the MoA which cannot be assessed by non-cellular ligand binding analyses. MAb Fab-domains display variable sequences that associate with antigen binding specificity and are directly related to the MoA, including neutralization, induction of apoptosis, or growth inhibition. The Fc-domain exhibits a constant sequence that is responsible for triggering effector functions such as complement-dependent cytotoxicity (CDC), antibody-

dependent cell cytotoxicity (ADCC) and antibody-dependent cellular phagocytosis (ADCP). [289] Therefore, it is important to have comprehensive assessments of both the Fab domain and Fc domain to validate the function and similarity of biosimilars. CBA are chosen and developed based on the reported MOAs and are unique to each biosimilar/reference pair.

The bioactivity assessments of Fab domains are well-established for mAbs, especially for mAbs whose biological function is primarily contributed by the Fab-domain, such as infliximab and adalimumab which inhibit pro-inflammatory signaling induced by a target protein TNF-α via the Fab-domain. Fab functionality assessments typically include cell binding assays and neutralization assays. The results of competitive cell-based assays can be informative to assess the similarity of biosimilar and reference mAb with respect to binding to TNF-α and can also characterize the binding function of the Fc-domain. Cell-based functional bioassays such as CD20 binding, Fc-effector function, and apoptosis activity were used to assess originator rituximab and its biosimilar. [68] To further characterize binding function, a neutralization assay can be used to assess the similarity of the biological functions that contribute to the clinical efficacy such as TNF-α and LT-α neutralization. Neutralization activity can be determined via apoptosis, cytotoxicity, or reporter gene assays. In a study of adalimumab biosimilar, ABP 501, inhibition of TNF-α-induced apoptosis was evaluated since TNF-α can induce apoptosis under the conditions in which activity of NF-κB is reduced. [270] Etanercept biosimilar, GP2015, compared its neutralization to reference using a reporter gene assay (Figure 1-11A, B). [79,288] Inhibition of target cell growth by blocking signaling pathways in cancer cells is one of the many modes of action for cancer therapeutic mAbs. [290] Therefore,

many biosimilars of antiproliferative therapeutic mAbs apply this approach to assess the potency of its inhibition of target cell growth. ABP 215 and its innovator, bevacizumab were evaluated for their similarity in antiproliferative function by using adenosine triphosphate (ATP)-specific luminescent reagent combined with lysed cell to determine the viability of the cell through amount of ATP presented. [275]

The assessment of effector function induced by the Fc-domain is necessary for therapeutic mAbs, especially those that Fc-effector functions have been proven to be part of their MOAs. To assess CDC activity, target cells and therapeutic mAbs are incubated and complement is introduced to opsonize target cells and induce lysis while monitoring cell viability by luminescence, fluorescence or ATP production with various commercially available reagents. [68,270,291] ADCC assays depend on mAb-mediated cross-linking of target cells and effector cells via binding with FcγRIIIa receptors on effector cells. Purified human natural killer (NK) cells are most widely used as effector cells in ADCC activity assessments, however, to more closely replicate the physiological environment, peripheral blood mononuclear cells can be used as effector cells since they are more representative of *in vivo* conditions including range of cell types and immune complexes. [96] ADCC cell death can be monitored through detection of prelabeled cells or production of cytosolic enzymes. [291] Successful ADCC assays require an optimization of the ratio of target cells to effector cells as the density of FcγRIIIa differs from donor-to-donor cell population. [292] Lastly, as the FcγRIIIa allotypes have different binding affinity against Fc domains of therapeutic mAbs, it is critical to compare the activity in both V/V and F/F genotype of FcγRIIIa. [293,294] Rituximab originator and adalimumab originator and their biosimilars were both evaluated for CDC and ADCC using methods described above.

[68,270,295] Cell-based assays can also be used to assess biosimilars such as filgrastim, a granulocyte colony-stimulating factor, which is not a mAb. Filgrastim bioactivity was assessed by incubating filgrastim with target cells, NFS-60, and luminescence was used to compare potency of each compound. [296] Although cell-based assays offer valuable knowledge of biosimilar functionality, they can be time-consuming and highly variable due to many extrinsic variables such as the assay matrix and are often difficult to validate. [297] (Figure 1-11C)

1.7 **Forced degradation studies**

Forced degradation studies have been utilized to support the drug development process and to evaluate manufacturability. [298] These studies are performed by applying thermal (elevated temperature, Freeze/thaw), chemical (low/high pH, oxidizing condition) or physical (agitation) stresses to drug substances and drug products. [299] Objectives of these studies are the following. (1) to determine the degradation pathway, (2) develop formulations, (3) develop analytical methods, (4) determine shelf-life, (5) evaluate manufacturability, (6) assess CQAs and (7) determine the intrinsic stability. [300] Recently, stresses have been utilized to compare biosimilarity as a comparative stability test in Biologic License Application submissions. [96,150,151,194,301] Analytical methods to assess degradation products are shown in Table 1-4.

1.7.1 Major degradation pathways

There are several major degradation pathways for mAbs. The most commonly observed pathways are (1) aggregation, (2) fragmentation, (3) deamidation and (4) oxidation. Under specific stress conditions, small amounts of impurities can be amplified. For example, levels of deamidation and disulfide bond scrambling can increase under

high pH conditions while levels of oxidation can increase under high- temperature conditions.

Table 1-4 *Selection of analytical methods to assess different types of degradation products*

Types of Degradation	Selected Analytical Methods
Soluble aggregation and fragments	SEC-HPLC, AF4, AUC, SDS-PAGE, Capillary electrophoresis
Subvisible aggregates, nanometer size range	DLS, NTA, AF4, MALLS, Turbidity, Static light scattering
Subvisible aggregates, micrometer size range	Light obscuration
Visible particles	Visual inspection
Secondary structure	Far-UV CD, IR, Raman spectroscopy
Tertiary structure	Near-UV CD, Intrinsic fluorescence, NMR, Second derivative UV spectrometry
Changes in hydrophobicity	RP-LC, extrinsic fluorescent dyes, Hydrophobic interaction chromatography
Chemical change (e.g, oxidation, deamication)	LC-MS, Peptide mapping, RP-LC, IEX-LC, IEF

1.7.2 Sources of stress

The most common method of forced degradation studies is the application of high temperature (thermal stress) that exceeds the normal storage temperature. For example, mAb drug products are required to be stored from 2-8 °C. Thus, 25 °C and temperatures above 35 °C are used for accelerated stability studies. This facilitates the formation of degraded substances, such as aggregates and fragments over the course of a short period of time. When a drug substance is in a solid form (such as lyophilized mAb drugs), high humidity may also be introduced in addition to thermal stress. [338,339]

Freeze-thaw is often utilized for forced degradation studies because drug substances can be exposed to low temperatures over the course of long-term storage

and lyophilization. This study is useful to assess drug stability upon accidental freezing and determine appropriates excipients that protect and stabilize the drug products during lyophilization.[340] The major degradation pathway for freeze-thaw is aggregation, including precipitation and particle formation. [341,342]

Drug substances and products can encounter agitation (stirring or shaking) as physical stresses during the entire drug manufacturing process, filling, shipping, and final administration. Thus, it is crucial to confirm a drug's robustness and stability against agitation. [340] Stirring, shaking, vortexing and sonication can be used for mechanical stress testing. [343–347] The major degradation pathway is aggregation after exposing the molecule to agitation.

Drug substances such as mAbs can be exposed to low or high pH conditions during purification. Low pH leads to aggregation and fragmentation, especially in solutions where mAbs are found at high concentration, resulting in precipitation. [334] High pH causes asparagine deamidation and disulfide bond shuffling, resulting in aggregation and fragmentation. [348]

During manufacturing, biologics are exposed to oxidizing condition by dissolved oxygen and free radicals derived from metal and oxidized surfactant impurities. Hydrogen peroxide and tert-butyl hydrogen peroxide are the most widely used reagents to test for forced methionine oxidation. Probing oxidation susceptible residues by forced oxidation is important since oxidation of site-specific residues (mainly Methionine) can result in decreased drug potency when the residue is located at the site of drug binding (antigen-binding sites). Often oxidation can occur aggregation since oxidation induced-conformation changes can occur. [334]

1.8 **Research scope**

My research contributes to a key foundational step in biosimilar development that requires extensive and robust analytical characterization to fill the gaps in knowledge resulting from the lack of disclosed information for innovator drug products. Through this research, one can characterize the quality attributes of a biosimilar and evaluate whether or not they closely match the structural and functional features of the originator. Based on the degree of similarity and residual uncertainty between an originator and a biosimilar, analytical characterizations can determine the extent of preclinical and clinical studies. The introduction highlights key characteristics of biosimilars including critical quality attributes and methods for analytical characterization of biosimilar structure and function. The work presented demonstrates the utility of various techniques to measure comparability between an originator and any prospective biosimilar.

1.9 **Thesis overview**

The overall goal of this thesis is to demonstrate biosimilarity and shed light on the minor differences between originator drugs and their respective biosimilars. To do this, we have compared different originator and biosimilar pairs; filgrastim, rituximab, bevacizumab and trastuzumab, using various analytical techniques. This thesis is composed of 5 chapters showing comparability studies of each originator and biosimilar pair regarding structure and functional aspects.

Chapter 2 of this thesis focuses on the analytical characterization of the originator filgrastim (Neupogen®) and its proposed biosimilar. This chapter first examines primary and higher order structures. This is accompanied by the analysis of variants that may

affect biological activity. Findings from this study can be used to support the claim of biosimilarity of a proposed biosimilar to filgrastim to a regulatory agency.

Chapter 3 assesses the biosimilarity of Rituxan®, the originator rituximab and Acellbia®, a biosimilar, using MAM workflow that can measure several attributes in a single assay. Outside of MAM, several different MS and LC separation techniques are utilized to characterize the higher order structure and product-related variants of rituximab, respectively. This chapter identifies key differences between the originator and a biosimilar that could lead to different biological activities, such as ADCC.

Chapter 4 evaluates the initial structural differences/similarities existing between three original mAb drugs and their biosimilars as well as their behaviors when subject to thermal stress. This stress condition could amplify subtle initial structural differences between the originators and biosimilars that might not be detected by individual analytical instruments. Findings from this work can be used when attempting to establish biosimilarity.

Chapter 5 highlights the final conclusions of each chapter and discusses the future direction for this work. Each chapter was prepared in a manuscript format. Chapter 1 was prepared with an invited submission to *Angewandte Chemie*. Chapter 3 was submitted for publication to *European Journal of Pharmaceutics and Biopharmaceutics*. Chapter 4 is written in a format for submission to *Analytical and Bioanalytical Chemistry.*

Chapter 2: Comparability Analysis of an Originator Filgrastim and its Proposed Biosimilar

2.1 Abstract

Filgrastim (brand name: Neupogen®), a recombinant human granulocyte colony-stimulating factor (rhG-CSF), is widely used to treat neutropenia by stimulating neutrophil maturation. Zarxio®, a filgrastim biosimilar, was the first biosimilar approved in the US due to its relatively simple structure compared to that of monoclonal antibody drugs. As of now, two filgrastim biosimilars have been approved in the US, but more may be approved in upcoming years. In this study, we compare Neupogen® and its proposed biosimilar regarding their structure (primary, higher order) and variants (size, oxidized, deamidated) using different mass spectrometry (MS) techniques, NMR and liquid chromatography (LC) techniques. No significant differences were detected regarding structure and variants levels except deamidation levels.

2.2 Introduction

Filgrastim is a recombinant human granulocyte-colony stimulation factor (rhG-CSF) product that has the same biological activity as endogenous G-CSF. Unlike human G-CSF, filgrastim contains an N-terminal methionine (Met) residue and is not glycosylated as it is expressed in *Escherichia coli.* [324] Filgrastim is used to treat neutropenia, a condition

derived from cancer chemotherapy and several other disease states, by stimulating neutrophil maturation. [325,326]

A biosimilar is a biological product that has no clinically meaningful differences from its reference product in terms of safety, purity and potency. [52] The market for biosimilars in the US has gained more attention, thanks in large part to the approval of the first biosimilar, Zarxio®. Zarxio®, a biosimilar filgrastim, was approved in 2015 and paved the way for the FDA approval of a second filgrastim biosimilar, Nivestim, in 2018. The number of biosimilars in development continues to rapidly increase due to the imminent patent expiration of many other biologic products and the release of an FDA guidance for biosimilar approval. However, dramatic cost savings for patients is highly unlikely due to the inherent requirement of more sophisticated procedures and higher operational cost for biologics, when compared to small molecule generics. [327] Contrary to small-molecule drugs, where the FDA provides an abbreviated regulatory pathway for generic drugs, biologics and their biosimilars present a difficult challenge in their regulatory pathway. The inherent complexity and variability in post-translation modifications (PTMs) observed for biologics and their biosimilars prevents the FDA from establishing an equivalent abbreviated pathway. [328] Therefore, the FDA encourages extensive fingerprint-like analytical assessment of biosimilars, as well as highly targeted animal and/or clinical tests, to ensure similarity between the biosimilars and their biologic reference product. In this regard, thorough characterization can provide the foundation allowing companies to determine the scope and extent of further animal and/or clinical tests [329]. While these assessments provide further confidence in the structure, potency and toxicity-based

similarities between biosimilars and reference biologics, they often come with the need to perform experiments using cutting-edge techniques and equipment. [52,67]

There are many tools available for characterizing biosimilarity. The primary structure of therapeutic proteins can be determined via peptide sequencing and mapping, and higher order structures can be characterized using circular dichroism (CD) spectroscopy and differential scanning calorimetry (DSC). Commonly employed methods for identifying impurities in biologic products include LC, SDS-PAGE and LC-MS. Information on protein binding affinity and kinetics is typically obtained using bioassays (ELISA, AlphaLISA, etc.) and surface plasmon resonance (SPR). [82,330–332]

In this study, we describe the physicochemical characterization of a potential filgrastim biosimilar and its reference product, Neupogen®, utilizing multivariate analytical techniques. Specifically, peptide mapping and PTM analysis were conducted to compare the primary structure of the products. Higher order filgrastim structures were compared by employing 1-dimensional (1D) and 2-dimensional (2D) NMR, ion mobility mass spectrometry (IM-MS) and intact mass spectrometry. Product impurity levels were evaluated using RP-UPLC and SEC UPLC analysis.

2.3 **Materials and methods**

2.3.1 Materials

Ammonium bicarbonate, acetonitrile (HPLC grade), dithiothreitol (DTT), iodoacetamide (IAM) and sorbitol were obtained from Fisher (Hampton, NH). Trifluoroacetic acid (TFA, for HPLC, ≥ 99.0%), formic acid (FA), sodium acetate, glacial acetic acid and deuterium oxide were purchased from Sigma-Aldrich (St. Louis, MO). Endoproteinase Glu-C and Progenta™ anionic acid labile surfactant were obtained from Protea (Morgantown,

WV). The original filgrastim (Neupogen®, lot numbers (0.6 mg/ml - 1056459, 1061003, 1057138), (0.3 mg/ml - 1048844, 1055570, 1050158) and biosimilar filgrastim (lot numbers (0.6 mg/ml - 3-Fin-2475, 3-Fin-2476, 3-Fin-2477) (0.3 mg/ml - 3-Fin-2479, 3-Fin-2480, 3-Fin-2481(0.3 mg/ml)) were provided by Adello biologics.

2.3.2 Enzymatic digestion

For digestion, 20 µg of samples were diluted in 100 mM Ammonium bicarbonate (pH 8.0) with 0.1% Anionic Acid Labile Surfactant. Proteins were reduced with DTT followed by 1 hour of incubation at 37°C. Alkylation was performed by adding IAM at a final concentration of 10 mM. Samples were then incubated in the dark for 30 minutes at room temperature. IAM was quenched using DTT. Glu-C enzyme was added to make a 1:20 enzyme to protein ratio after which the samples were incubated overnight at 30°C. Following digestion, samples were immediately acidified with FA and stored at 4°C until analysis.

2.3.3 Peptide mapping

We analyzed the protein digests using MS/MS on an Electrospray ionization (ESI) Q exactive mass spectrometer (ThermoFisher, Waltham, MA) interfaced with an Acquity UHPLC system (Waters, Milford, MA). LC separation was performed on an analytical column (AdvanceBio Peptide Mapping C18, 2.1 x 150 mm 2.7 µm) (Agilent, Santa Clara, CA) at a flow rate of 150 µl/min with a 50 min reverse phase gradient. The mass spectrometer was operated in a data-dependent acquisition mode. The 2 most intense multiply charged ions in each regular MS scan were subjected to MS/MS analyses. Precursor ions were scanned at 70,000 resolution, while fragment ions were scanned at 17,500 resolution. Mass accuracy, sensitivity, and fragment isolation were assessed by

injecting 1 pmol of Pierce Peptide Retention Time Calibration Mixture prior to data acquisition. Byonic™ search software was used for the analysis of LC-MS/MS data from digested samples. The precursor peptide mass was measured in the first stage of MS/MS (MS1), with the resulting fragment ion masses being measured in the second stage of MS/MS (MS2). Byonic™ analyzes peptide ions by matching the mass of the precursor mass (MS1) with the expected fragment ion masses (MS2) and its calculated masses based on an in-silico filgrastim sequence digest. Byonic™ can provide a search of variable modifications such as the oxidation of methionine and tryptophan residues and deamidation of asparagine and glutamine residues.

Byologic® software employs a label free quantification approach, utilizing extracted ion chromatogram areas (XIC areas) to quantify PTMs with respect to their unmodified counterparts. XIC extraction and data organization were performed automatically by Byologic® using the data derived from Byonic™ search software.

2.3.4 Ion mobility mass spectrometry

Samples were buffer exchanged with 100 mM ammonium acetate using a 10K MWCO Microcon filter device. Sample aliquots (~7 µL) were analyzed in triplicate for each lot by IM-MS on a Synapt G2 HDMS quadrupole-ion mobility-time-of-flight mass spectrometer (Q-IM-ToF MS) instrument (Waters, Milford, MA). Protein was ionized by nano-ESI in the positive mode with a capillary voltage of 1.2 – 2.0 kV and cone voltage of 60 V. To generate ion mobility separation, Direct Current (DC) voltage with 600 m/s of wave velocity and 40 V of wave height was applied.

2.3.5 Collision induced unfolding

The ions gained collision energy in the traveling-wave-based ion trap prior to reaching the IM separator to carry out protein CIU. The 8+ charge state of the intact protein was chosen by tandem-MS using quadrapole selection. The collision voltage increases in a 5 V stepwise manner from 5 to 90 V to construct the fingerprint data, a profile of energy-dependent arrival-time distribution.

All mass spectra were processed using Masslynx 4.1 software. CIU data were extracted as a function of collision voltage and drift time using Drift Scope (Waters, Milford, MA). Analysis of Extracted CIU data was performed using CIUSuite. Corresponding 2D-contour plots were generated by the CIUSuite_gen module where the strongest intensity was shown in red and normalized with a maximum value of 1 by a Savitzky−Golay filter. Average CIU fingerprints and standard deviation plots were generated for multiple lots of innovator and its biosimilar using the CIUSuite_stats module.

2.3.6 1 and 2-dimensional NMR analysis

Each sample (13 prefilled syringes - 480 µg of filgrastim each) were concentrated using pre-rinsed Amicon® Ultra centrifugal filter units (0.5 mL, 3000 Da MWCO). Centrifugation was performed at 4,000 X g for 4 x 20 min at room temperature. The final sample volume was adjusted to 280 µL with filtrate. 20 µl of D_2O was added and loaded into a Shigemi tube (5 mm diameter and 8 mm length at the bottom (Shigemi Inc., Tokyo, Japan)).

HSQC spectra (1D and 2D) were obtained on a 600 MHz Bruker NMR spectrometer equipped with a cryogenic probe. The spectral width of the ^{1}H and ^{15}N dimensions were 16.0221 and 32 ppm, respectively. For each spectrum, 2048 points were used for F1 and

128 points were used for F2. After being zero filled to 2048 points in both F1 and F2 (without linear prediction), data were Fourier transformed with a squared-sine-bell (SSB) window function. Topspin was used for data processing and Sparky was used for data analysis. The data was acquired with 2D 1H-15N correlation via double INEPT transfer, using sensitivity enhancement via an Echo/Antiecho-TPPI gradient selection method. Trim pulses were used during INEPT transfer. Decoupling was applied during acquisition. Total experimental analysis was performed for 84 h at 15 °C.

Multi-variable linear regression of NMR values and drug categories were performed to evaluate the similarity between Neupogen® and the proposed biosimilar. Drug category was regarded as dependent variable, with the proposed biosimilar defined as 1 and Neupogen® defined as 0. Two-dimensional NMR parameters (X and Y values, or ^{1}H and ^{15}N values) were used as independent variables. The regression was executed using Excel software, and regression statistics including R Squared, an ANOVA table and estimated parameters, were obtained.

2.3.7 Intact protein analysis

LC separation was obtained by injecting 1 µg of sample on an 1290 Infinity system (Agilent, Santa Clara, CA) with an Poroshell 300SB-C8 column (1 X 75 mm, 5 µm) (Agilent, Santa Clara, CA) at a flow rate of 0.2 ml/min. Mobile phase A was 0.1% FA in water, and B was 0.1% FA in acetonitrile. The gradient started linearly ramped from 5% to 99% B over 6 min and was held at 99% B for 0.5 min, then ramped back to 5% B after 0.5 min, and held at 99% B for 1 min. MS analysis was conducted on an Agilent 6530 Mass QTOF coupled to ESI in positive dual ESI ion mode with a capillary voltage of 3500 V. Intact data was acquired over the mass range between 500-5000 m/z. System suitability was assessed

by injecting 1 µg of intact mAb mass check standard. (Waters, Milford, MA) Data processing was performed with Agilent MassHunter Workstation Software (Version B. 05. 01).

2.3.8 Size exclusion chromatography

UPLC analyses were performed on an Acquity UPLC H-class system (Waters, Milford, MA) using an Acquity SEC BEH 125Å column (1.7µm, 2.1mm x 100mm, 1K-80K; Waters, Milford, MA). UV detection at 215 nm was chosen. The mobile phase was 20 mM ammonium bicarbonate (pH 7) with an isocratic flow rate of 0.3 mL/min, run for 10 min. Injection volume was 5 µL, and data analysis was performed using Empower 3 software.

2.3.9 Reverse phase chromatography

An Acquity UPLC BEH C_{18} column (1.7 µm, 2.1 mm × 100 mm; Waters, Milford, MA) was used with UV detection at 215 nm, with column temperature set at 60°C. Mobile phase A was acetonitrile with 0.1% TFA and mobile phase B was water with 0.1% TFA. A linear gradient was used, ramping from 25% to 55% mobile phase A over 13 min and then ramping from 55% to 75% mobile phase A over 17 min. The column was equilibrated with 25% A for 10 min between each injection. The injection volume was 5 µL, and data analysis was performed using Empower 3 software.

2.4 **Results**

2.4.1 Primary structures and post-translational modifications

The primary structures of Neupogen® and its proposed biosimilar were determined by LC-MS/MS amino acid sequencing following Glu-C digestion. Figure 2-1 shows the total peptide coverage for 3 vial lots of biosimilar and Neupogen®. Total peptide coverage was 100% (175 of 175) in all 6 samples. Figure 2-2 shows the major modifications of filgrastim in 3 vial lots of biosimilar and Neupogen® as observed by LC-MS/MS. Oxidation and

deamidation were observed mostly at trace levels (<6 %). Peptides containing oxidized or deamidated residues are highlighted by red marks in Figure 2-1. Oxidation levels were comparable between Neupogen® and the proposed biosimilar while deamidation levels were significantly different between the two at Gln12, (4 -7 % deamidation in Neupogen® vs. <1 % in the biosimilar).

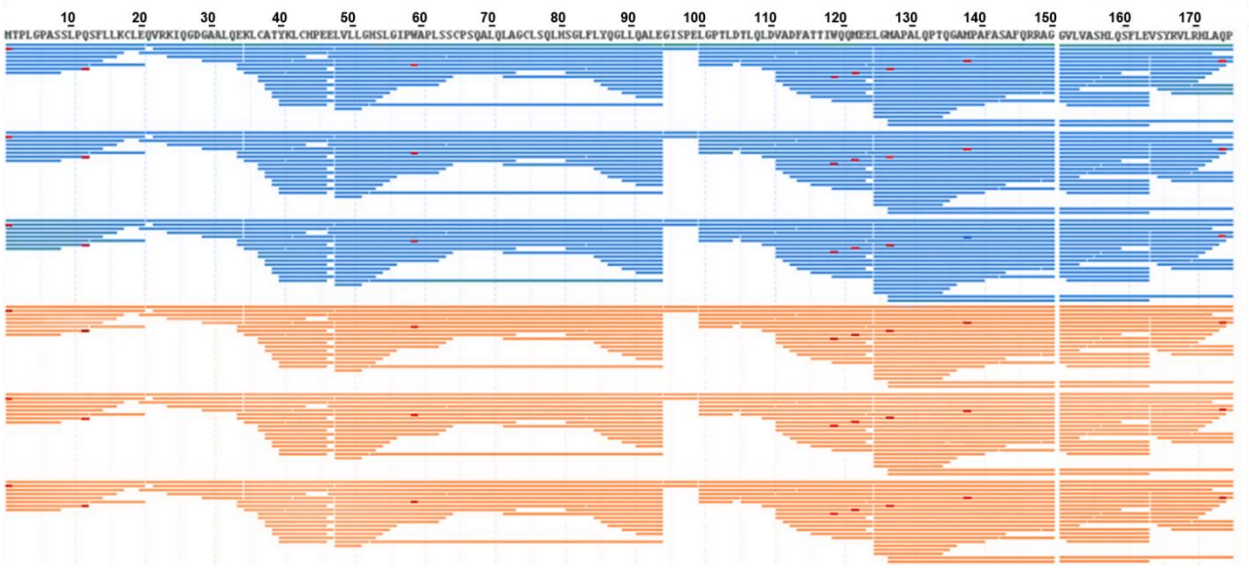

Figure 2-1 *Sequence coverage map of Neupogen® (blue) and biosimilar filgrastim (orange). We confirmed 100% sequence coverage and identical amino acid sequence between the two.*

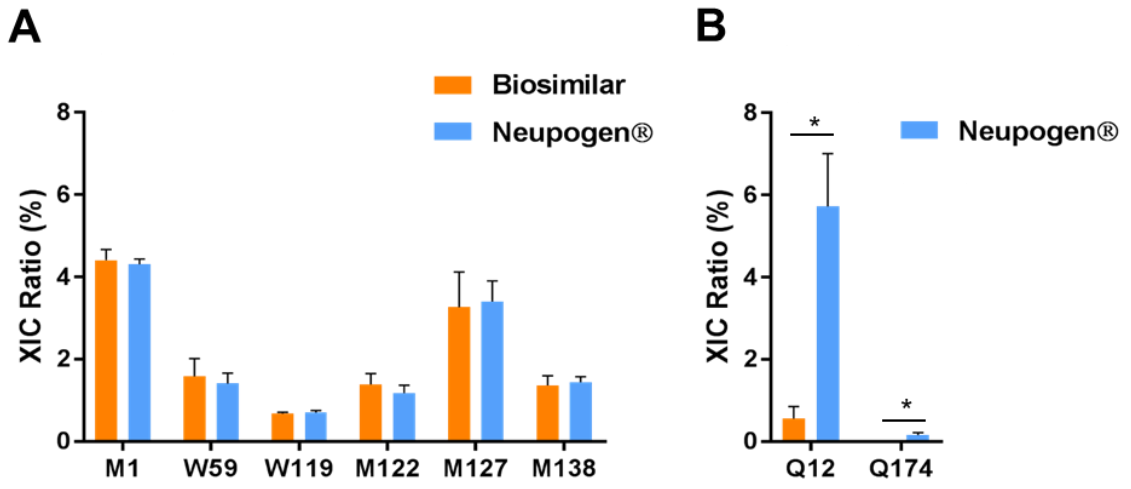

Figure 2-2 *(A)Oxidation and (B) deamination levels of filgrastim in 3 vial lots of Neupogen® and its proposed biosimilar observed in LC-MS/MS. Peptides containing oxidized or deamidated residues are highlighted by red marks in Figure 2-1. N = 3; mean ± SD, Student's t-test, NS: not significant, *p<0.05, **p<0.01) M: Methionine, W: Tryptophan, Q: Glutamate*

Table 2-1 *Detailed percentage values for the major modifications of filgrastim in 3 vial lots of Neupogen® and its proposed biosimilar observed in LC-MS/MS.*

Modification	Modified amino acid	Residue number	% PTM observed					
			Vial lot biosimilar			Vial lot Neupogen®		
			Lot 1	Lot 2	Lot 3	Lot 1	Lot 2	Lot 3
Deamidation	Glutamine	12	0.89	0.35	0.43	5.69	4.46	7.03
	Glutamine	174	0.00	0.01	0.00	0.19	0.09	0.19
Oxidation	Methionine	1	4.61	4.12	4.50	4.23	4.24	4.46
	Tryptophan	59	1.22	1.45	2.07	1.18	1.69	1.35
	Tryptophan	119	0.70	0.63	0.69	0.67	0.76	0.68
	Methionine	122	1.55	1.08	1.53	0.99	1.38	1.16
	Methionine	127	2.94	2.60	4.24	2.83	3.62	3.76
	Methionine	138	1.35	1.14	1.60	1.44	1.58	1.32

2.4.2 Higher order structure analysis

A stable higher order structure is essential for a therapeutic protein to be functional [333]. To compare higher order structures between Neupogen® and its biosimilar, we performed CIU-IM-MS and 1D, 2D-NMR analysis. ESI MS spectra showed highly similar charge state distributions with the highest intensity of 8+ charge in both cases. Their 2D-IM-MS plots showed comparable spectra patterns without detecting aggregates such as a dimer and trimer. (Figure 2-3) Then, their gas phase unfolding dynamics were compared using the 8+ charge ions. The ion intensities are represented by the color axis to the right of plots. The averaged CIU contour map appeared to be similar with both drugs. On the contour map, three distinct CIU features were detected for the +8 charge state. (Figure 2-4) The most compact form in the gas phase was the first feature, which represents the ground state,

experiencing unfolding at the lowest trap collision voltage. Two additional unfolded states were observed as the trap collision voltage increased, with each CIU transition initiated under nearly identical acceleration voltages (around 30 V).

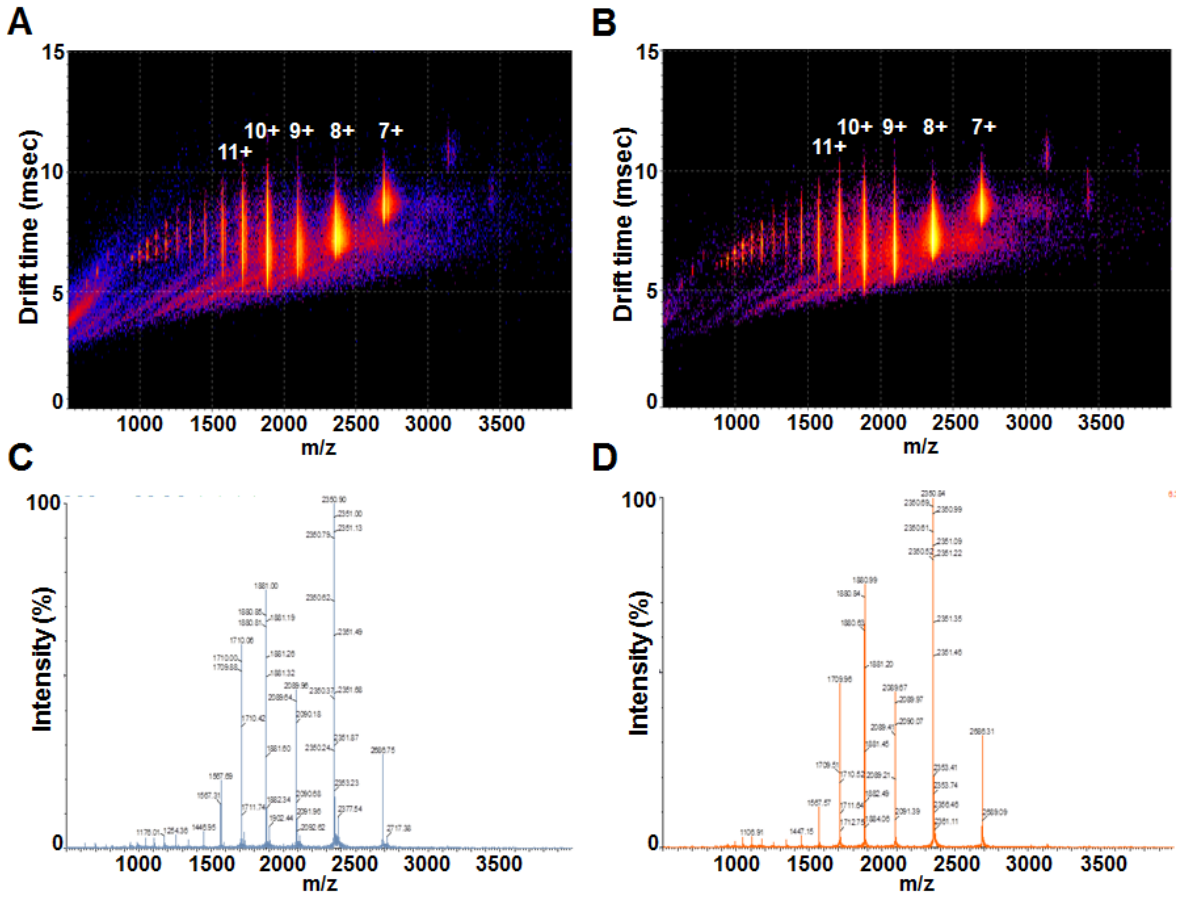

Figure 2-3 *Representative 2D IM-MS plots of (A) Neupogen® and (B) biosimilar and ESI MS spectra of (C) Neupogen® and (D) biosimilar*

1D ^{1}H-NMR spectra revealed high structural similarity between the two products. Notably, the amide backbone region did not show any differences between 6 and 9 ppm. However, each signal appeared to be highly overlapped. (Figure 2-5). To overcome the overlapping, 2D-^{1}H-^{15}N HSQC was carried out at natural abundance levels of ^{15}N to obtain H-N correlations. The peaks shown in the spectra (Figure 2-6) were mainly from the

backbone amide groups. Trp side-chain Nε-Hε groups at 129.5/9.65 ppm and 128.5/9.75 ppm and Asn/Gln side-chain Nδ-Hδ groups between 110-115 ppm/6.3-7.5 ppm were also visible. Amide peaks in the spectra were well-dispersed from 6.3 ppm-9.75 ppm indicating a well-folded protein. There were 108 total NMR signal observations. The R squared value was 8.80392E-06, which indicates there was no significant linear relationship between NMR parameters and drug category, meaning there were no detectable differences between these two drugs in terms of their NMR characteristics.

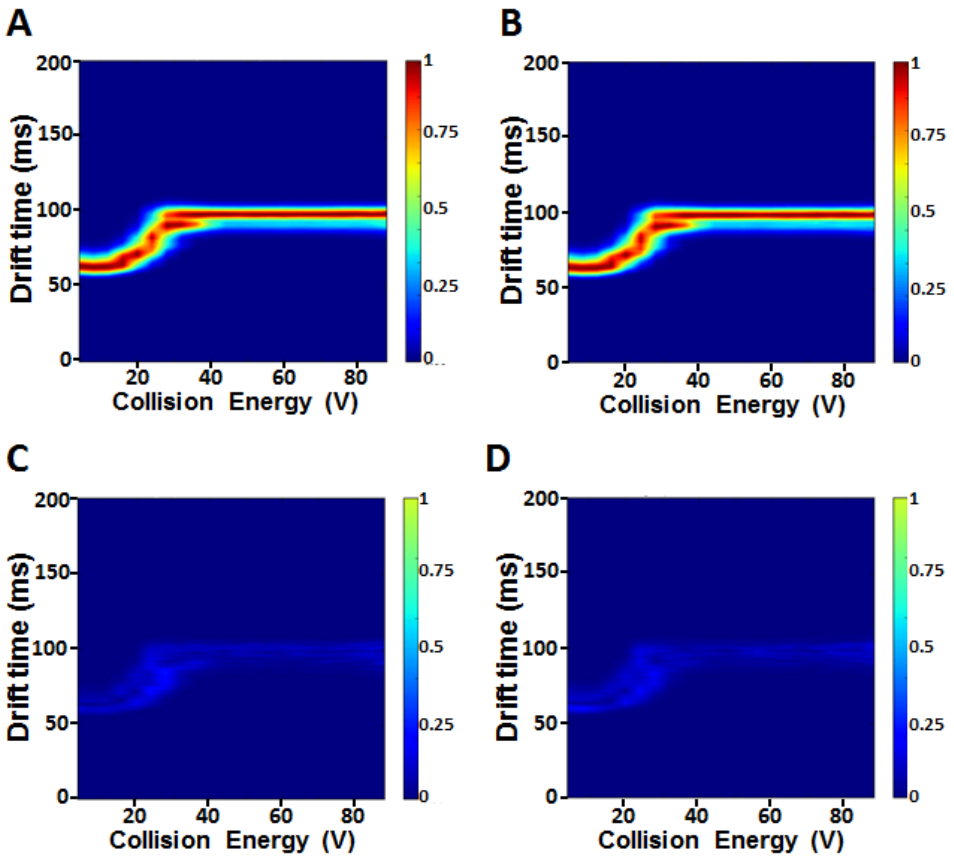

Figure 2-4 *Collision-induced unfolding (CIU) fingerprint of (A) Neupogen® and (B) biosimilar. Standard deviation plot for (C) Neupogen® and (D) biosimilar.*

2.4.3 Molecular weight distribution

Intact mass analysis was performed to determine filgrastim's molecular weight (MW). The resulting deconvoluted spectra showed highly similar MW distribution between Neupogen® and its proposed biosimilar (Figure 2-7). Multiple peaks were observed in both cases with highly similar abundances, which represented the mass of the main peak (18799.0 Da), a +21 Da sodium adduct (18820.0 Da), a +39 Da potassium adduct (18838.0 Da), and a -133 Da N-methionine clipped peak (18666.0 Da).

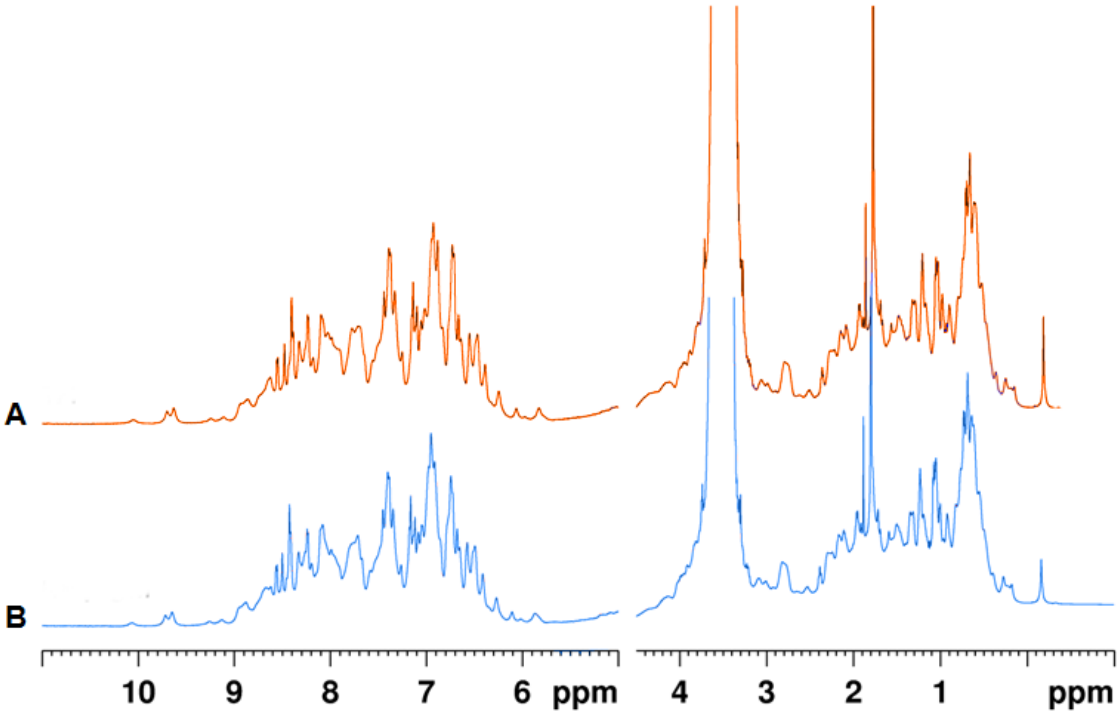

Figure 2-5 *Comparison of 1D 1H NMR specta for (A) biosimilar and (B) Neupogen®. Both NMR spectra revealed high structural similarity.*

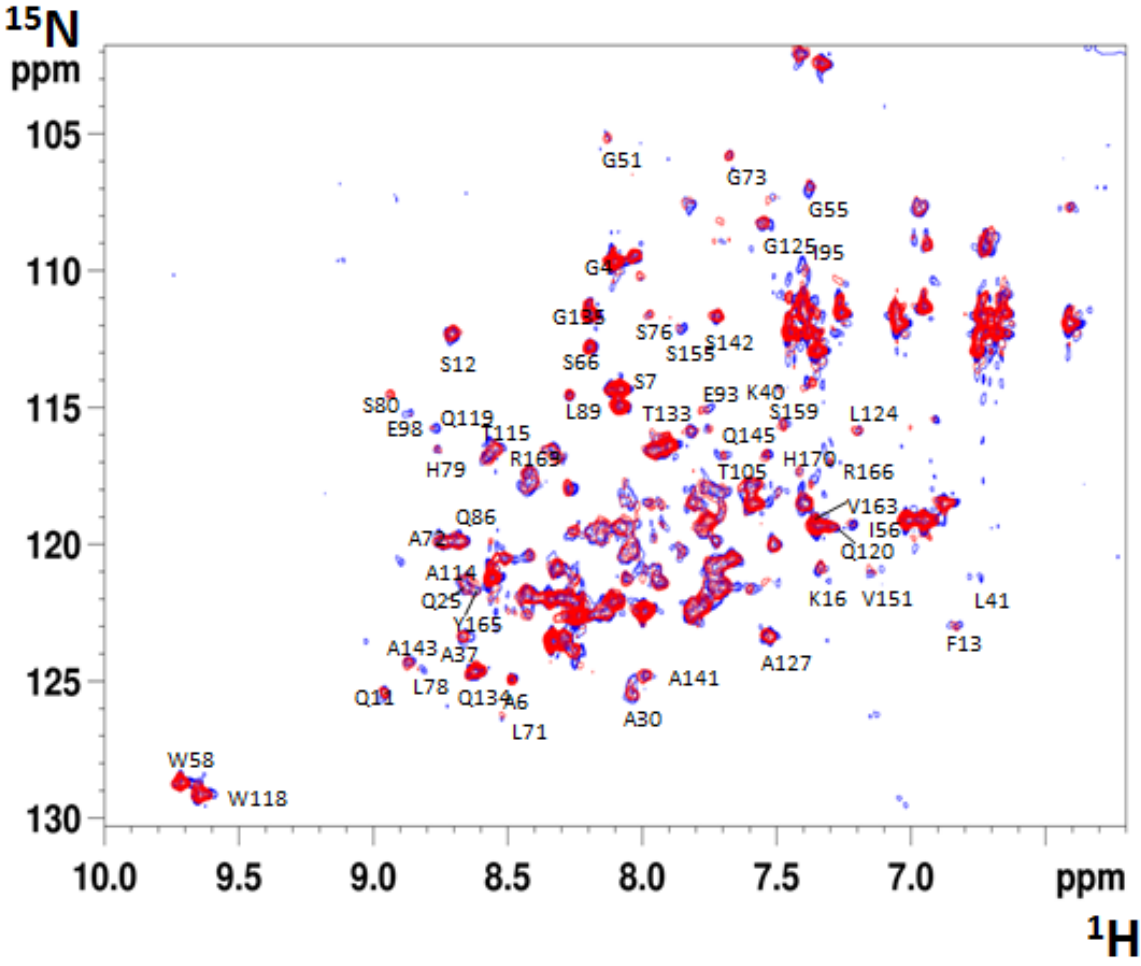

Figure 2-6 *A plot of the overlay of Neupogen® (red) and biosimilar (blue) 600 MHz 2D 1H-15N NMR spectra at 15°C (1H range: 6.2 to 10 ppm, 15N range 101.7 to 130.3 ppm). Sample similarity can be directly assessed by visual comparison of spectral overlays. Resonance are overlaid under the red peaks.*

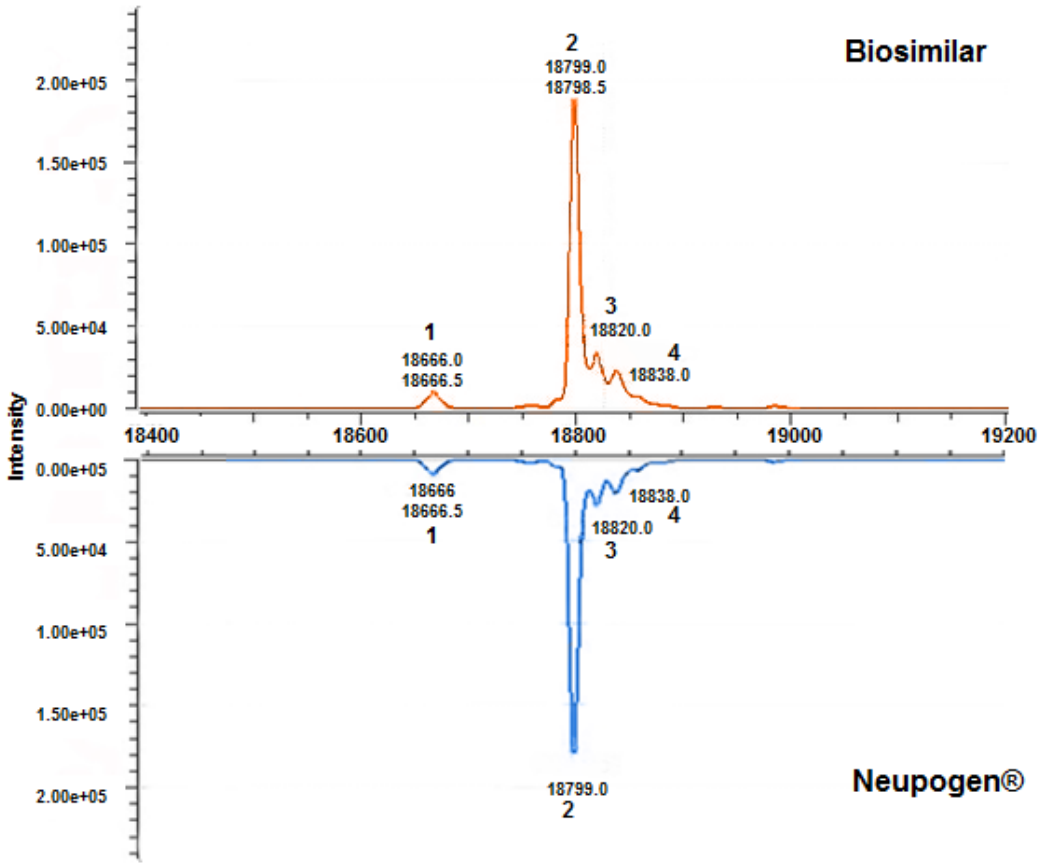

Figure 2-7 *A representative mirror plot of deconvoluted intact mass between innovator (VL158) and biosimilar filgrastim (VL81). (1) N-methionine clipped filgrastim [M-met], (2) filgrastim [M], (3) filgrastim+Na adduct [M+Na]- and (4) filgrastim+K adduct [M+K]+.*

2.4.4 Variants analysis

Size exclusion and reversed phase liquid chromatography (SEC-LC and RP-LC) are used to detect product-related variants such as high molecular weight (HMW), deamidated and oxidized species. Because HMW species (aggregates) can lead to immunogenicity, characterization of soluble aggregate content is required for the development of biologics and biosimilars. In our study, both drugs showed very low levels of high molecular species for all lots, with comparable levels shown. In addition to LC-MS/MS analysis on deamidation and oxidation levels, we also performed RP-LC analysis. Oxidized variants elute out earlier

than the main filgrastim peak while deamidated variants elute out later. RP-LC data showed both low and comparable levels of oxidation (Neupogen®: 0.79 ± 0.18 %, its proposed biosimilar: 0.74 ± 0.05 %). In terms of deamidation, both showed highly similar levels at 1.08 relative retention times (Neupogen®: 0.56 ± 0.24 %, its proposed biosimilar: 0.57 ± 0.05 %), while two lots of biosimilar showed very low levels at relative retention time 1.09 (0.2 %).

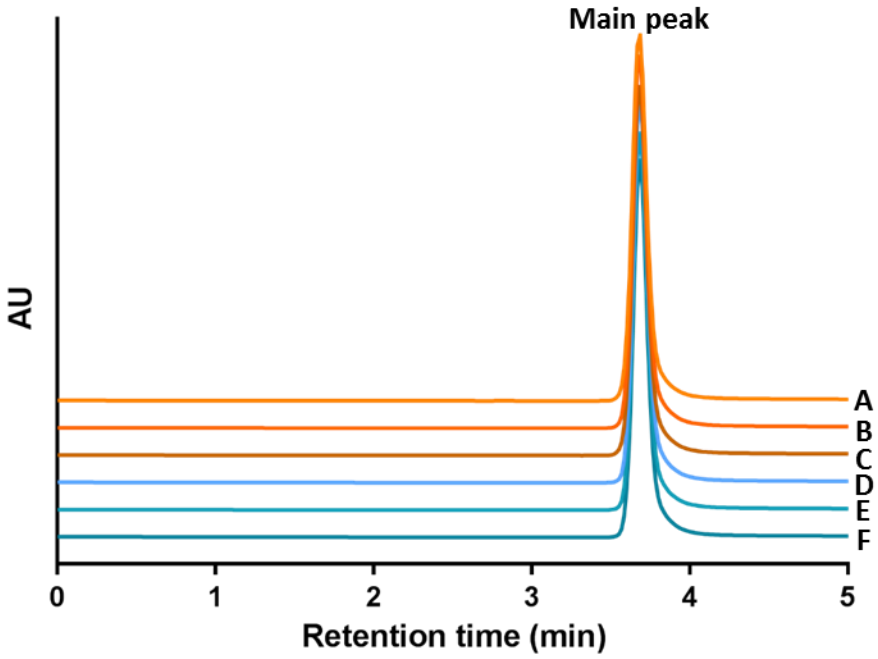

Figure 2-8 *Overlays of SEC-UPLC chromatograms of (A-C) the biosimilar and (D-E) Neupogen®. Both showed very low high molecular weight species and fragmented species.*

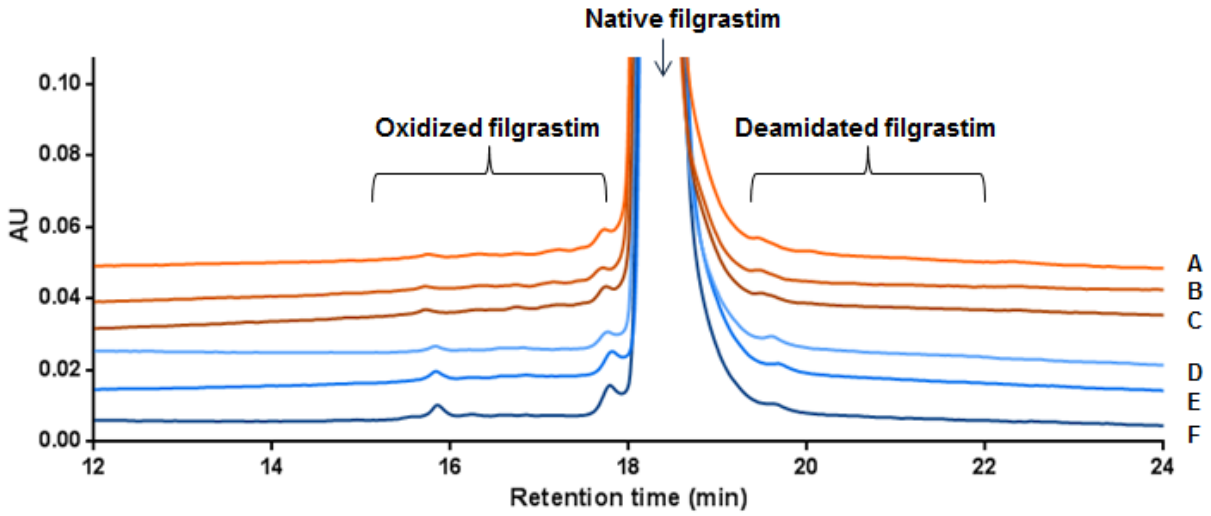

Figure 2-9 *Overlays of reversed-phase UPLC chromatograms of the innovator and its biosimilar. Three biosimilar syringe lots (A-C) were used to show oxidized and deamidated variants as compared to Neupogen syringe lots: (D-F)*

2.5 **Discussion**

Biosimilar development requires extensive physicochemical characterization as a foundation to generate a highly similar biosimilar product. To support a fingerprint-like analysis, orthogonal techniques are used to elucidate the complex structure of protein drugs. We performed a comparative analysis of Neupogen® and its potential biosimilar using LC-MS/MS peptide mapping based multi-attribute method (MAM). The primary amino sequence between Neupogen® and the proposed biosimilar appeared to be the identical as shown by MS/MS peptide mapping. Glu-C was used to digest filgrastim, cleaving Asp or Glu.

Filgrastim contains 4 Met residues, which are prone to oxidize into sulfoxide derivatives. Met oxidation is one example from a broad list of PTMs that can affect a protein or peptide's biological activity. [192] Outside of methionine 1 (non-functional), it has been known that oxidation of the other three methionine residues (122, 127 and 138), which are located in close proximity and all facing the protein's interior, are closely related to a

decrease of potency. [336,337] Thus, comparison of oxidation levels can be useful for identifying the source of discrepancies in potency. In this analysis, oxidation levels were comparable between Neupogen® and its proposed biosimilar filgrastim. Methionine 1 showed the highest level of oxidation, which was expected since the N-terminal Met is the most easily accessible of the four residues. [338] To support this data, a further study on potency would be helpful. Interestingly, Neupogen® showed significantly higher levels of deamidation of glutamine residues 12 and 174. Although deamidation was not related to its biological activity, the lower deamidation level is desirable since it is one of the degraded products of filgrastim.

Both proteins had comparable high order structures and MW profiles based on IM-MS, NMR and intact MS analyses. CIU-IM-MS analysis can be a useful tool to evaluate biosimilarity since CIUs have been applied to detect subtle differences such as glycosylations and disulfide bonds in innovator IgG drug products and their biosimilars. [54,108,339] This is the first time CIU analysis has be used to compare filgrastim biosimilarity based on the rationale that proteins of high structural similarity will show almost identical unfolding patterns. During the CIU process, both the innovator and biosimilar showed the same number of structural features upon the addition of collision energy. The CIU patterns in the gas phase between Neupogen® and the biosimilar appeared to be comparable regarding feature shapes, drift time and transition values of collision voltage. 1D-1H NMR analysis provides a fast and simple structural analysis, but showed a highly overlapped signal due to the protein’s complex structure and non-selectivity towards excipients. This limitation can be overcome by 2D NMR analysis. [340] Recently, 2D-NMR analysis for biotherapeutics has been used to provide a comprehensive readout of the drug

conformation along the polypeptide chain at an atomic level while providing a higher order structural comparison between innovator and biosimilar. [341,342] Intact analysis is used to assess characteristics of protein purity and heterogeneity. Based on this, we were able to get accurate estimates of filgrastim's MW. N-terminal Met truncated species were detected in both cases, but their presence was not expected to decrease the activity of filgrastim since G-CSF also lacks an N-terminal Met. Regarding impurity analyses using LC separation, both showed similar oxidation and deamidation levels, however LC-MS/MS data showed significantly lower deamidation levels in the biosimilar. This discrepancy is due to the different resolution between analysis methods. LC-MS/MS provides site specific quantification by showing percent modified of individual amino acid modification with high sensitivity, while LC-C18 quantifies relative amount of the entire molecule depending on affinity to the column. [344] Also, SEC separation confirmed very low levels of high molecular weight species below 0.1 % in both.

Taken together, we have applied MAM analysis to confirm the identical primary structure, similar oxidation and significantly different deamidation level between neupogen® and its biosimilar. Although we have only acquired data on amino acid modifications such as deamidation and oxidation using MAM, MAM can be used to provide a much wider variety of data such as glycosylation, glycation, clips, isomerization and host cell protein with biotherapeutics in single assay. Such MAM assay will provide comprehensive and timely support for analytical characterization. Also, we have demonstrated comparable higher order structure and molecular weight distribution with different MS techniques and 2D-NMR. Interestingly, we have confirmed different resolution

depending on analytic methods on the same attribute – LC-MS/MS and LC-C18 analysis that necessitate to perform analyses on the same attribute with orthogonal methods.

Chapter 3: Multifaceted Assessment of Rituximab Biosimilarity: The Impact of Glycan Microheterogeneity on Fc Function

3.1 Abstract

Biosimilars are poised to reduce prices and increase patient access to expensive, but highly effective biologic products. However, questions still remain about the degree of similarity and scarcity of information on biosimilar products from outside of the US/EU in the public domain. Thus, as an independent entity, we performed a comparative analysis between the innovator, Rituxan® (manufactured by Genentech/Roche), and a Russian rituximab biosimilar, Acellbia® (manufactured by Biocad). We evaluated biosimilarity of these two products by a variety of state-of-the-art analytical mass spectrometry techniques, including bottom-up protein digestion followed by LC-MS/MS, HX-MS, IM-MS, and intact MS. Both were found to be generally similar regarding primary and higher order structure, though differences were identified in terms of glycoform distribution levels of C-terminal Lys, N-terminal pyroGlu, charge variants and soluble aggregates. Notably, we confirmed that the biosimilar had a higher level of afucosylated glycans, resulting in a stronger FcγIIIa binding affinity and increased ADCC activity. Taken together, our work provides a comprehensive characterization and comparison of Rituxan® and Acellbia® to support biosimilarity.

3.2 **Introduction**

A biosimilar is a follow-on biologic drug that has highly similar physicochemical properties to the innovator product with no clinically meaningful differences in terms of safety and efficacy. [305] Recent patent expirations for lucrative biopharmaceutical products has led to the regulatory approvals for a number of biosimilars. So far, 45 biosimilars have been approved by the European Medicines Agency (EMA) and 17 biosimilars have been approved by the Food and Drug Administration (FDA). Among these approved biosimilars, twelve are monoclonal antibody (mAb) based drugs. [324,325] In contrast to generic small molecule products, biosimilars are not identical copies of the innovator products. Biosimilar mAbs are especially challenging to develop due to their structural complexity, including several functional domains, post translational modifications (PTMs), and possible immunogenicity. [326,327] The most frequently observed structural differences in biosimilar mAbs are in glycosylation profile, charge variants, incorrect disulfide bridging, and C-terminal or N-terminal amino acid variations. [53–55,66,68,226,328,329] In most cases, multiple orthogonal analytical methods are utilized to complementarily investigate each quality attribute as there is no single, perfect method to reveal biosimilarity as a whole. Biosimilar development for FDA approval requires the consideration of a totality-of-evidence and a step-wise approach to demonstrate biosimilarity by filling the gaps between residual uncertainty after analytical characterization for prediction of clinical similarity. [64,305]

Rituxan® or MabThera® is the rituximab innovator product developed by Genentech/Roche, and was approved by the FDA in 1997. [330] Rituximab is a chimeric human/murine mAb against CD20 on the surface of malignant B cells. [331–333] It is

administered to treat non-Hodgkin's lymphoma, chronic lymphocytic leukemia and refractory autoimmune disorders. [334–337] One of the main mechanisms of action of rituximab is antibody dependent cellular cytotoxicity (ADCC), which results in tumor cell lysis. [331–333] Once bound CD20 on the malignant B cell, rituximab's fragment crystallizable (Fc) region binds to the FcγIIIa receptor on effector cells, such as NK cells and macrophages, which leads to the degranulation of lytic enzymes, resulting in tumor cell death. [338,339] It is known that afucosylated glycoforms show stronger binding affinity to the FcγIIIa receptor, resulting in rituximab's higher ADCC activity. [340–342] Therefore, comprehensive glycoform profiling and functional bioassays are important to verify mAb biosimilarity.

Since rituximab's patent expirations in 2018 (US) and 2013 (Europe), [343] many companies have been developing potential rituximab biosimilars. These include Truxima® (Celltrion) approved in February 2017 [344] by EMA as the first mAb biosimilar for an oncology indication, followed by approval of Rixathon® from Sandoz in June 2017. [345] Following initial rejection by FDA of both rituximab biosimilar products, Truxima® was eventually approved in November 2018[325], whereas the application for Rixathon® was withdrawn. [346] Additionally, multiple rituximab biosimilars have been approved outside of the US and EU in India, Latin America and Russia. For example, there are currently five rituximab biosimilars available in India, including Maball® (Hetero), RituxiRel® (Reliance) and Reditux® (DRL). [347] Similarly, there are currently two approved rituximab biosimilars in Russia, AcellBia® (Biocad) and Reditux® (DRL). [348] These differences in rituximab biosimilars availability reflect vastly different requirements for biosimilar approvals from country to country.

Approval of biosimilar products by the FDA/EMA is often accompanied by a publication from a biosimilar developer summarizing product analytical comparability data used in the regulatory filling. [54,55,66,275] In stark contrast, only limited amounts of information is available about the biosimilars approved in countries outside of the EU/US. In addition, few publications on biosimilar characterization are authored by the analytical laboratories independent from the biosimilar developer. Here, we compare innovator rituximab (Rituxan®) and a biosimilar rituximab (AcellBia®) that has been approved in Russia, Latin America, and Asia. We utilize orthogonal techniques to evaluate their primary sequence, higher order structure, PTMs, including glycosylation patterns, charge variants, oxidation, deamidation, FcγRIIIa binding affinity and ADCC activity. We aim to define a correlation between structural and functional differences between the innovator and biosimilar rituximab drug products, with an enhanced focus on glycosylation and ADCC.

3.3 **Materials and methods**

3.3.1 Materials

Rituximab biosimilar (Acellbia®) and rituximab innovator (Rituxan®) lots were purchased and stored at 4ºC until use. All materials used were before their expiry date.

3.3.2 Digestion

Antibody samples (50µg) were digested using AccuMAP™ Low pH protein digestion kits (Promega) according to the manufacturer's protocol. In short, samples were denatured with guanidine hydrochloride, reduced with tris(2-carboxyethyl)phosphine, and alkylated with iodoacetamide. The samples were predigested with AccuMAP™ Low pH resistant rLys-C for 1 hour then digested with AccuMAP™ Modified Trypsin and Accumap™ Low pH resistant rLys-c at 37°C for 3 hours. All steps were performed at mildly acidic conditions to

suppress artificial deamidation. Finally, the samples were acidified with trifluoroacetic acid and purified with a SepPak C18 Plus light cartridge.

3.3.3 Peptide mapping

Digested samples (500ng) were analyzed by a Dionex RSLC-nano UHPLC system interfaced with a Q Exactive HF mass spectrometer (ThermoFisher). The samples were separated by an EASY-spray system PepMap RSLC C18 column (500 mm, 75 µm, particle size: 2 µm, pore size: 100Å) (ThermoFisher) using 1% acetic acid / acetonitrile gradients at 300 ml/min and introduced into a Q Exactive HF mass spectrometer. Data were collected in the range of m/z 600-2000 using Orbitrap for detection. LC-MS/MS data were searched by Byonic™ search software and validated by Byologic® (Protein Metrics Inc.). Peptide ions were identified using the search software by comparing computed masses to precursor peptide masses (MS1) and expected fragment ion masses (MS2), enabling the search of various protein modifications such as deamidation, oxidation (mono-, di-), N-terminal glutamate to pyroglutamate conversion and an N-glycan. N-glycan species were automatically assigned based on a predetermined library of 50 biantennary glycans.

3.3.4 Ion mobility mass spectrometry

Innovator and biosimilar were supplied as solution of identical formulations (Rituximab, sodium chloride, sodium citrate dihydrate, and polysorbate 80). All samples were diluted with pure water to a concentration of 1 mg/mL (~6.7 µM) and then samples were buffer exchanged into 200 mM ammonium acetate buffer using Micro Bio-Spin 30 columns (Bio-Rad). Antibody aliquots (~7 µL) were analyzed by IM-MS on a quadruple-ion mobility-time-of-flight mass spectrometer (Q-IM-ToF MS) (Synapt G2 HDMA, Waters). Antibody ions were generated using a nESI source in positive ion mode. The electrospray

capillary was operated at voltages of 1.5-1.7 kV with the sampling cone operated at 40 V. The trap traveling-wave ion guide was pressurized to 4.96×10^{-2} mbar of argon gas. The traveling-wave ion mobility separator was operated at a pressure of ~2.6 mbar. Ion mobility separation was achieved with a DC generated wave operated at 40 V wave height traveling at 600 m/s. The ToF-MS was operated over the m/z range of 1000−10,000 at a pressure of 1.5×10^{-6} mbar. Mass spectra were calibrated externally using a solution of cesium iodide (100 mg/mL) and processed with Masslynx V4.1 software (Waters). Exact molecular masses of intact antibody samples were calculated by assigning the charge states based on the set that gives the lowest standard deviation for a given average mass assignment.

3.3.5 Collision induced unfolding

Antibody ions were subjected to collision in the travelling-wave ion trap prior to IM separation to perform antibody CIU. Tandem-MS (quadrupole selection) was used to select the 23+ charge state of the intact antibody ion. The collision voltage was ramped from 5 to 200 V in 5 V increments to construct the CIU fingerprints data. Drift time data was extracted at each collision voltage in DriftScope (Waters) using TWIMExtract. [349] These extracted drift time data were analyzed using a home-built software package, CIUSuite 2. [350]

CIU “fingerprint” data was plotted as a 2D contour plot such that the intensity was normalized between data sets to a maximum value of 1 at each collision voltage and smoothed once using a Savitzky-Golay filter. Features in these fingerprints are detected by grouping the observed drift times for each collision voltage. The settings for feature detection were a minimum of 5 steps, an allowed drift time width of 0.75 ms, and a maximum CV gap length of 0 Following feature analysis the CIU50 values were calculated by fitting the transition regions between features with a logistic function. We define the

CIU50 value as the voltage in which 50% of a relatively compact state transition to a more extended state.

3.3.6 Hydorogen exchange mass spectrometry

Stock solutions (10 mg/mL) of innovator and biosimilar rituximab were dialyzed with 10K MWCO Slide-A-Lyzer MINI devices for 20 hours (buffer exchanged at 6 hours) at 4 °C in protein buffer (25 mM citrate buffer with 150 mM sodium chloride, pH 6.5). After dialysis, protein concentrations were measured by a Bradford assay and adjusted to 2.4 mg/mL for HX experiments. HX experiments were performed on a LEAP Technologies H/X PAL robot. Deuterated samples were prepared by diluting 3 µL of mAb (2.4 mg/mL) with 57 µL of protein buffer in D_2O (25 mM sodium citrate, 150 mM NaCl, pD 6.5). Samples were labeled, in triplicate, at 25 °C for 20, 100, 500, 2500, 12500, and 62500 seconds. Labeling was quenched at 0 °C by a 1:1 dilution with quench buffer (200 mM phosphate, 3 M guanidine hydrochloride, 0.5 M Tris(2-carboxyethyl)phosphine hydrochloride, pH 2.5). Following quench, 4.8 µg of sample was injected into the sample loop in a temperature-controlled chromatography cabinet at 0 °C connected to an Agilent 1260 infinity series LC. Injected sample was passed over an immobilized pepsin column (2.1 mm x 50 mm) prepared in house [351] at 200 µL/min for 180 seconds with 0.1% formic acid in water. After digestion peptic peptides were captured on a C8 trap (InfinityLab Poroshell 120 EC-C8, 2.1 x 5 mm, 2.7 µm) and desalted for 60 seconds at 200 µL/min with 0.1% formic acid in water. Peptic peptides were then separated on a C-18 column (ZORBAX RRHD 300Å Stable Bond C-18, 2.1 x 50 mm, 1.8 µm) with a 12 min linear gradient of 0.1% formic acid in acetonitrile increasing from 15% to 35%. Peptides masses were measured on an Agilent 6530 Quadrupole Time-of-Flight mass spectrometer running in ESI-positive mode. Raw HX-MS

data was processed in Sierra Analytics HDExaminer and exported to Microsoft Excel for post-processing. Relative deuterium uptake is expressed as the peptide mass increase divided by the number of peptide backbone amides. When the second residue of the peptide is not proline, the number of peptide backbone amides was decreased by one to account for rapid back-exchange by the amide adjacent to the N-terminal residue. [352] The criterion for significance in individual HX differences was defined by pooled standard deviation obtained from the entire collection of 2676 HX differences, 0.032 Da. The pooled standard deviation was propagated as random error through an HX difference and multiplied by Student's *t* for a two-tailed difference at 99% confidence for four degrees of freedom, 4.604. This yielded a threshold of significance for individual HX differences of 0.21 Da.

3.3.7 Intact mass spectrometry

Intact mass antibody characterization was performed in 2 different ways; without enzyme treatment and deglycosylated. First, each antibody sample (50 µg) was diluted with water and exchanged 4 times into a 20% acetonitrile solution containing 1% acetic acid using a 10 KDa Nanosep filter (Pall). Protein was recovered from the filter in water and concentration determined by a Qubit fluorometer (Invitrogen). For intact mass analysis: sample concentration was reduced to 0.5 mg/mL with HPLC grade water. For deglycosylated intact mass: 20 µg of antibody was incubated with 3 µL PNGase F (Promega) in 50 mM ammonium bicarbonate at 37°C for 3 hr. Samples were analyzed by LC-MS using a C4 column (X-Bridge BEH C4 2.1 x 50 mm) (Waters) interfaced to a Q Exactive mass spectrometer (ThermoFisher). 500 fmols or 5pmols was injected for intact or reduced samples, respectively. Data were acquired from 600-4000 *m/z* at a resolution

of 17,500 FWHM (at 400 *m/z*) with ten µscans per spectrum (intact mass), or 600-2500 *m/z* at a resolution of 17,500 FWHM (at 400 *m/z*) with three µscans per spectrum (reduced mass). Spectral deconvolution was performed with Intact Mass™ ver 3.3 (Protein Metrics Inc.).

3.3.8 Cation exchange chromatography

Antibody samples (10 mg/ mL) were filtered with a 0.45 µm filter. 5 µL of samples was injected into Waters Alliance HPLC onto a MAbPac SCX-10 column (4 x 150 mm, 5 µm) (Thermofisher). Mobile phase A was 20 mM MES buffer (pH 5.6) and mobile phase B was 20 mM MES buffer with 300 mM NaCl (pH 5.6), ran at flow rate of 1 mL/min at 30°C for 20 min using a linear 30-60% B gradient.The signal was detected at 280 nm. To confirm C-terminal Lys truncation, samples were incubated with carboxypeptidase B (Worthington Biochemical) for 2 hours at 37°C and then analyzed by the cation exchange chromatography method above.

3.3.9 Size exclusion chromatography

Antibody samples (10 mg/mL) were diluted 2-fold and filtered with a 0.45 µm filter. 5 µL samples were injected into Waters Alliance HPLC system and separated with a TSKgel SuperSW mAb HR column (7.8 mm x 30.0 cm, 4 µm, 25 nm) (Tosoh). 0.2 M phosphate buffer (pH 6.7) with 0.05% NaN_3 was chosen for the mobile phase, with a flow rate of 0.8 mL/min. The signal was detected at 280 nm.

3.3.10 Glycan profiling by fluorescent labelling and LC analysis

N-glycans were prepared from antibody samples (15 µg) using a GlycoWorks RapiFluor-MS N-Glycan kit (Waters) according to the manufacturer's protocol. Briefly, antibody samples were denatured and deglycosylated with PNGase F. Resulting N-glycans

were labeled with RapiFluor-MS and cleaned-up with a HILIC microelution plate. Labelled N-glycan samples were separated on a UPLC Glycan BEH amide column (2.1 X 150 mm, 130 Å, 1.7 µm) (Waters) at a flow rate of 0.4 mL/min at 60°C with mobile phase A (50 mM ammonium formate pH 4.4) and mobile phase B (acetonitrile) following manufacturer's instructions for gradient preparation.. The signal was detected with a fluorescence detector at an excitation wavelength of 265 nm and emission wavelength of 425 nm.

3.3.11 FcγRIIIa binding assessment by biolayer interferometry

The interaction of the Fc regions with FcγRIIIa for both innovator and biosimilar rituximab were measured by BLI with a BLITZ® instrument (Fortebio), equipped with protein G biosensor tips. We followed a previously reported BLI method. [53,353,354] Rituximab samples were dialyzed with PBS buffer (50 mM sodium phosphate, 150 mM sodium chloride, pH 7.4) and diluted to 0.4 µM with kinetic buffer (PBS buffer containing 1 mg/mL casein as a blocking agent). Following sample preparation, the protein G biosensor tips were loaded (120 sec) with innovator or biosimilar rituximab. A baseline (240 sec) was established followed by the association (180 sec) and dissociation (360 sec) of FcγRIIIa, as measured by dipping the tips into different concentrations of FcγRIIIa solution and PBS kinetic buffer, respectively. After each binding assay, the regeneration procedure was used for the biosensor tip, which consisted of two cycles of 30 seconds in 10 mM HCl and 60 seconds in PBS kinetic buffer. For the determination of the dissociation constant (K_D) of innovator and biosimilar rituximab, the concentration range of FcγRIIIa was varied by 2-fold serial dilutions from 0.4 to 3.2 µM. Data were produced in triplicate and globally fitted to a 1:1 binding model by BLITZ® pro software (Fortebio) to obtain ka, kd and K_D.

3.3.12 Antibody-dependent cell-mediated cytotoxicity (ADCC) reporter bioassay

ADCC Reporter Bioassay (Promega) was used per the manufacturer's instruction to assess ADCC activity. Briefly, the target WIL2-S cells, CD-20 positive human B lymphoblastoma cells, were seeded in each well of a 96-well assay plate. After seeding, either serially diluted innovator or serially diluted biosimilar rituximab was added to the assay plate. As effector cells, either V158 (high affinity FcγRIIIa) or F158 (low affinity FcγRIIIa) variant Jurkat T-lymphocyte cells engineered to stably express FcγRIIIa receptors were co-cultured with rituximab treated target cells at an effector cell to target cell ratio of 6:1 for 6 hours at 37 °C in a humidified 5% CO_2 incubator. Once bound to the antibody, engineered Jurkat T-lymphocyte cells activated gene transcription through the nuclear factor of activated T-cells (NFAT) pathway, inducing the expression of firefly luciferase. Lastly, luciferase activity was quantified using luciferase assay reagent by a SpectraMax M3 plate reader (Molecular Devices).

3.4 **Results**

3.4.1 Primary structure

According to FDA and EMA regulations, the primary sequence of the biosimilar should be identical to the innovator. [13,64] To confirm the identical sequence between the innovator and biosimilar, protein digestion and pre-digestion steps were performed with trypsin/Lys-C at mild acidic conditions. This procedure was completed at mildly acidic conditions to suppress any artificial non-enzymatic protein modifications commonly induced during peptide mapping sample preparation. Base peak chromatograms generated post digestion were shown in Figure 3-1. Both innovator and biosimilar had identical sequence with 100% coverage. The presence of N-terminal pyroGlu, oxidation and deamidation

products were observed for both the biosimilar and the innovator as discussed in detail later in the manuscript.

3.4.2 Higher order structure

Appropriate higher order structure (HOS) is crucial for proteins to ensure proper biological activity. [355] Thus, HOS should be thoroughly evaluated by orthogonal methods to reveal potential differences. To evaluate the HOS of innovator and biosimilar rituxmabs, we performed a mass spectrometry (MS) based analysis using ion mobility MS (IM-MS) and hydrogen exchange MS (HX-MS).

Collision induced unfolding (CIU) fingerprints acquired by IM-MS have recently emerged as a powerful method to differentiate higher order structural information for intact mAbs. [53,99,102,356] CIU fingerprints are generated by increasing the internal temperature of antibody protein ions in a stepwise fashion through collisions with a background gas, resulting in unfolding that is then followed by IM separation and MS analysis. CIU fingerprint plots track the amount of applied collision voltage used to generate the observed protein ion unfolding transitions. Previous CIU fingerprint analysis of mAbs have distinguished unique conformational features including: antibody subclass, glycosylation states, antigen binding potential, domain exchange, and biosimilarity. biosimilarity. [53,99,102,357]

The 23+ charge state for both the innovator and biosimilar was chosen based on its relative intensity (Figure 3-2A and D), and ability to provide CIU fingerprints containing a suitable number of transitions for high-confidence mAb analysis. Three prominent CIU features were detected for both the innovator and biosimilar, including an initial, compact state and 2 unfolded states (Figure 3-2B and E). Median drift times values for each feature

were determined to be near identical between the innovator and biosimilar suggesting similar collision cross sections (Figure 3-3A).

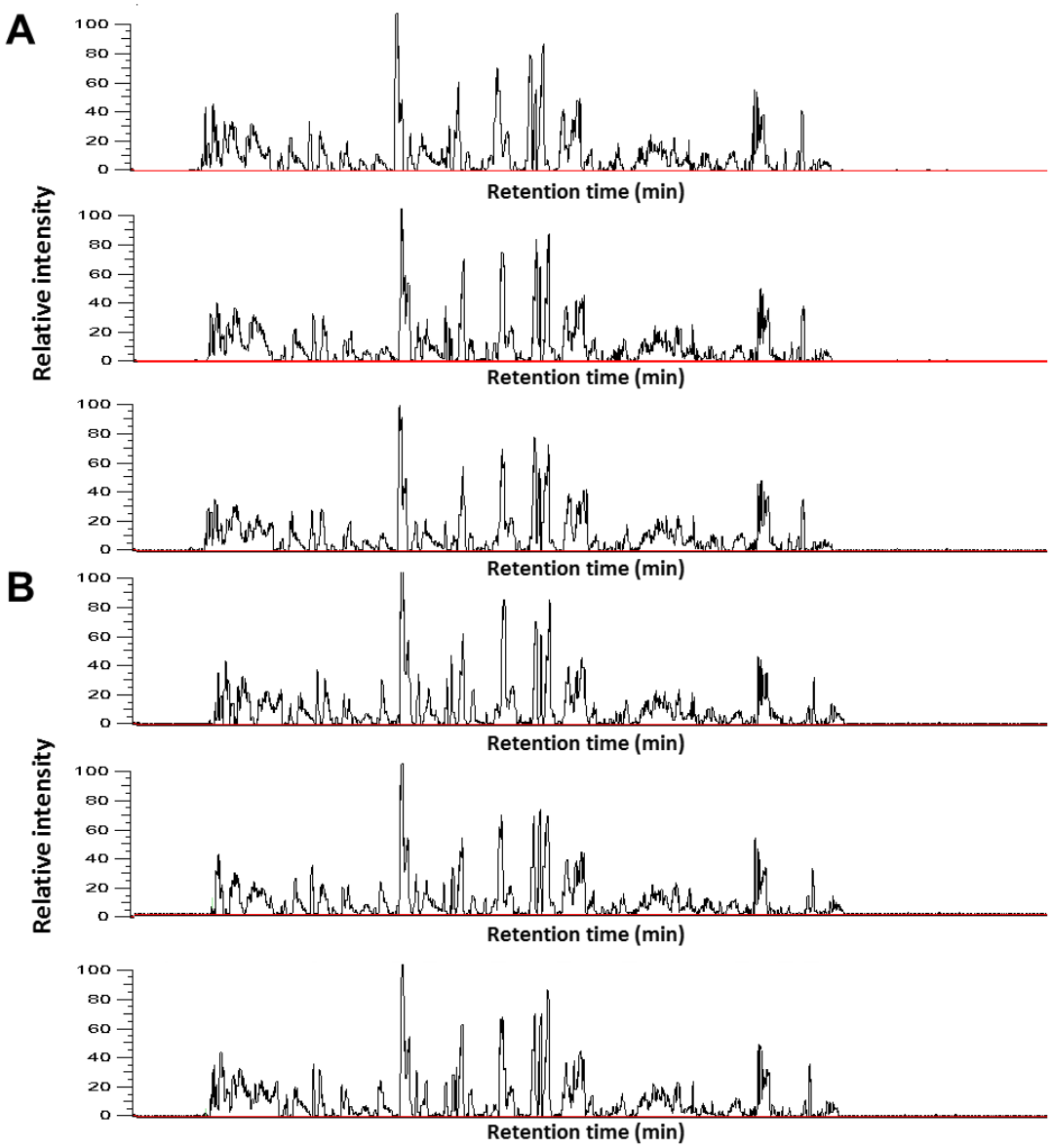

Figure 3-1 *Base peak chromatogram of LC-MS/MS analysis of (A) innovator and (B) biosimilar.*

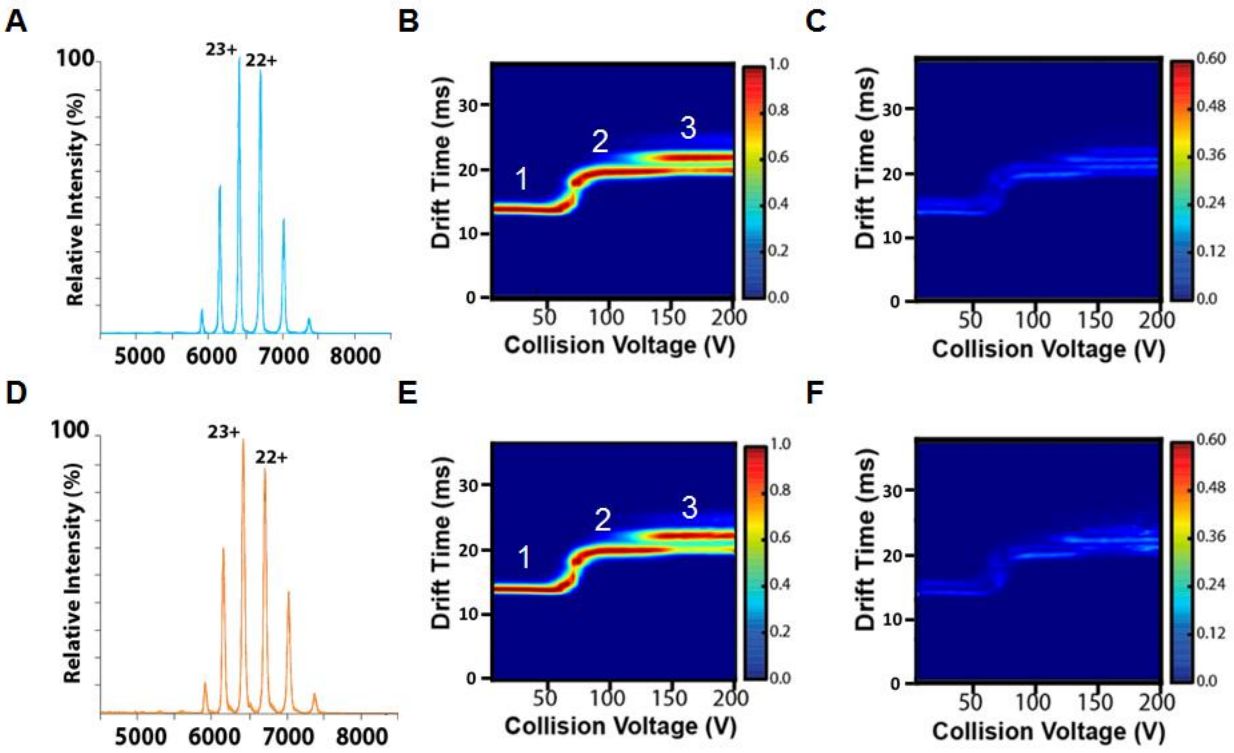

Figure 3-2 *Ion mobility mass spectrometry of (A) innovator and (D) biosimilar. Average CIU fingerprints of (B) innovator and (E) biosimilar rituximab. Standard deviation of rituximab (C) innovator and (F) biosimilar. (n = 3) 1: initial compact state, 2,3: unfolded states.*

The CIU fingerprints were further analyzed using sigmoidal fitting to determine CIU50 values, the collision voltages where the most intense feature decreases to below 50% of the relative intensity of its neighboring feature, for each mAb. While the initial transitions occurred at nearly identical collision voltages ($CIU50_1$) of 69.8 V, there were noticeable differences between the CIU50 values recorded for the second transitions ($CIU50_2$), specifically 148.7 V and 143.7 V, for the innovator and biosimilar respectively (Figure 3-3 and 3-4). We also detected subtle differences in the standard deviations between CIU replicates recorded for innovator and biosimilar 23^+ ions at collision voltages greater than 150 V (Figure 3-2C and F).

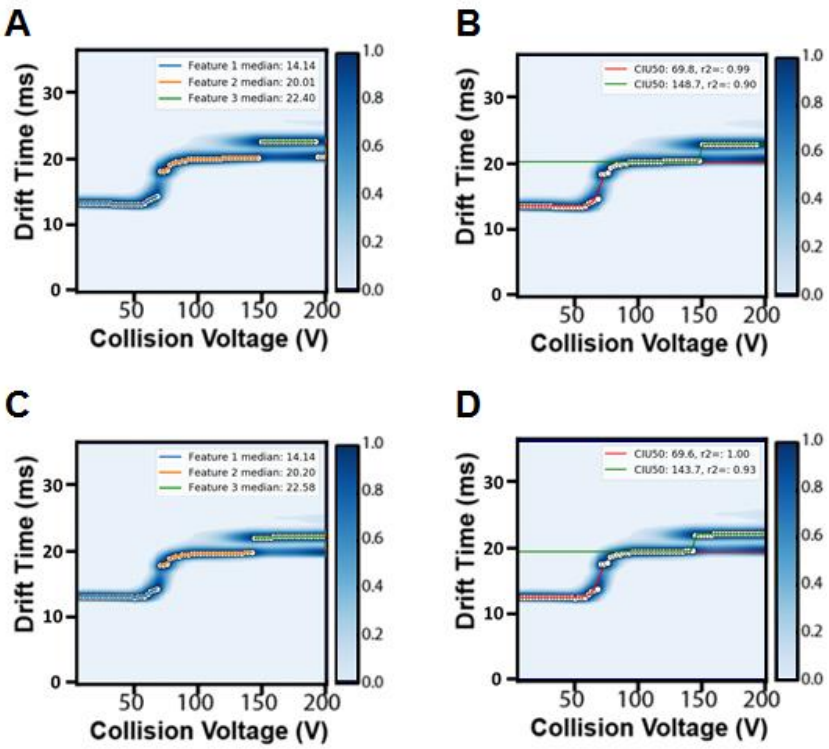

Figure 3-3 *Median drift times for (A) innovator and (C) biosimilar rituximab. CIU50 values between dominant features (between initial compact state and the next unfolded state, between two unfolded states) for (B) innovator and (D) biosimilar.*

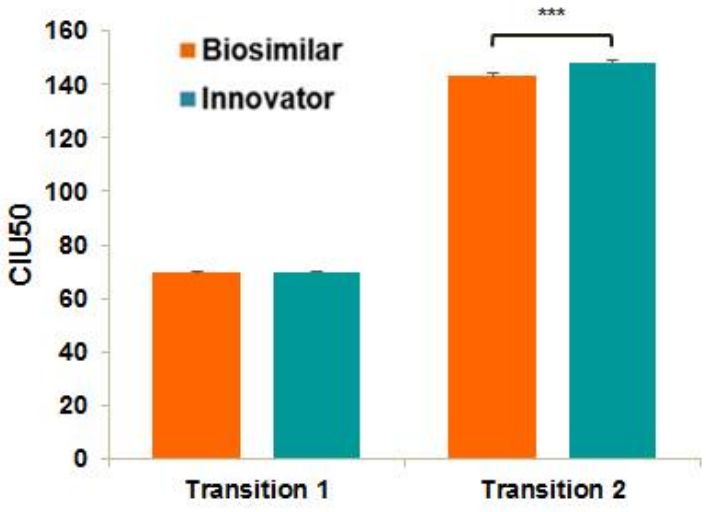

Figure 3-4 *CIU50 values of innovator and biosimilar at transition 1 and 2. (***p<0.001, student t test)*

The conformational dynamics of the innovator and biosimilar rituximab were further compared by HX-MS. The rate of protein backbone amide hydrogen exchange with solvent deuterium is dependent on backbone structure and dynamics. [358] Flexible regions of the protein exchange rapidly while rigid regions exchange slowly. After exchange, peptic digestion followed by MS analysis provides a peptide resolution of hydrogen exchange kinetics, providing information on localized protein backbone conformational dynamics that can serve as a probe for higher order structure comparability. [359]

HX profiles, illustrated as a butterfly plot (Figure 3-5), are highly symmetrical when comparing average HX measurements across six labeling times for innovator and biosimilar rituximab. Relative deuterium uptake is plotted on the vertical axis for each label time of each peptic peptide monitored on the horizontal axis. HX was monitored for 223, MS/MS confirmed, peptic peptides giving 98.8% total sequence coverage. Peptides containing G0F, G1F, and G2F at heavy chain (HC) Asn 301 as well as pyroGlu at HC and light chain (LC) Gln 1 were monitored for both innovator and biosimilar rituximab. Deuterium uptake at each label time for each peptide was compared between the innovator and biosimilar rituximab. All deuterium uptake differences were less than 0.19 Da and none exceeded the significance limit of 0.21 Da (Figure 3-6). Thus, there were no significant differences when comparing HX of innovator to biosimilar rituximab.

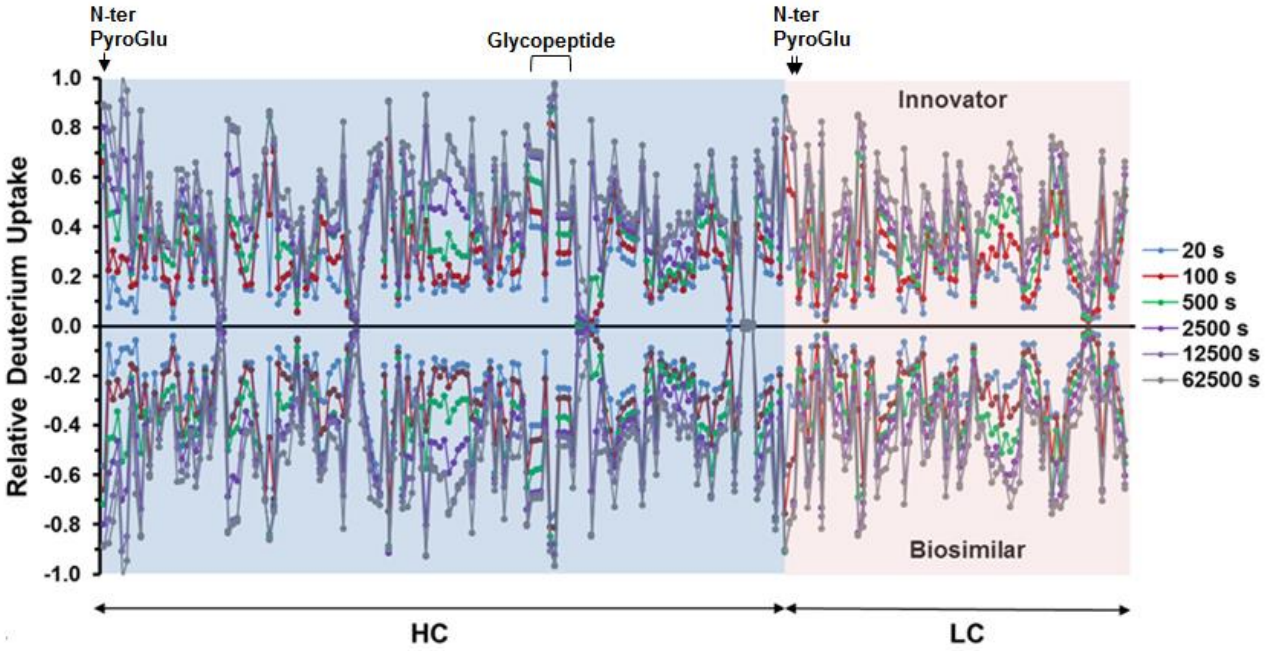

Figure 3-5 *HDX-MS butterfly plot comparing innovator (top) and biosimilar (bottom) rituximab average relative deuterium uptake for each peptic peptide monitored from labeling times of 20 (blue), 100 (red), 500 (green), 2500 (purple), 12500 (light purple), and 62500 (grey) seconds. (N = 3) HC: Heavy chain, LC: Light chain*

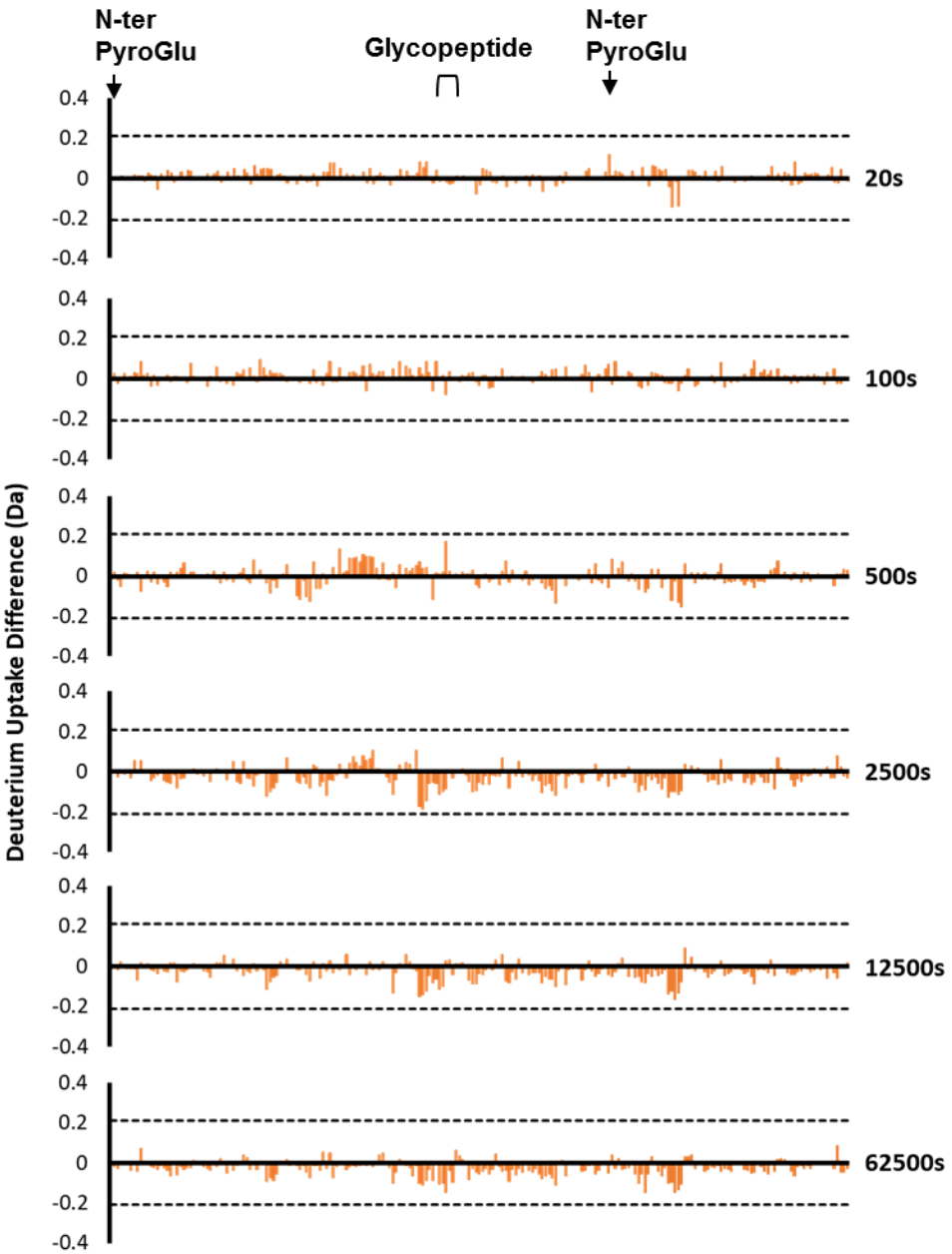

$$\Delta D = \sum_{i=1}^{n_t} \#D_i^{RB} - \#D_i^{RO}$$

Figure 3-6 *Deuterium uptake difference (Biosimilar – Innovator) at each label time for each peptide. Significance line at 0.21 Da representative of 99% confidence level from pooling 2,676 experimental standard deviations from all peptides and label times measured. #DiRB was subtracted from #DiRO, anything in the positive direction (faster exchange) would suggest RB is more flexible relative to RO and anything in the negative direction (slower exchange) would suggest RB is less flexible relative to RO.*

3.4.3 Intact antibody mass analysis

Intact mass spectrometry provides a rapid assessment of the potential differences between innovator and biosimilar mAbs, including the presence of low molecular weight impurities, covalent aggregates, N-terminal/C-terminal modifications and relative glycoform distributions. We performed intact mass analyses of the two products in both their fully glycosylated and deglycosylated (Figure 3-7). Expected major intact mass modifications are altered glycosylation patterns, N-terminal conversion of Gln to pyroGlu (-17 Da mass difference) and absence of C-terminal Lys (-128 Da mass difference). [163] Peak assignments were obtained by mass calculations of amino acid sequences and various glycan compositions.

First, the intact masses of innovator and biosimilar rituximab were acquired in their fully glycosylated state. The three most abundant charge states were z = 52, 53 and 54 in both cases. The glycoform distributions analyzed from the deconvoluted spectra for the biosimilar and innovator are shown as a mirror plot in Figure 3-7A. In both cases, the most abundant glycoforms were G0F/G0F, G0F/G1F and G0F/G2F or $(G1F)_2$. A Man5/Man5 peak was detected with a relative intensity of 5%, but only for innovator rituximab. The most significant difference detected was the mass peaks containing one C-terminal Lys found in the biosimilar, relative to innovator. These peaks are marked with red asterisks in Figure 3-7A and exhibit mass differences of approximately +128 Da from the more prominent (-)Lys peaks.

To further characterize structural modifications of biosimilar and innovator rituximab, mAbs were deglycosylated by PNGase F. When deglycosylated, two main peaks were detected from the deconvoluted intact mass analysis (Figure 3-7B) that are likely attributed

to an N-terminal 4 pyroGlu and/or glycation (+161 Da). The presence of a peak containing one C-terminal Lys was observed for the biosimilar, but not for the innovator.

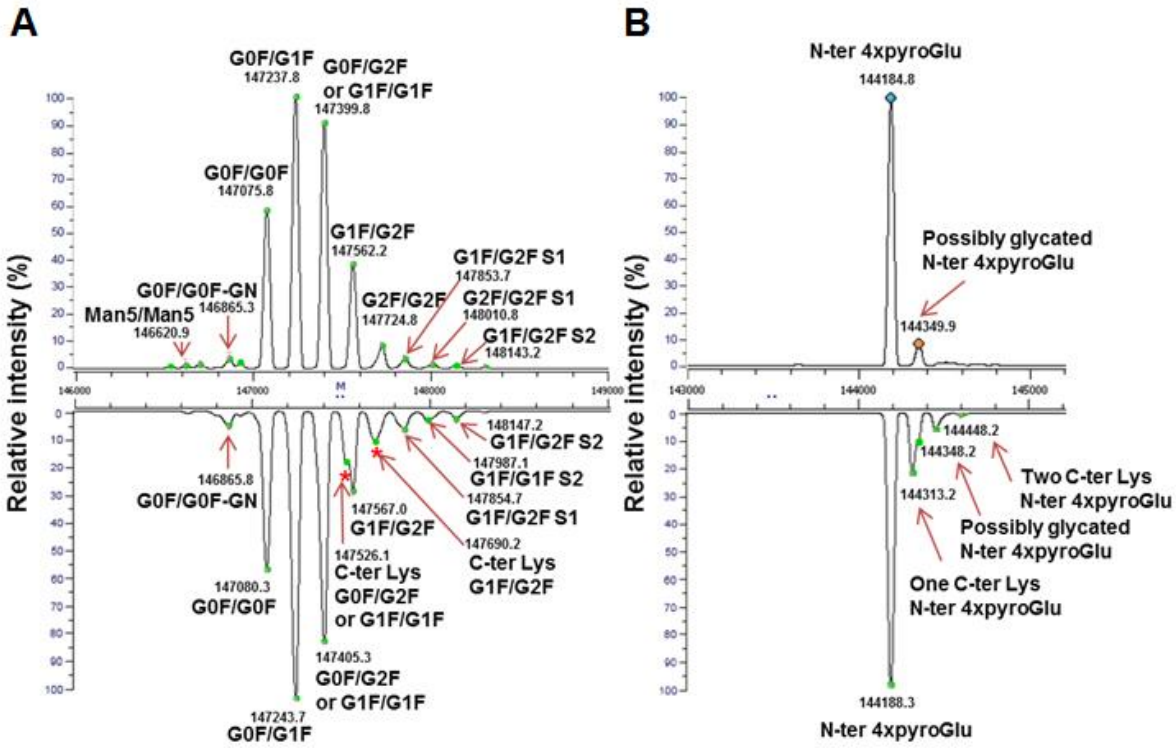

Figure 3-7 *(A) Mirror plot of deconvoluted intact mass spectrum of innovator and biosimilar rituximab. (B) Mirror plot of deconvoluted intact mass spectrum of deglycosylated innovator and biosimilar rituximab.*

3.4.4 Amino acid modification

Multiple attribute analyses (MAM) allows us to evaluate a variety of protein PTMs in a single mass spectrometry assay by computationally analyzing mass data following a enzymatic digest of the biosimilar and innovator pair. [53,318] The MAM analysis of Rituxan® and Acellbia® is shown in Figure 3-8A, B and C, and Table 3-1 with statistically significant differences in oxidation, deamidation and pyroGlu levels determined by a Student's *t* test. The levels of single amino acid oxidation were comparable except Trp 47 oxidation which was higher for the innovator at 0.23 ± 0.1% relative to 0.2 ± 0.0% for the

biosimilar ($p < 0.05$). In addition, deamidation levels of Asp 55 on HC as well as Asp 136 on LC were significantly higher for the biosimilar product relative to the innovator. Due to the presence of N-terminal Gln, rituximab has tendency towards the formation of cyclized Glu. [329] We found different levels of the N-terminal Glu to pyroGlu conversion (Figure 3-8C). Percentage of N-terminal pyroGlu conversion on HC was 98.8 ± 0.1% for the biosimilar and 98.5 ± 0.1% for the innovator ($p < 0.05$), while the levels of N-terminal pyroGlu conversion on LC was only 58.1 ± 1.0% for the biosimilar and 81.2 ± 6.4% for the innovator ($p < 0.01$).

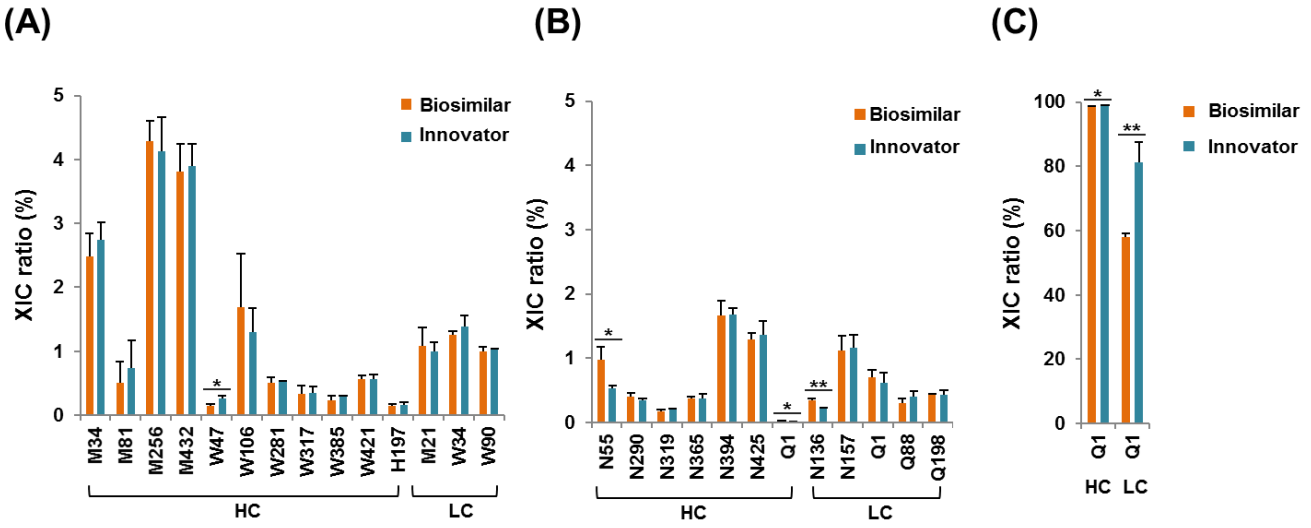

Figure 3-8 *LC-MS/MS analysis of tryptic digested rituximab biosimilar and innovator: levels of (A) oxidation, (B) deamidation, and (C) formation of N-terminal pyro glutamic acid. M: Methionine, W: Tryptophan, H: Histidine, N: Asparagine Q: Glutamine, HC: Heavy chain, LC: Light chain (N = 3; mean ± SD, Student's t-test, *p<0.05, **p<0.01).*

3.4.5 Charge and size variant profiles

Cation exchange (CEX) chromatography separates molecules using a negatively charged ion exchange resin that interacts with positively charged molecules on the surface. MAbs are prone to have charge variants resulting from PTMs, including the presence of C-terminal Lys, N-terminal pyroGlu and deamidation, which could potentially affect their quality, safety and efficacy. [190,360] As shown in Figure 3-9A, both biosimilar and innovator rituximab exhibited three distinct variant groups: main peak, acidic variants and basic variants containing one or two C-terminal Lys. The sums of the innovator and biosimilar acidic variants were 17.0 ± 0.1% and 21.3 ± 0.5%, respectively. The slight difference between the sums of the acidic variants was attributed to common sources of acidic variants such as sialylation and deamidation. [190] However, unlike the acidic variants, significant differences were observed in the basic charged variant patterns for two rituximab products. The sum of basic variants was calculated as 6.0 ± 0.2% for the innovator and 27.7 ± 0.3% for the biosimilar. To examine if the basic variants in the biosimilar correspond to the presence of C-terminal Lys, biosimilar samples were treated with carboxypeptidase B (CPB) and reanalyzed by CEX. The percentage of basic variants of biosimilar decreased to 9.8 ± 0.2% following CPB treatment (Figure 3-10), confirming the presence of C-terminal Lys in Acellbia®, which is in line with the intact mass results.

Protein aggregation the primary stability concern for biopharmaceutical products. [76] The presence of aggregates could impact protein efficacy and safety as the presence of aggregates could lead to increased product immunogenicity. [252] Size variants for innovator and biosimilar rituximabs were determined by size exclusion chromatography, separating molecules by size difference as a function of their diffusivity into a porous matrix

of resin particles. As seen in Figure 3-9B, the biosimilar showed higher levels of dimerization (3.0 ± 0.0%) compared to the innovator (0.5 ± 0.2%).

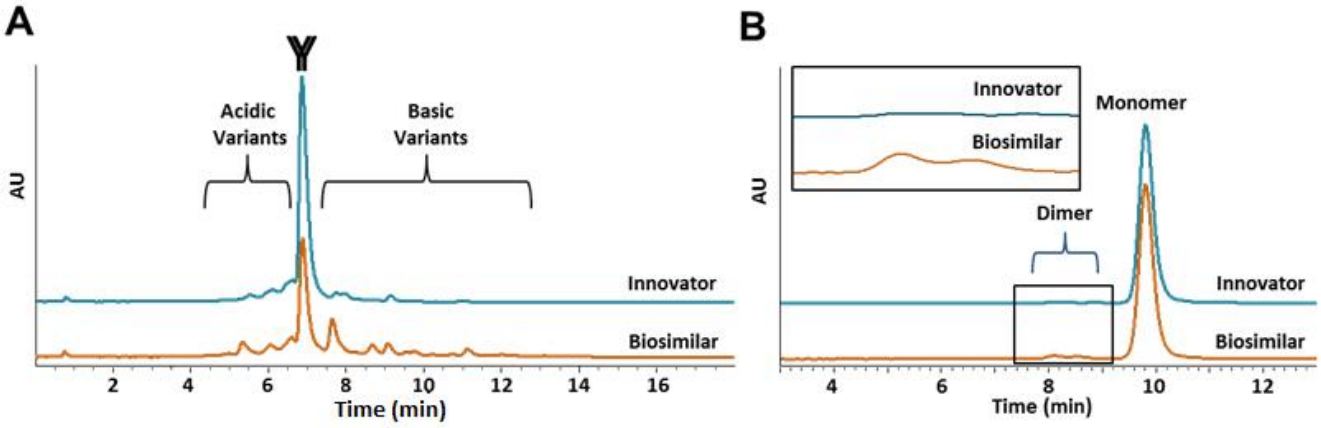

Figure 3-9 *(A) Representative charge variant profile and (B) representative size exclusion Chromatogram of rituximab biosimilar and innovator.*

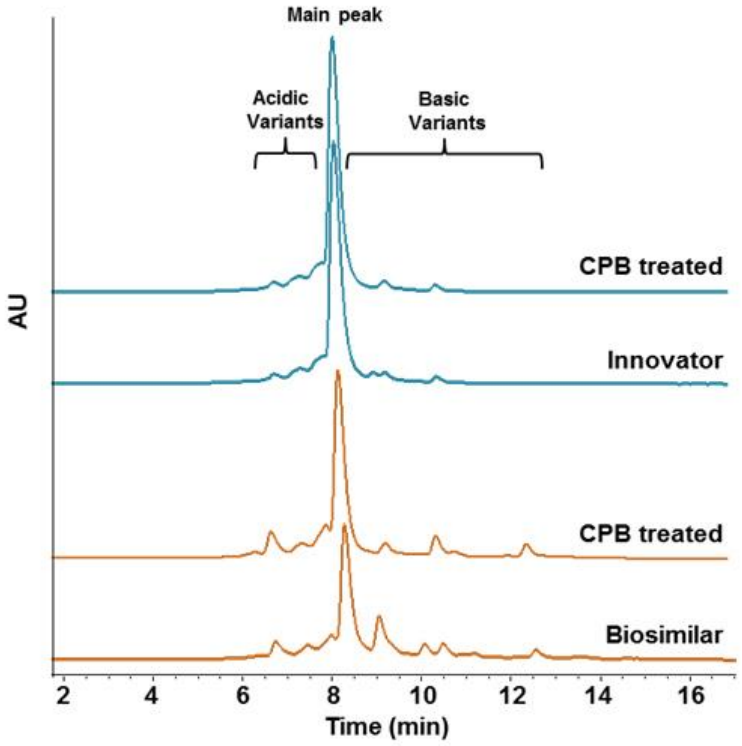

Figure 3-10 *(A) Representative charge variant profiles of the innovator and biosimilar rituximab with or without carboxypeptidase B (CPB) treatment.*

3.4.6 Glycoform distribution

Glycosylation affects mAb's effector functions and pharmacokinetic profile. [340] Therefore, understanding the differences in glycan distribution between a biosimilar and its innovator is crucial for filling the gap between its analytical residual uncertainty and clinical efficacy. Specifically in the context of tumor targeting, different glycoforms lead to variable binding affinities between the Fc region and FcγIIIa receptor, resulting in different ADCC activity. [361] We analyzed the glycan profiles of the biosimilar and innovator rituximab using two different methods; liquid chromatography analysis following fluorescent glycan labeling (LC-FLR) and quantitative bottom-up protein digestion followed by LC-MS/MS MAM analysis (Figure 3-11, 3-12, 3-13 and Table 3-2, 3-3). With both methods, the most abundant glycoforms appeared to be the same in the biosimilar innovator, including G0F, G1F and G2F fucosylated biantennary glycans (Figure 3-12A, 3-13A).

However, some differences in glycoform distributions were detected. A total of 32 glycoforms were detected by LC-MS/MS, while only 13 glycoforms were detected by our LC-FLR methodology. Among these glycoforms, there were 16 afucosylated glycans detected by LC-MS/MS compared to 4 detected by LC-FLR. This difference is mainly due to the presence of HM glycans. While HM glycoforms were not detected by our LC-FLR method, 5 of top 10 most abundant glycoforms were HM glycans as detected by LC-MS/MS. For LC-FLR method, percentage of afucosylated glycan for the biosimilar and innovator were 4.5 ± 0.1 % and 2.0 ± 0.3 %, respectively ($p < 0.001$). For LC-MS/MS method, percentage of afucosylated glycan for the biosimilar and innovator were 8.8 ± 0.1 % and 4.0 ± 0.1 %, respectively ($p < 0.0001$) (Figure 3-12B, 3-13B). For both methods,

biosimilar rituximab showed double the amount of afucosylated glycans, although the absolute afucosylation levels were the method-dependent.

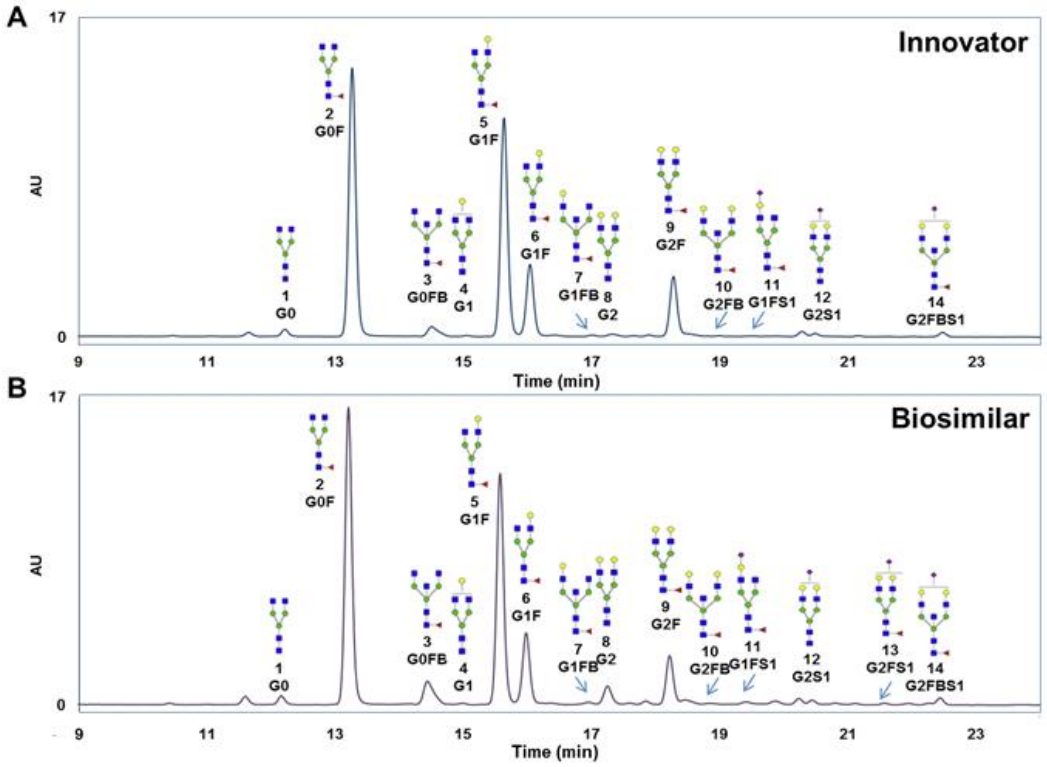

Figure 3-11 *N-glycan profiles of rituximab (A) innovator and (B) biosimilar by fluorescence LC analysis.*

3.4.7 FcγRIIIa binding affinity

Bio-layer interferometry (BLI) is an optical analytical technique that measures the interference pattern prior to and following the interaction between two biomolecules. [362] We chose V158 polymorph FcγRIII variants for this analysis that have been shown to exhibit a higher affinity to rituximab's Fc region. FcγRIIIa is an essential mAb mechanism of action (MOA), especially where immune-mediated cell killing mechanisms such as ADCC, are involved. Based on biosimilar rituximab's higher afucosylation level, the biosimilar was expected to have a stronger FcγRIIIa binding affinity than the innovator.

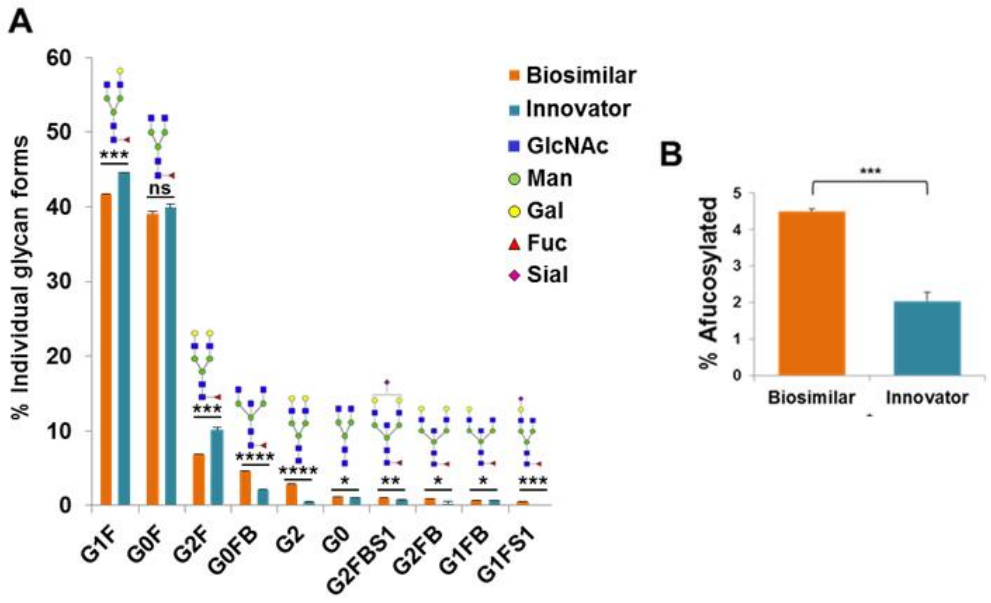

Figure 3-12 *(A) N-glycan quantification by fluorescence LC analysis and (B) total percentage of afucosylated glycans. (N = 3; mean ± SD, Student's t-test, *p<0.05, **p<0.01, ***p<0.001, ****p<0.0001)*

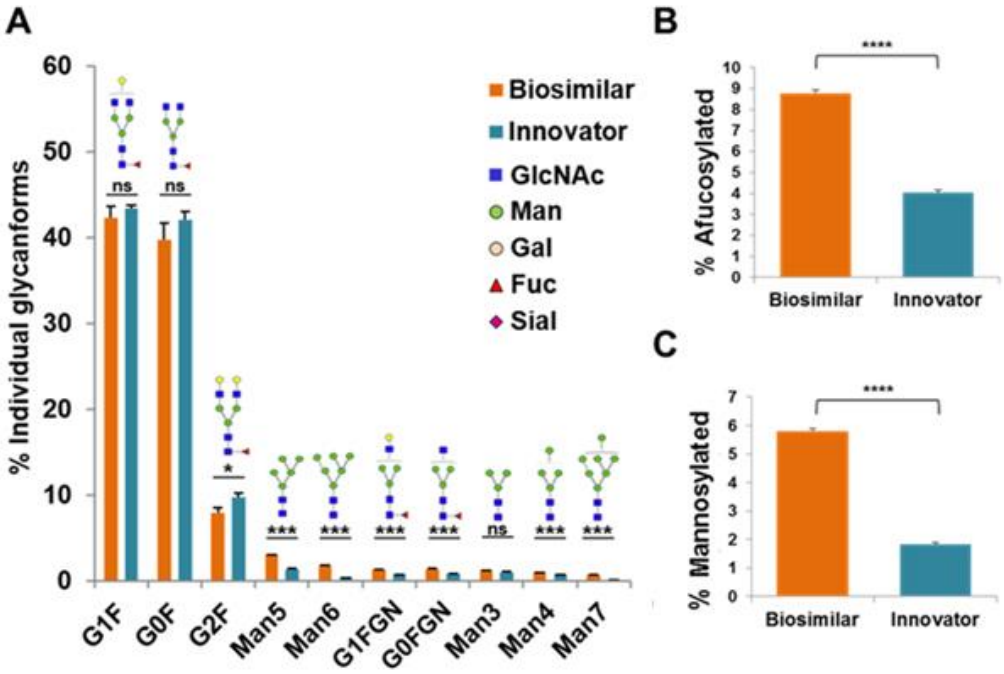

Figure 3-13 *(A) N-glycan quantification by LC-MS/MS, (B) total percentage of afucosylated glycans (C) high mannosylated glycans. (N = 3; mean ± SD, Student's t-test, *p<0.05, **p<0.01, ***p<0.001, ****p<0.0001)*

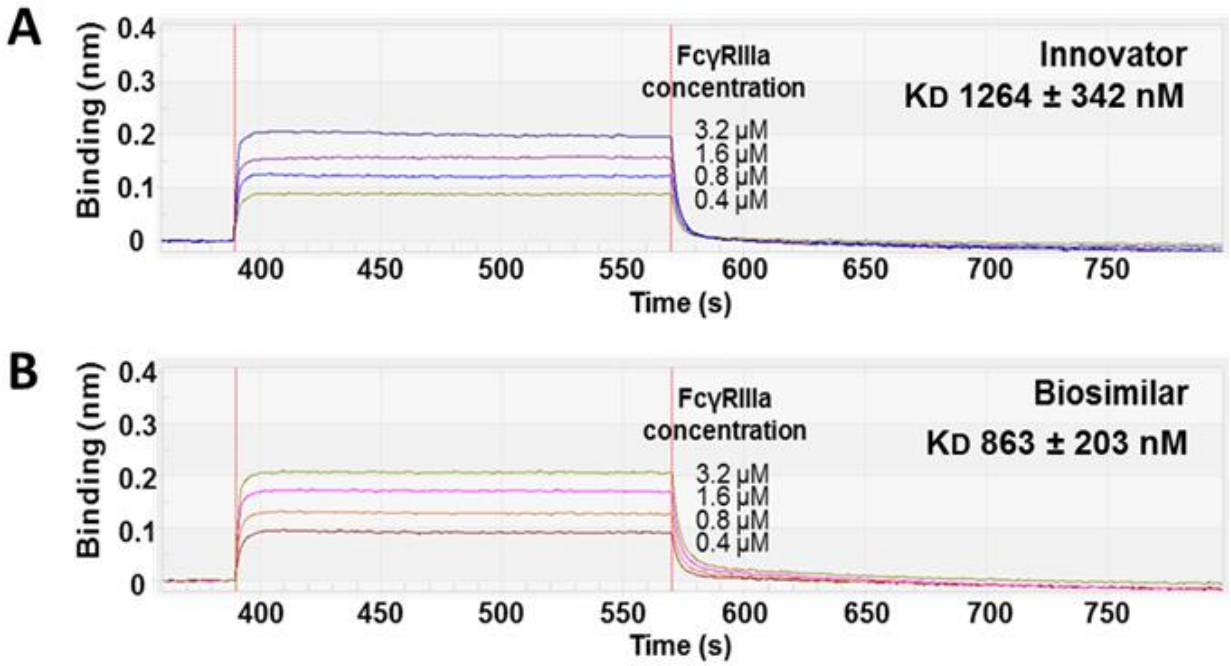

Figure 3-14 *Representative BLI sensograms to FcγIIIa receptors of rituximab (B) innovator and (C) biosimilar. (N = 3; mean ± (RSD))*

Correspondingly, biosimilar rituximab showed a lower mean K_D value (868 ± 203 nM) than innovator rituximab (1264 ± 342 nM) as measured by BLI (Figure 3-14).

3.4.8 ADCC activity

ADCC is the critical MOA of anti-cancer mAbs, where antibodies recruit FcγR-bearing effector cells to target “diseased” cells for destruction. To evaluate ADCC activity of rituximab, we used WIL2-S target cells, a CD-20 positive human B lymphoblastoma cell, and Jurkat effector cells, T lymphocyte cells that stably express either the V158 (high Fc affinity) or F158 (low Fc affinity) FcγRIIIa variants. The simultaneous binding of mAbs with both target (WIL2-S) and effector (Jurkat) cells leads to the induction of measurable nuclear factor of activated T-cells (NFAT) luciferase fluorescence. Biosimilar rituximab exhibited higher ADCC activity (Figure 3-15) as a measurement of potency for both V158 and F158

FcγRIIIa variants. In the presence of the V158 variant, the half maximal effective concentrations (EC_{50}) indicated a significantly higher potency for the biosimilar (1.1 x 10^{-8} g/mL) than the innovator (2.1 x 10^{-8} g/mL) ($P < 0.001$). Likewise, in the presence of the F158 (low Fc affinity) variant, the EC_{50} values indicated a higher potency for the biosimiliar (5.2 x 10^{-8} g/mL) than the innovator (6.9 x 10^{-8} g/mL). Statistical differences were compared with a two-tailed Student's *t* test. Taken together, the biosimilar's higher afucosylated glycan levels resulted in stronger FcγRIIIa binding affinity and higher ADCC activity.

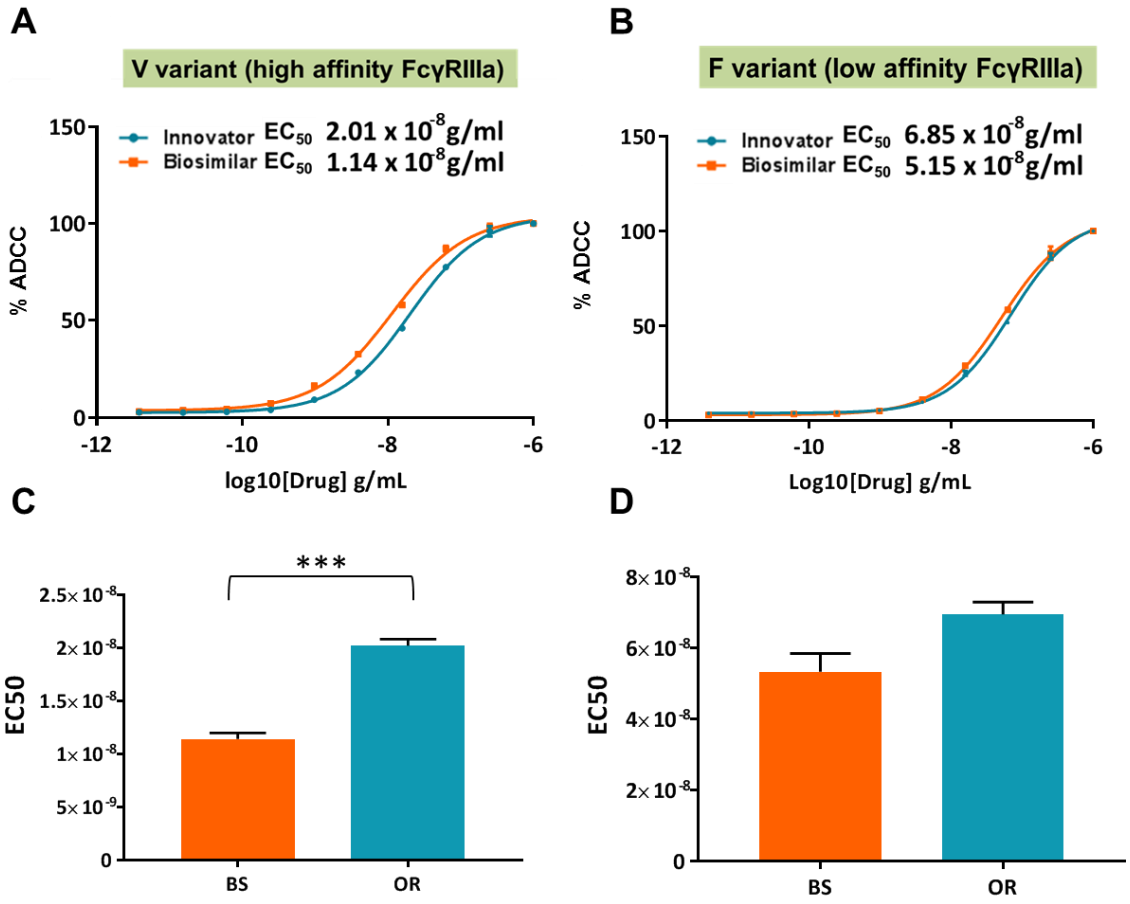

Figure 3-15 *Results of ADCC Reporter bioassay of rituximab innovator and biosimilar to (A)V variant (high affinity FcγRIIIa) and (B) F variant (low affinity FcγRIIIa) Statistical comparison using two-tailed Student's t test of (C) V variants and (D) F variants. (N = 3; ***p < 0.001)*

3.5 **Discussion**

Even with the patent expirations of many top-selling mAb based drugs, the approval of their respective mAb biosimilars has been limited by the lack of a concrete answer to the question, “How similar is similar enough?” To answer the similarity question and hasten the biosimilar approval process, it is necessary to devise an acceptable list and range of relevant critical quality attributes, highlighting differences between innovator and biosimilar products. [42,76,305] In our efforts to devise this list, we characterized and compared the underlying differences between Acellbia® and Rituxan® in primary structure, PTMs, and HOS using various MS-based techniques. We sought to find a relationship between structural differences and mAb functional activity, with an enhanced focus on glycosylation differences and their relationship with ADCC. Additionally, we compared innovator-biosimilar rituximab’s numerical differences detected in our study with similar numerical differences reported for other EU/FDA approved innovator-biosimilar pairs.

For our initial characterization, the primary structures of Acellbia® and Rituxan® were elucidated by performing bottom-up protein digestion followed by LC-MS/MS analysis. LC-MS/MS revealed comparable oxidation and deamidation levels for the two products but lower N-terminal pyroGlu formation levels for (58.1% vs 81.2%). In a similar study, lower N-terminal pyroGlu levels (95.7%) were observed for Truxima®, an EU/US approved rituximab biosimilar, when compared with its rituximab innovator (97.6 %). [363] However, it has been previously been shown that differences in pyroGlu formation have no effect on mAb HOS, potency and *in vivo* clearance, indicating limited clinical relevance. [191,193,363]

We then investigated the impact of primary structure differences (deamidation, oxidation and glycosylation) on HOS. [176,364–366] We confirmed that similar primary structures corresponded to comparable HOS by IM-MS and HX-MS. Recent studies have reported that IM-MS can provide a rapid characterization of mAb disulfide bonding and glycosylation states. [53,99,318] By focusing on CIU_{50} values in our analysis, we minimize the influence of overall signal intensity and focus on mAb stability shifts. It has been previously observed that mAb glycosylation can affect observed CIU_{50} values. [99] Thus, we rationalize the observed difference in the second CIU_{50} is related to glycosylation profile differences we detect between the innovator and biosimilar. The similarities in CIU fingerprint features, standard deviation, median feature drift time, and CIU50 values indicate that the biosimilar is comparable to the innovator rituximab.

Previous HX-MS studies have characterized the impact of PTMs on IgG1's localized structure. [367,368] Recently, More *et al.* revealed by HX-MS that the conformational integrity of the C_H2 and C_H3 domains are sensitive to different glycoforms. [369] In knowing this, we conducted HX-MS experiments and determined that there was an absence of significant differences in localized HX-MS conformational dynamics. These results supported the previously mentioned structural similarity determined by IM-MS. However, it is important to note that structural perturbations due to primary sequence modifications are likely below the limit of detection for HX-MS and, therefore, may still be present. We also measured any impact on the higher order structure of size variants by HX-MS and detected a presence of less than 2.5% for the variants. Taken together, the peptide level resolution of HX-MS combined with HOS level analysis by IM-MS seems to provide the confidence to support a complete analytical assessment of innovator and biosimilar mAbs.

Additionally, the macroscopic characterization and comparison of biosimilar and innovator rituximab was performed by intact MS, CEX and SEC analysis. Previous biosimilar studies have revealed differences in charge variants derived from the presence/absence of C-terminal Lys.[55,66] For example, Mvasi®, an EU/US approved bevacizumab biosimilar, showed higher levels of basic variants (8.6%) when compared to its innovator (6.1%). This was caused by unprocessed HC C-terminal Lys present in the biosimilar. In contrast, Inflectra®, an EU/US approved infliximab biosimilar lacking HC C-terminal Lys, showed lower levels of basic variants (41.5%) than its innovator (46.2%). [55,66,194,275,301]

In our study, the biosimilar was found to have higher levels of both acidic and basic variants, with basic variants corresponding to the presence of C-terminal Lys. This was confirmed by CPB treatment and intact MS. However, it has been previously shown that the rapid C-terminal Lys clipping upon IV administration is unlikely to alter potency or safety nor impact ADCC activity.[55,370] We also found significantly increased levels of high molecular weight aggregates in Acellbia® (3.0%) relative to Rituxan® (0.5%). Our results reflected those from a recent study on Inflectra® which revealed a relatively higher amount of high molecular weight aggregates for the biosimilar (0.8%) when compared to its innovator (0.2%). We note, however, that this difference in aggregates did not affect clinical immunogenicity for Inflectra®.[54,55] In AcellBia®, the clinical relevance of the effect of the higher amounts of aggregate on immunogenicity still needs to be assessed.

Lastly, we investigated the impact of different levels of afucosylated glycans on FcγRIIIa binding affinity and ADCC activity between the biosimilar and innovator rituximab. In some biosimilar documents, glycoform analysis was considered as moderate to low (tier

2 or 3) in terms of its potential impact on biological activity, safety or immunogenicity. [96,301,371] However, several studies have reported a positive relationship between afucosylated glycan levels, FcγRIIIa binding affinity and ADCC activity. [328,363,372–375] For example, the levels of afucosylated glycans appeared to be approximately ~ 1.5-fold higher for the anti-TNF-α innovator Remicade® than its biosimilar Remsima® (10.0% vs 6.2% as determined by LC-FLR and 19.7 vs 13.2% as determined by LC-MS/MS). This difference is reflected in an approximately 2-fold higher FcγRIIIa binding affinity and ADCC activity for Remicade® than for Remsima®. In a clinical setting, the difference in FcγRIIIa binding affinity and ADCC activity appear to alter the responsiveness of Crohn's disease patients to Remsima® vs. Remicade®. [53,328,376]

The relationship between afucosylation, FcγRIIIa binding affinity and ADCC activity is even more critical for cancer mAb therapeutics where ADCC is the drug's primary MOA. In our study, both LC-FLR and LC-MS/MS methods revealed that the biosimilar contained a higher percentage of afucosylated glycans. Differences in the number of detected glycans were method-dependent in a similar manner to previous Remicade®/Remsima® comparison reports. [53,328] These differences may reflect the necessity of orthogonal methods to thoroughly analyze glycoform distributions without overlooking certain species.

Our results confirmed that higher levels of afucosylated glycans in AcellBia® resulted in enhanced FcγRIIIa binding affinity and increased ADCC activity when compared with the innovator rituximab. Specifically, twice as many afucosylated glycans were observed for AcellBia® relative to Rituxan® (4.5% vs 2.0% detected by LC-FLR method and 8.8% vs 4.0% detected by LC-MS). This difference in afucosylation corresponded to a 2.5-fold difference in EC_{50} ADCC value (3.7×10^{-9} g/mL for AcellBia® vs 9.2×10^{-9} g/mL for

Rituxan®) in presence of effector cells containing a high affinity (V) FcγRIIIa variant. Higher levels of afucosylated glycans for Truxima® relative to Rituxan® were also reported by Celltrion (3.8 % vs 2.8 % measured by LC-FLR). However, these differences did not result in higher ADCC when measured using PBMC effector cells. In the case of Truxima®, the numeric difference in afucosylated glycans levels relative to Rituxan® was smaller than those found for AcellBia®/Rituxan® and Remicade®/Remsima® pairs. In addition, Celltrion has shown an excellent correlation between afucosylation levels and FcγRIIIa (V variant) binding/ADCC over a range of 5-50% rituximab afucosylation. Only a limited correlation was observed at afucosylation levels below 5%, which is likely due to the assay's low sensitivity. [363]

Moving forward, it will be critical to examine if the higher ADCC for AcellBia® will result in better efficacy for the biosimilar relative to the innovator, especially in patients with the V/V polymorph of the *FCGR3A* gene showing higher binding affinity to therapeutic mAb's Fc portion. In summary, additional research into the relative differences in afucosylation, ADCC and clinical activities between multiple biosimilar-innovator pairs is critical for establishing an Fc function similarity framework for biosimilar approval.

Table 3-1 *Levels of oxidation, deamidation and pyroGlu of Rituxan® and Acellbia®.*

		Oxidation			
		Rituxan®		Acellbia®	
	Modification site	**Average (%)**	**Stdev (%)**	**Average (%)**	**Stdev (%)**
Rituximab heavy chain	M34	2.74	0.27	2.48	0.36
	M81	0.74	0.43	0.51	0.33
	M256	4.13	0.53	4.28	0.32
	M432	3.89	0.35	3.81	0.44
	W47	0.26	0.05	0.15	0.03
	W106	1.30	0.37	1.69	0.84
	W281	0.53	0.00	0.51	0.08
	W317	0.35	0.10	0.33	0.14
	W385	0.30	0.01	0.23	0.07
	W421	0.56	0.08	0.57	0.05
	H228	0.32	0.09	0.29	0.08
	H272	0.08	0.02	0.07	0.03
Rituximab light chain	M21	1.00	0.14	1.09	0.28
	W34	1.38	0.18	1.25	0.06
	W90	1.02	0.02	0.99	0.08
	H197	0.16	0.05	0.14	0.04
		Deamidation			
		Rituxan®		Acellbia®	
	Modification site	**Average (%)**	**Stdev (%)**	**Average (%)**	**Stdev (%)**
Rituximab heavy chain	N55	0.98	0.20	0.53	0.04
	N290	0.41	0.05	0.35	0.02
	N319	0.17	0.03	0.21	0.01
	N365	0.37	0.03	0.37	0.07
	N394	1.67	0.23	1.68	0.10
	N425	1.29	0.10	1.37	0.21
	Q1	0.02	0.01	0.01	0.00
Rituximab Light chain	N136	0.34	0.03	0.23	0.00
	N157	1.12	0.23	1.17	0.20
	Q1	0.70	0.12	0.62	0.16
	Q88	0.30	0.07	0.40	0.09
	Q198	0.43	0.02	0.43	0.07
		PyroGlu			

		Rituxan®		Acellbia®	
	Modification site	**Average (%)**	**Stdev (%)**	**Average (%)**	**Stdev (%)**
Rituximab heavy chain	Q1	98.82	0.13	98.54	0.10
Rituximab Light chain	Q1	81.20	6.39	58.11	0.97

Table 3-2 *Glycoform profiles for Rituxan® and Acellbia® by LC-FLR.*

Glycan	**Rituxan®**		**Acellbia®**	
	Average (%)	**Stdev(%)**	**Average (%)**	**Stdev (%)**
G0	1.04	0.04	1.18	0.04
G0F	39.9	0.59	39.10	0.30
G0FB	2.12	0.02	4.56	0.07
G1	0.14	0.01	0.22	0.03
G1F	33.10	0.07	31.29	0.13
G1F	11.52	0.30	10.39	0.08
G1FB	0.53	0.02	0.66	0.02
G2	0.53	0.07	2.87	0.02
G2F	9.75	0.35	6.83	0.06
G2FB	0.24	0.27	0.95	0.01
G1FS1	0.00	0.00	0.48	0.08
G2S1	0.32	0.24	0.22	0.04
G2FS1	0.10	0.06	0.26	0.02
G2FBS1	0.71	0.06	0.99	0.04
Total	100.00		100.00	
Afucosylated	4.49	0.11	2.03	0.26

Table 3-3 *Glycoform profiles for Rituxan® and Acellbia® by LC-MS/MS.*

Glycan composition	Glycan	Rituxan®		Acellbia®	
		Average (%)	Stdev (%)	Average (%)	Stdev (%)
HexNAc(1)	-	0.04	0.00	0.07	0.01
HexNAc(2)Hex(4)	Man4	0.00	0.00	0.00	0.00
HexNAc(2)Hex(4)Fuc(1)	Man4F	0.09	0.01	0.04	0.00
HexNAc(2)Hex(5)	Man5	1.35	0.07	2.91	0.05
HexNAc(2)Hex(6)	Man6	0.31	0.00	1.69	0.07
HexNAc(2)Hex(7)	Man7	0.08	0.00	0.71	0.03
HexNAc(2)Hex(8)	Man8	0.10	0.01	0.48	0.05
HexNAc(2)Hex(9)	Man9	0.00	0.00	0.02	0.00
HexNAc(3)Hex(3)	G0-GN	0.17	0.02	0.21	0.04
HexNAc(3)Hex(3)Fuc(1)	G0F-GN	0.79	0.08	1.28	0.16
HexNAc(3)Hex(4)	G1-GN	0.02	0.00	0.06	0.00
HexNAc(3)Hex(4)Fuc(1)	G1F-GN	0.68	0.02	1.29	0.05
HexNAc(3)Hex(5)	Man5-GN	0.13	0.01	0.22	0.01
HexNAc(3)Hex(6)	Man6-GN	0.03	0.00	0.14	0.06
HexNAc(4)Hex(3)	G0	0.96	0.09	1.06	0.09
HexNAc(4)Hex(3)Fuc(1)	G0F	41.19	0.95	38.49	1.99
HexNAc(4)Hex(4)	G1	0.66	0.02	0.97	0.01
HexNAc(4)Hex(4)Fuc(1)	G1F	42.49	0.41	40.96	1.21
HexNAc(4)Hex(5)	G2	0.09	0.02	0.11	0.01
HexNAc(4)Hex(5)Fuc(0)NeuAc(1)	G2S1	0.00	0.00	0.00	0.00
HexNAc(4)Hex(5)Fuc(1)	G2F	9.50	0.50	7.61	0.66
HexNAc(4)Hex(5)Fuc(1)NeuAc(1)	G2FS1	0.65	0.16	0.69	0.05
HexNAc(4)Hex(5)Fuc(1)NeuAc(1)NeuGc(1)	G2FS1N1	0.00	0.00	0.00	0.00
HexNAc(4)Hex(5)Fuc(1)NeuAc(2)	G2FS2	0.36	0.03	0.56	0.15
HexNAc(4)Hex(5)Fuc(1)NeuGc(1)	G2FS1	0.00	0.00	0.01	0.00
HexNAc(4)Hex(6)Fuc(1)	G2FGal1	0.03	0.00	0.01	0.00
HexNAc(4)Hex(6)Fuc(1)NeuAc(1)	G2FS1Gal1	0.00	0.00	0.00	0.00
HexNAc(4)Hex(7)Fuc(1)	G2FGal2	0.00	0.01	0.00	0.01
HexNAc(5)Hex(4)	G1B	0.00	0.00	0.13	0.03
HexNAc(5)Hex(4)Fuc(1)	G1FB	0.01	0.01	0.26	0.03
HexNAc(5)Hex(5)Fuc(1)	G2FB	0.00	0.00	0.01	0.00
HexNAc(5)Hex(5)Fuc(1)NeuAc(2)	G2FBS2	0.01	0.00	0.00	0.00
	Total	100.00		100.00	
	Afucosylated	4.04	0.14	8.78	0.14

Chapter 4: Assessment of Biosimilarity Using Forced Degradation: Rituximab, Bevacizumab and Trastuzumab Originators and Biosimilars

4.1 Abstract

Biosimilars are highly similar to, but not identical with, their originator products. As a result, structural differences between originators and biosimilars can be difficult to detect and characterize without the appropriate analytical tools. Therefore, we first focus on identifying initial structural differences between rituximab, bevacizumab, and trastuzumab originator and biosimilar pairs and later address how these differences change after applying thermal stress at 40ºC with orbital shaking for 4 weeks. Prior to incubation, we detected comparable secondary and tertiary structures for each pair and identified different levels of soluble aggregates, charge variants, and molecular weight variants due to differences in glycoforms and the number of C-terminal lysines. Over the course of incubation, we detected differences in charge variants and unfolding patterns. Taken together, our study provides a comparability exercise, providing information on the minor differences present between originator and biosimilar products and how those differences are impacted by stress.

4.2 Introduction

The development of biosimilars, especially monoclonal antibodies (mAbs), is now on the rise due to the patent expiry of many lucrative biologic drugs. As of now, 20 biosimilars have been approved by U.S. Food and Drug Administration (FDA), 13 of which are mAbs [377]. Unlike generic small molecule drugs, there may be minor structural

discrepancies between biosimilars and their originator drug products due to differences in cell line as well as manufacturing and storage conditions. Even when the same cell line and manufacturing processes are used, variations in post-translational modifications (PTMs) can contribute significantly to functional and structural differences between a reference product and proposed biosimilar. [378] Various studies have reported different levels of PTMs, including oxidation, deamidation, charge variants, size variants, glycosylation, glycation and incorrect disulfide bond formation, between originator and biosimilar mAbs. [53–55,226,227,270,275,379,380] In addition, some biosimilars are not formulated with the same excipients and buffer system as the originator product. [381–385] Together, all of these factors make up the potential sources of variability between originators and biosimilars.

For any biosimilar development program, it is pivotal to perform extensive biophysical characterization with robust methodologies in order to detect structural differences between the reference product and proposed biosimilar. Additional structural information can be obtained by subjecting each product to different stresses in attempt to exacerbate existing differences while simultaneously providing a product stability profile. Forced degradation studies typically use stress conditions such as pH, temperature, light and agitation. [300] This is commonly used in industry for manufacturability evaluation, formulation optimization, analytical method development and determination of product shelf-life. [298] Degradation studies have also provided an integral framework for the assessment of biosimilarity in regulatory filings [96,150,151,194,301], since these stress conditions highlight subtle structural differences that may not be readily detected without forced degradation. [318] The results of forced degradation studies may vary depending

on the stress condition and type of mAbs being evaluated on top of the inherent differences between the originator (OR) and biosimilar (BS). For example, both infliximab OR and BS showed significant formation of high molecular weight forms, resulting in reduced TNF-α binding, when stressed at pH 2.9 under 5ºC for 8 days, while increased deamidation, resulting from thermal stress at 45 ºC for 10 days, had no impact on TNF-α binding. [150] In addition, rituximab OR and BS showed different rates of aggregate formation after 15 days of incubation at 50 ºC. [66]

In this study, we used three different innovator and biosimilar pairs; rituximab, bevacizumab, and trastuzumab. Our objective was to determine which methods are best suited for detecting initial structural differences between the OR and BS. We subsequently investigated how these differences changed over the course of 4 weeks of incubation at 40ºC, with orbital shaking at 250 RPM, by comprehensive structural analysis using an array of highly sensitive chromatographic and biophysical assays.

4.3 **Materials and methods**

4.3.1 Samples and reagent

All drugs were purchased and stored at 4ºC until use (Rituxan®, Avastin®, Herceptin® (Genetech), Acellbia®, HERtiCAD®, Avegra® (Biocad)). Bacteriostatic 0.9% sodium chloride injection, USP was purchased from Pfizer Inc. (New York City, NY, US) All MS grade reagents were from Fisher Scientific (Hampton, NH, US). The chemicals were purchased from Sigma-Aldrich (Milwaukee, WI, US).

4.3.2 Sample incubation

Samples were diluted to 1 mg/mL using 0.9% bacteriostatic sodium chloride injection, USP. Samples were incubated at 40 ºC with 250 RPM orbital shaking for 4 weeks.

4.3.3 Circular dichroism

CD was carried out using Jasco J-815 CD spectrometer equipped with temperature controller (CDF-426S/15) and Peltier cell (Jasco, Oklahoma City, OK) at 25 °C. CD data were collected from 190 to 260 nm with scanning speed of 50 nm/min, band width of 1nm and a DIT of 1 sec using Spectrosil® far UV quartz cells with 1 mm pathlength. CDPro analysis (CONTIN) was used for analyzing CD spectra to determine the secondary structure contents. CD data were plotted after being converted to mean residual ellipticity (MRE) using the following equation.

$$[\theta]_{mrw,\lambda} = MRW\ X \frac{\theta\lambda}{10\ X\ d\ X\ c}$$

θ_λ: observed ellipticity in degrees at wavelength λ

d: path length (cm)

c: concentration (g/mL)

4.3.4 Intrinsic fluorescence

Intrinsic fluorescence of antibody samples (1 mg/mL) was measured in ultra-micro cell black quartz cuvettes (1.5 x 1.5 mm optical path length) (Hellma, Müllheim, Germany) using a SpectraMax3 (Molecular devices, San Jose, CA) with excitation at 280 nm and emission ranging from 280 nm to 450 nm.

4.3.5 Ion mobility mass spectrometry and collision induced unfolding

All antibody samples, native and thermally stressed, were buffer exchanged into 200 mM ammonium acetate buffer using Micro Bio-spin 30 columns (Bio-Rad, Hercules, CA). Buffer exchanged samples were then diluted to a working concentration of 1 mg/mL (~6.7 μM).

Antibody samples were analyzed using a quadrupole-ion mobility-time-of-flight mass spectrometer (Q-IM-ToF MS) instrument (Synapt G2 HDMS, Waters, Milford, MA). Sample was transferred to a gold-coated borosilicate capillary needle (prepared in-house), and ions were generated by direct infusion using a nano-electrospray ionization (nESI) source in positive mode. The electrospray capillary was operated at voltages of 1.5-1.7 kV with the sampling cone operated at 40 V. The backing pressure was set to ~7.9-8.1 mbar. The helium cell flow was operated at 200 mL/min and pressurize to $1.40x10^3$ mbar. The trap traveling-wave ion guide was pressurized to 4.93×10^{-2} mbar with argon gas. The traveling- wave IM separator was operated at a pressure of ~3.4 mbar. IM separation was achieved with a travelling wave operated at 40 V wave height traveling at 600 m/s. The ToF-MS was operated over the m/z range of 100−10,000 at a pressure of 1.5×10^{-6} mbar.

Antibody ions were subjected to collisions in the travelling-wave ion trap prior to the IM separation to perform all charge state antibody CIU. The collision voltage was ramped from 5 to 200 V in 5 V increments to construct the CIU fingerprint data. The dwell time for each 5 V step was 6 seconds. Drift time data was extracted at each collision voltage in DriftScope (Waters, Milford, MA) using TWIMExtract. [349] These extracted drift time data were analyzed using a home-built software package, CIUSuite 2. [350]

4.3.6 Intact mass spectrometry

Each antibody sample was buffer-exchanged 4 times into a 20% acetonitrile solution containing 1% acetic acid using a 10 KDa Amicon® Ultra filter (EMD Millipore, Burlington, MA). Antibody was recovered from the filter unit in water and concentration was measured by a Qubit fluorometer (Invitrogen, Carlsbad, CA). Sample concentration was reduced to 0.5 mg/mL with LC-MS grade water. Samples were separated and analyzed by a C4 column (X-Bridge BEH C4 2.1 x 50 mm) (Waters, Milford, MA) interfaced to a Q Exactive mass spectrometer (ThermoFisher, Waltham, MA). Data were acquired from 600-4000 *m/z* at a resolution of 17,500 FWHM (at 400 *m/z*) with 10 µscans per spectrum (intact mass). Spectral deconvolution and analysis were performed using Intact Mass™ ver 3.3 (Protein Metrics Inc., San Carlos, CA).

4.3.7 Cation exchange chromatography

CEX was performed on an Alliance HPLC (Waters, Milford, MA) equipped with PDA detector. Antibody samples were centrifuged for 10 min at 15,000 RPM and injected (30 µL) onto a MAbPac SCX-10 column (4 x 150 mm, 5 µm) (Thermofisher, Waltham, MA). Mobile phase A was 20 mM MES buffer (pH 5.6) and mobile phase B was 20 mM MES buffer with 300 mM NaCl (pH 5.6). The flow rate was 1 mL/min at 30°C for 20 min using a linear 30-60% B gradient. The signal was detected at 280 nm.

4.3.8 Size exclusion chromatography

Antibody samples were centrifuged for 10 min at 15,000 RPM. Samples (25 µL) were injected into a Waters Alliance HPLC system and separated with a TSKgel SuperSW mAb HR column (7.8 mm x 30.0 cm, 4 µm, 25 nm) (Tosoh, Tokyo, Japan). 0.2

M phosphate buffer (pH 6.7) with 0.05% NaN_3 was used for the mobile phase with a flow rate of 0.8 mL/min. The signal was detected at 280 nm.

4.3.9 SDS-PAGE

SDS-PAGE was performed under reducing and non-reducing conditions in pre-cast NuPAGE® 3-8% tris-acetate gel (Invitrogen, Carlsbad, CA). Antibody samples (7.5 µg) were mixed with NuPAGE® LDS sample buffer (Invitrogen, Carlsbad, CA) to make a final volume of 10 µL. For reducing SDS PAGE, 1 µl of NuPAGE® reducing agent was added. Samples were heat denatured at 70 °C for 10 minutes. HiMark prestained protein standard (Invitrogen, Carlsbad, CA) was used for the protein ladder. For reducing SDS PAGE, 0.5 ml of antioxidant was added to the running buffer in the upper chamber. Electrophoresis was carried out at a constant voltage of 150 V for 1 hour with XCell SureLock Mini-Cell (Invitrogen, Carlsbad, CA). Gels were stained with SimplyBlue Safe stain (Thermofisher) and analyzed by Fluorchem M (ProteinSimple, San Jose, CA).

Table 4-1 *Formulation of mAbs.*

	Rituximab	**Bevacizumab**	**Trastuzumab**
Concentration	10 mg/ml	25 mg/ml	21 mg/ml
Form	Solution	Solution	Lyophilized powder
Buffering agent	7.35 mg/ml Sodium citrate dihydrate	5.8 mg/ml Sodium phosphate monobasic monohydrate 1.2 mg/ml Sodium phosphate dibasic anhydrous	1.9 mg/ml L-Histidine 2.4 mg/ml L-Histidine HCl
Tonicity modifier	9 mg/ml Sodium chloride		
Lyo-protector	60 mg/ml α, α-trehalose dihydrate		19.1 mg/ml α, α-trehalose dihydrate
surfactant	0.7 mg/ml Polysorbate 80	1.6 mg/ml Polysorbate 20	0.09 mg/ml Polysorbate 20
pH	6.5	6.2	6

4.4 **Results**

4.4.1 Initial structural differences between the originator and the biosimilar

First, we performed far UV circular dichroism (CD) (190-260 nm) and intrinsic fluorescence (IF) to detect differences of secondary and tertiary structure. Circular dichroism detects secondary structure of proteins by measuring absorbance differences of left and right circularly polarized light. [74] Intrinsic fluorescence measures the conformational changes of proteins derived from the fluorescence of aromatic amino acids, which are sensitive to local environment changes. [386] CD spectra for three mAb pairs were shown in Figure 4-1 a-c and were well overlapped between OR and BS. Also, the resulting structural contents (α-helix, β-sheet, β-turn, and random coil) were highly similar between OR and BS with their secondary structure being mainly composed of β-sheet, turns and random coil (Table 1). In addition, IF spectra for the three mAb pairs are shown in Figure 4-1 d-f. IF spectra were well-overlapped for each mAb pair. The emission wavelength of maximum intensity for the rituximab pair was found to be 335 nm, while the emission wavelength of maximum intensity for bevacizumab and trastuzumab pairs was found to be 340 nm. Altogether, there were no significant secondary or tertiary structural differences detected by CD and IF between OR and BS.

Next, we utilized ion mobility mass spectrometry (IM-MS), which has previously been implemented in biosimilar comparison studies by detecting subtle differences in features such as glycosylation and disulfide bonds [53,56,318], for the characterization of intact mAbs and generation of collision-induced unfolding (CIU) fingerprint plots. By

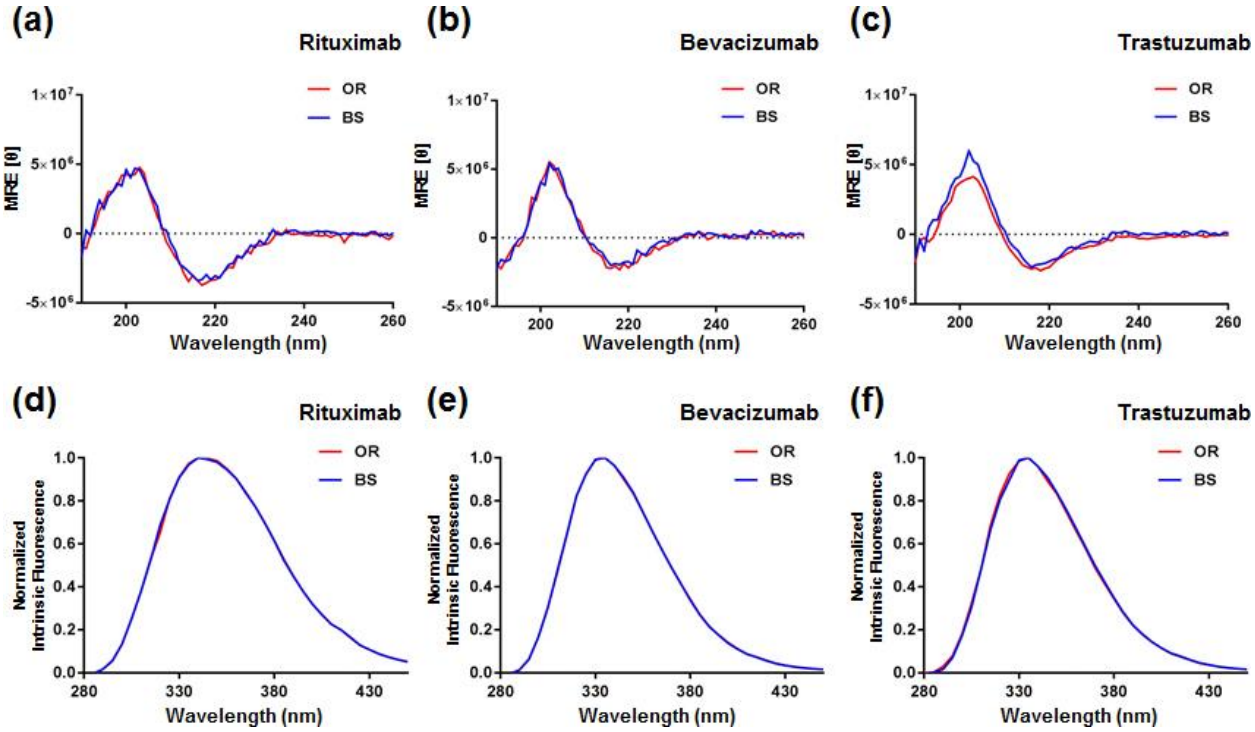

Figure 4-1 *Representative far UV circular dichroism spectra of (a) rituximab pair, (b) bevacizumab pair and (c) trastuzumab pair. Representative intrinsic fluorescence spectra of (d) the rituximab pair, (e) the bevacizumab pair and (f) the trastuzumab pair.*

calculating the CIU50 (the voltage at which 50% of a relatively compact state of the protein transitions to an unfolded state), we are able to compare the stability for all transitions across different CIU fingerprints. [350] The 24+ charge states were used to generate CIU plots, providing suitable transition numbers between features with high confidence. The resulting CIU plots are shown in Figure 4-2. We observed 1 stable and 2 unfolded states for all 3 OR-BS pairs. Also, we did not detect any significant differences in the stability of mAb structure between OR and BS based on the collision energy required to unfold the antibody, with the exception of the rituximab pair at the second transition (Figure 4-2d).

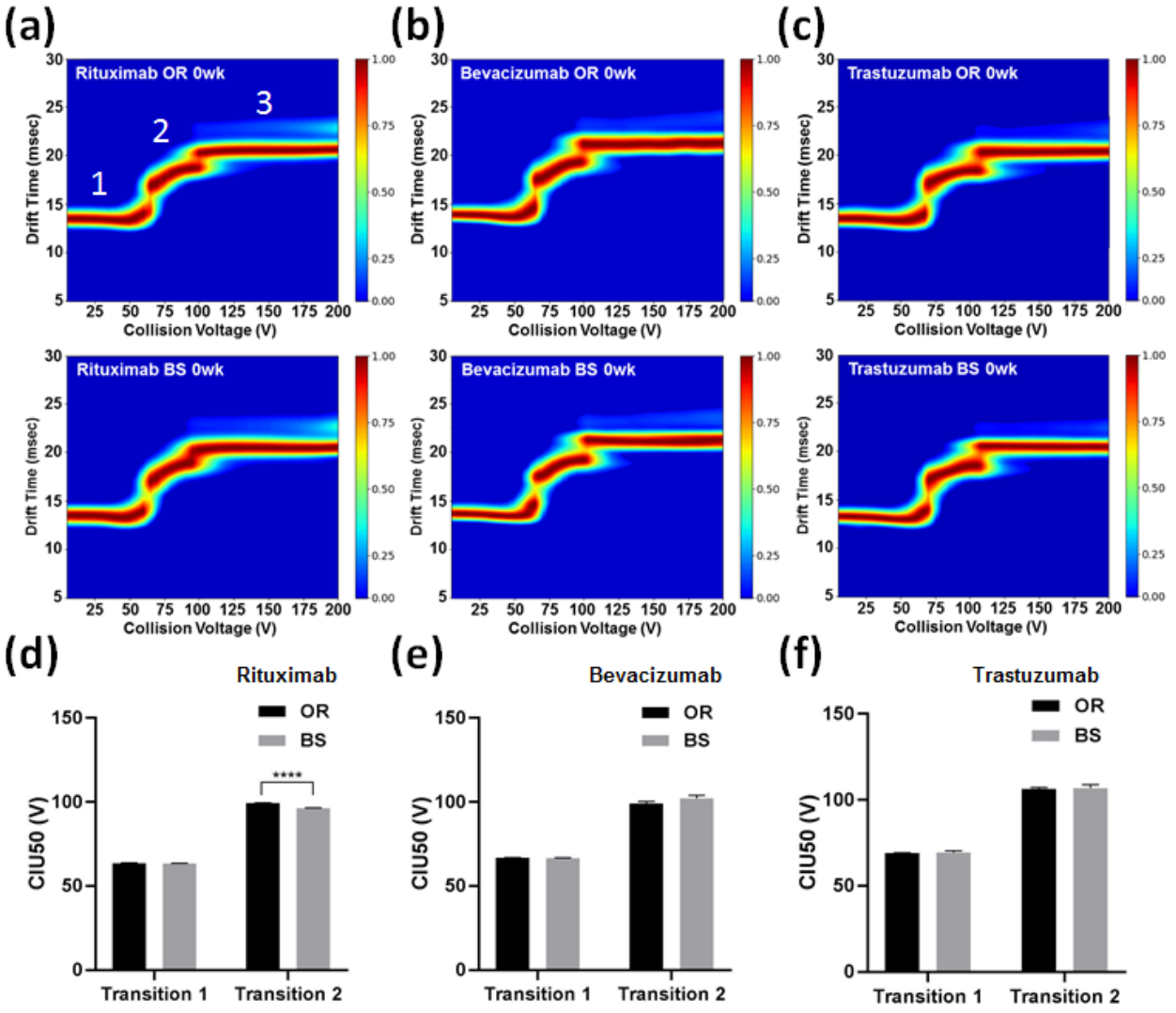

Figure 4-2 *Representative CIU fingerprints of (a) the rituximab pair (b) the bevacizumab pair and (c) the trastuzumab pair and CIU50 values of (d) the rituximab pair (e) the bevacizumab pair and (f) the trastuzumab pair. (N = 3; mean ± SD, Student's t-test, ****p<0.0001)*

Then, a molecular weight (MW) of each antibody was measured by intact mass analysis. By comparing observed mass with a protein's expected mass (based on amino acid sequence), information on each antibody's glycoform profile and PTMs can be obtained. The deconvoluted MS spectra of each mAb pair are shown in Figure 4-3 as a mirror plot. The presence of various glycoforms and C-terminal Lys species were assigned based on deconvoluted MS values. Each mAb showed multiple MW peaks,

corresponding to mAb molecules with different N-linked glycoforms and different amounts of C-terminal lysine residues (a mass difference of ~162 corresponds to galactose and N-acetylglucosamine, ~291: sialic acid, ~146: fucose, and ~128: C-terminal Lys). We detected initial MW distribution differences between OR and BS. In general, more MW peaks were detected for BS samples, including split peaks shown in rituximab and trastuzumab BS samples.

The rituximab OR contained four of the most abundant glycoforms (G0F/G1F, G0F/G2F or $(G1F)_2$, $(G0F)_2$ and G1F/G2F) along with a series of less abundant glycoforms. The rituximab BS possessed similar glycoforms, but split peaks were detected with MW corresponding to the presence of C-terminal Lys immediately to the left of its respective glycoform. There were no new glycoforms detected between the OR and BS. The bevacizumab OR showed a simple MW distribution with four glycoforms: ($(G0F)_2$, G0F/G1F G0F/G2F or $(G1F)_2$ and G1F/G2F). In contrast, the bevacizumab BS showed more MW peaks than the OR, with differences derived from the presence of 1 or 2 C-terminal Lys with similar major glycoforms. Glycoforms containing sialic acid were not observed in both the OR and the BS. The trastuzumab OR and BS showed similar major glycoforms (G0F/G1F, $(G1F)_2$ or G0F/G2F, $(G0F)_2$, G1F/G2F, G0/G0F, and $(G2F)_2$), but showed differences of minor glycoforms. For example, $(Man5)_2$ and $(G2F)_2$ glycoforms were only detected in the OR. Differences between the OR and the BS were detected as split peaks, corresponding to having one or two C-terminal Lys (like the rituximab pair).

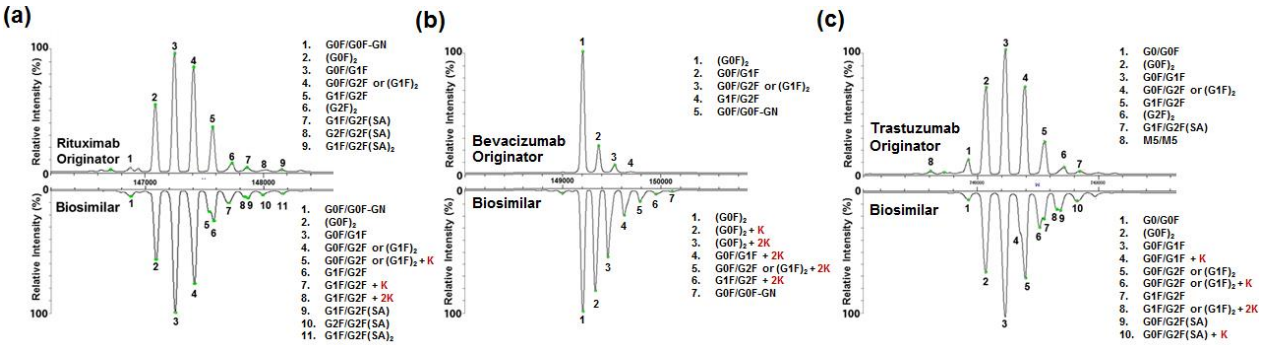

Figure 4-3 *Comparison of deconvoluted mass spectra with annotated glycoforms and C-terminal Lys of (a) the rituximab pair, (b) the bevacizumab pair and (c) the trastuzumab pair.*

In addition, we profiled charge variants in the three mAb pairs using CEX (Figure 4-4). Charge variants in mAbs stem from PTMs during manufacturing, such as sialylation and C-terminal Lys clipping, as well as degradation during storage, such as deamidation. These charge variants are specified as acidic or basic relative to the main species. For CEX, acidic variants will elute out earlier than the main species while basic variants will elute out later. The main peak was defined as the largest peak observed for the OR of each pair. For all 3 mAb pairs, the BS product contained a smaller main peak fraction and a larger portion of basic variants compared to the OR. We confirmed that basic variants were mainly derived from C-terminal Lys variations by treating mAbs with carboxypeptidase B (CPB), an enzyme that selectively cleaves C-terminal Lys. Overall, the CEX data aligned well with the intact mass results and clearly identified differences in the number of C-terminal Lys between the OR and BS pairs.

Lastly, we assessed the presence of mAb aggregates and fragments using SEC. SEC is a widely used method to separate protein molecules based on their size in solution. [387] The SEC chromatograms are shown in Figure 4-5. The size variants were highly similar for each of the 3 mAb pairs, with only the rituximab BS showing a small (2.6

± 0.1%) but statistically significant difference in the presence of aggregates compared to the OR product.

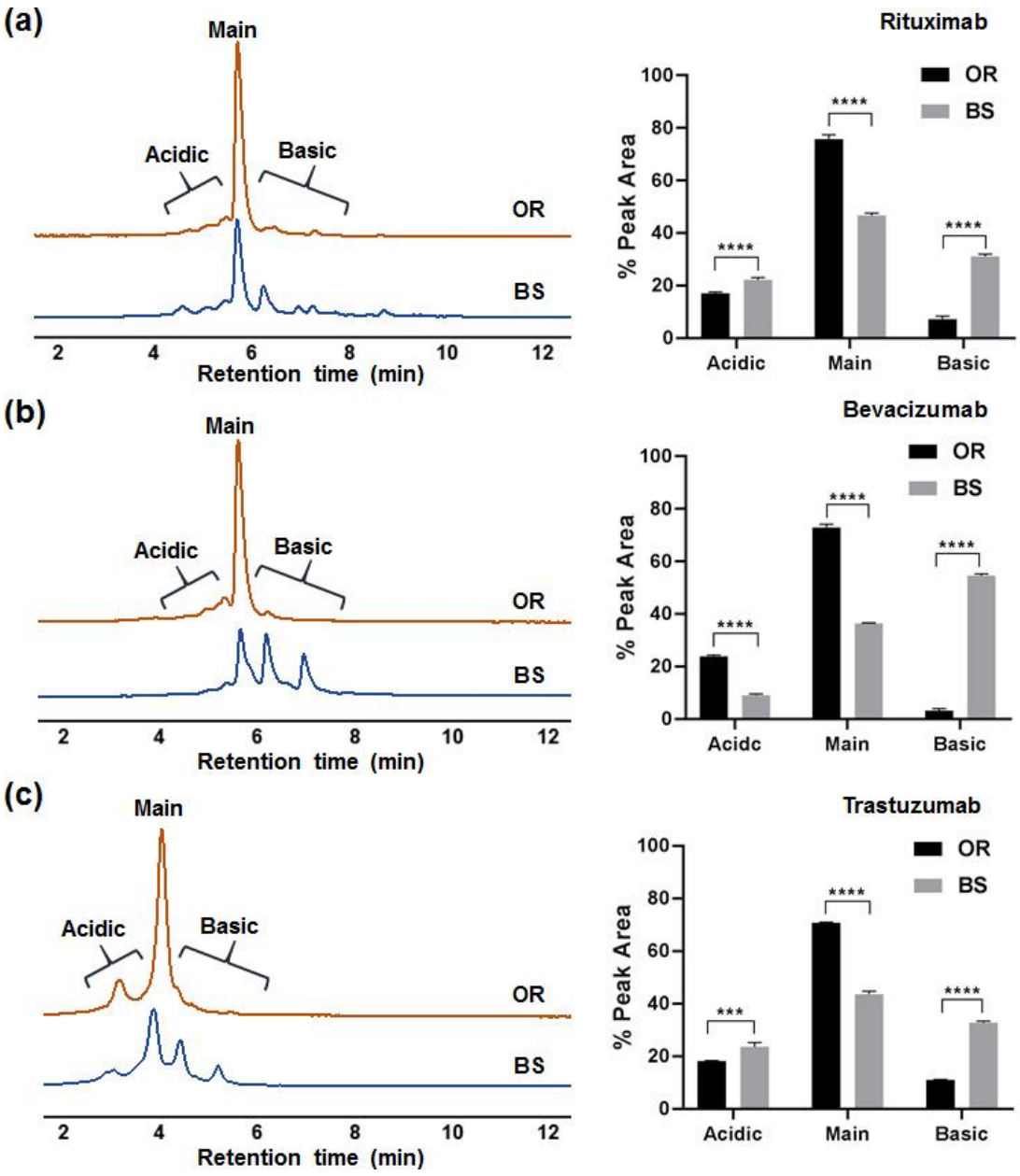

Figure 4-4 *Cation exchange chromatograms and relative percentage peak area of charge variants of (a) the rituximab pair, (b) the bevacizumab pair and (c) the trastuzumab pair (UV detection at 280 nm). (N = 3; mean ± SD, Student's t-test, ***p<0.001, ****p<0.0001)*

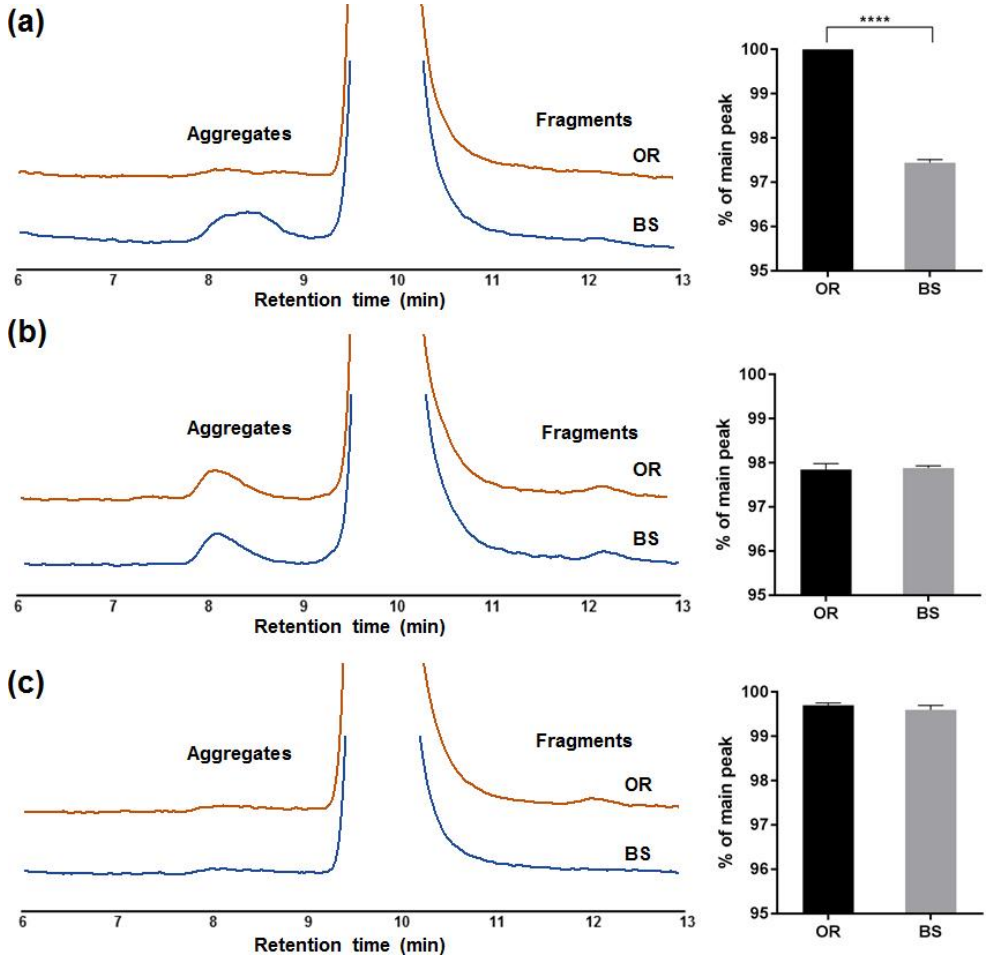

Figure 4-5 *Representative SEC chromatograms and relative percentage main peak area of for (a) the rituximab pair, (b) the bevacizumab pair and (c) the trastuzumab pair. (N = 3; mean ± SD, Student's t-test, ****p<0.0001)*

Altogether, our initial structural characterization of the 3 mAb pairs revealed a high degree of similarity with minor differences in unfolding and aggregation pattern (the rituximab pair) as well as differences in glycoform distribution and charge profiles (all pairs). In order to amplify these initial differences between the OR and BS products, we subjected each mAb to a 4-week incubation at 40 ºC with orbital shaking.

4.4.2 Assessment of structural differences after stress

Over the course of incubation, no structural changes were detected via CD and IF. The CD spectra were nearly identical between each OR and BS pair before and during

stress, indicating that the secondary structure remained unchanged during incubation. The IF spectra were also identical for each mAb pair regardless of incubation time point, indicating a high degree of similarity in protein-folding state. (Figure 4-9 and Table 4-2)

Regarding IM-MS, there were a number of subtle, but statistically significant changes after the 4-week incubation. The rituximab OR showed a decreased CIU50-2 value at week 4, corresponding to a minor destabilization, whereas there were no significant difference in the resulting CIU50 values between the stressed OR and BS indicating the presence of a terminal CIU50 value for stressed rituximab (Figure 4-9b). With the bevacizumab pair, the BS had a higher CIU50-2 (7% difference) than the OR, but still within standard deviation of the unstressed BS, suggesting the BS is more stable than the OR (Figure 4-9d). The trastuzumab OR showed a higher CIU50-1 than the BS after incubation, and both the OR and BS showed similar increases (approximately 2%) in CIU50-2 (Figure 4-9f), indicative of a small and unexpected increase in stability of both mAbs after incubation that may be related to variance in secondary structure as a result of incubation as indicated by the CD data for transtuzumab.

The post-stress intact MS data for the rituximab and trastuzumab pairs were identical to the data obtained from the unstressed samples (Figure 4-3a and c and Figure 4-10a and c). In short, each OR-BS pair possessed similar major glycoforms, with minor differences manifesting as split peaks that correspond to different numbers of C-terminal lysines. However, for the bevacizumab pair, we detected the cleavage of N-acetylglucosamine from the G0F glycan as well as cleavage of the entire G0F glycan from the bevacizumab OR upon incubation (Figure 4-3b).

The CEX profiles of all 6 mAbs showed a decrease in main peak area and increases in a combination of acidic and basic-peak areas over the course of the 4-week stress period (Figure 4-6). In general, the largest changes in charge variant distribution occurred in the 3 OR products. The main peak areas for the Rituximab, Bevacizumab, and Trastuzumab OR products decreased by 14%, 11%, and 29%, respectively. In contrast, the main-peak areas of the 3 BS products decreased by 5%, 1%, and 19%, respectively. Interestingly, the trastuzumab pair showed the most changes during the incubation, with both the OR and BS products having statistically significant differences in acidic, main, and basic-peak areas when comparing unstressed to 4-week stressed samples (Figure 4-6h and i). As with the unstressed samples, we confirmed that basic variants in all 3 pairs were derived from C-terminal Lys variations by treating mAbs with carboxypeptidase B (CPB), an enzyme that selectively cleaves C-terminal Lys.

Across all 3 mAb pairs, the incubation period brought about no significant changes in the levels of aggregates and fragments based on SEC data. The initial differences between each OR-BS pair in terms of aggregation and fragmentation accounted for any differences observed over the course of the incubation (Figure 4-7a and b). To confirm the SEC results, we also performed reducing and non-reducing SDS-PAGE as an orthogonal method (Figure 4-7c). In general, the data from SDS-PAGE supported the observations made by SEC. SDS-PAGE data were corresponded well to SEC data where the presence of dimer for the rituximab BS and bevacizumab pair. In addition to monomer mAb bands, smaller molecular weight bands (approximately 100 kDa : 2 heavy chain and 125 kDa: 2 heavy chains and 1 light chain) were also observed under non-reducing conditions, which have been commonly observed in previous studies. [318,388–390] No

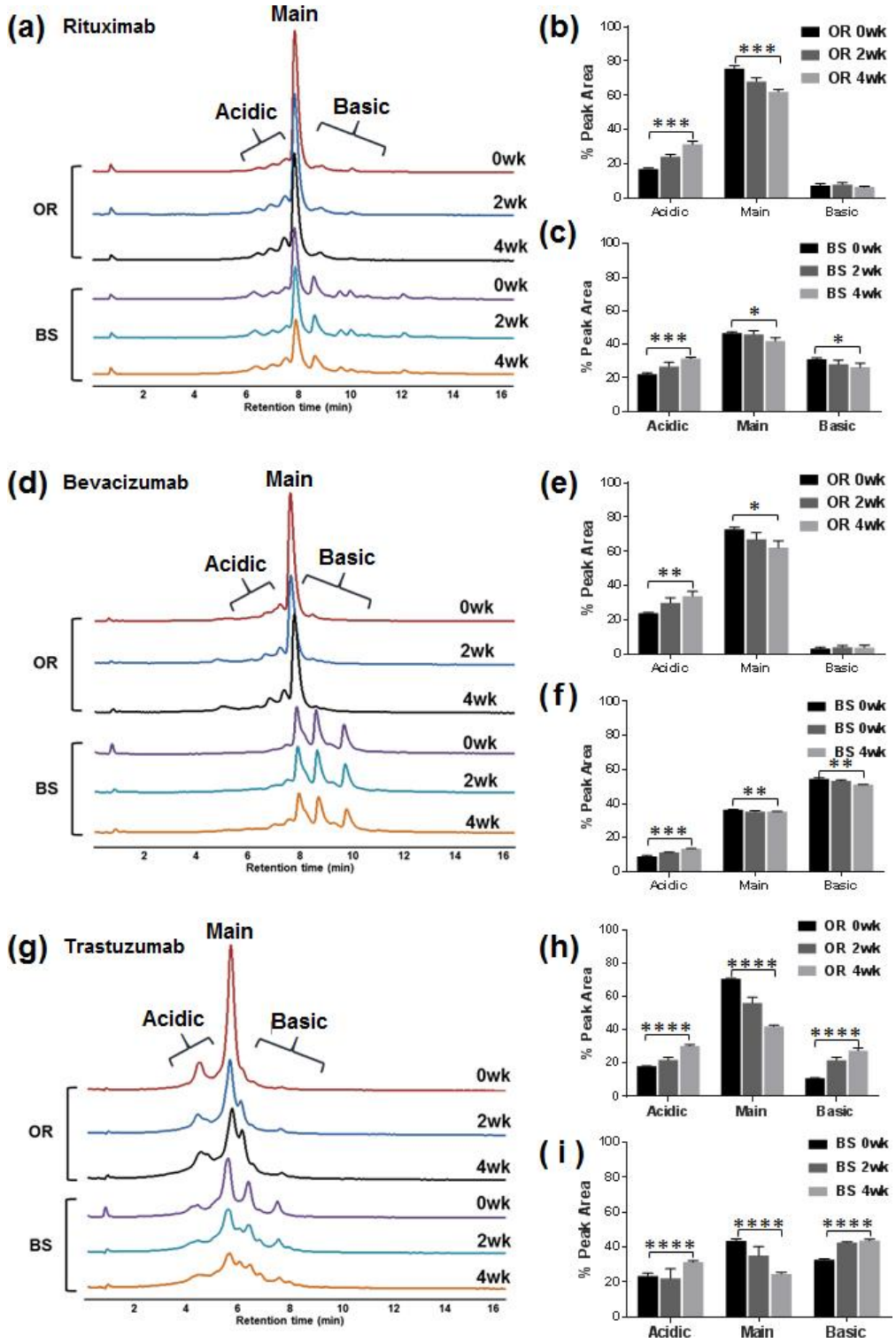

Figure 4-6 *Representative CEX chromatograms of (a) the rituximab pair, (d) the bevacizumab pair and (g) the trastuzumab pair. The calculated percentage area of acidic, main and basic peaks of (b, c) the rituximab pair (e, f) the bevacizumab pair and (h, i) the trastuzumab pair. (N = 3; mean ± SD, Student's t-test, *p<0.05, **p<0.01, ***p<0.001, ****p<0.0001*

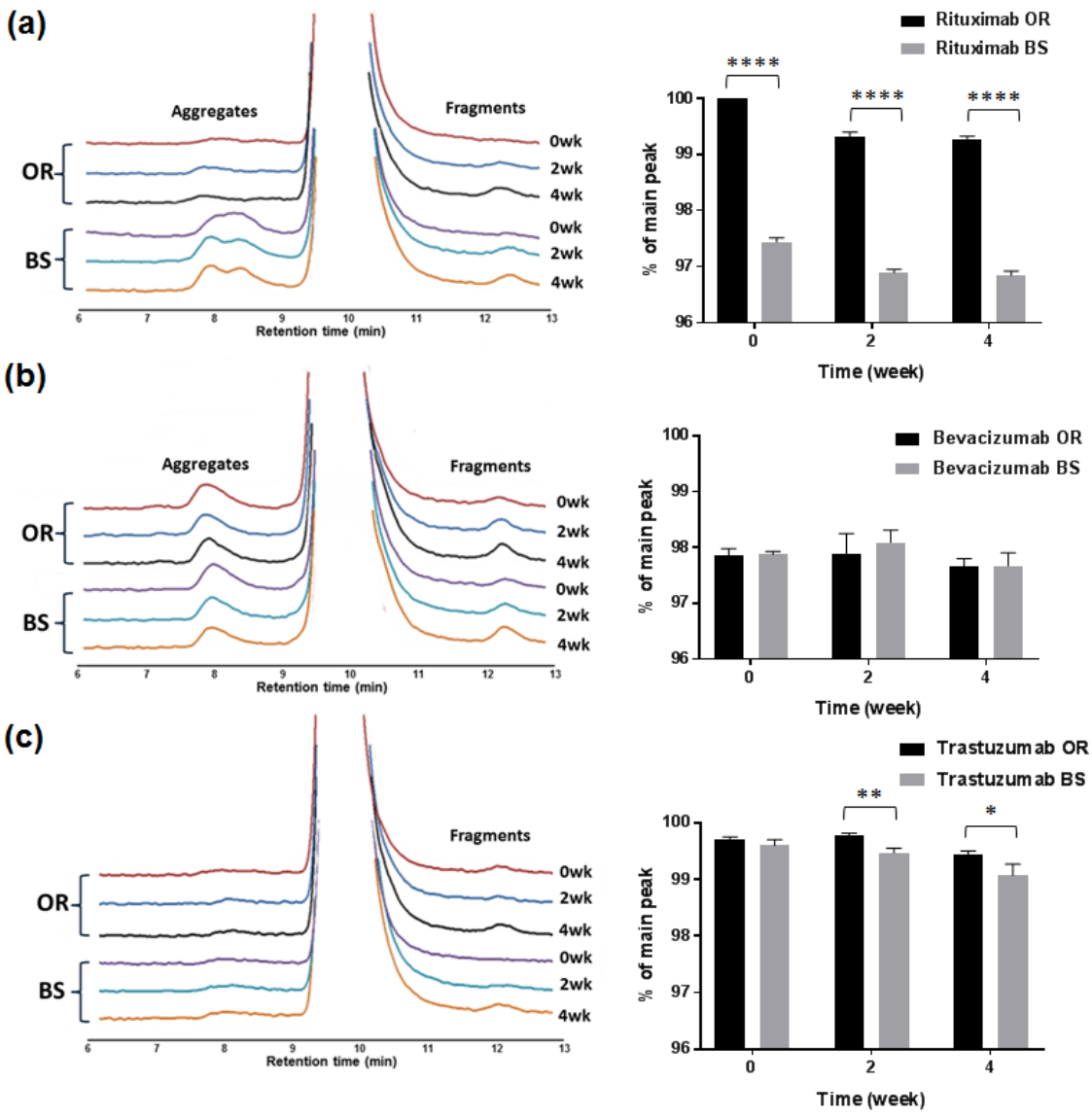

Figure 4-7 *Representative SEC chromatograms and the calculated percentage of main peak of (a) the rituximab pair, (b) bevacizumab pair and (c) trastuzumab pair. (N = 3; mean ± SD, Student's t-test, *p<0.05, **p<0.01, ****p<0.0001)*

significant difference was detected for each band over the course of incubation. Two distinct bands were detected under reducing conditions, corresponding to heavy and light chain. Only the bevacizumab pair showed faint bands around 41 KDa, which indicates a degraded heavy chain, with a band intensity that gradually increased upon incubation. (Figure 4-8)

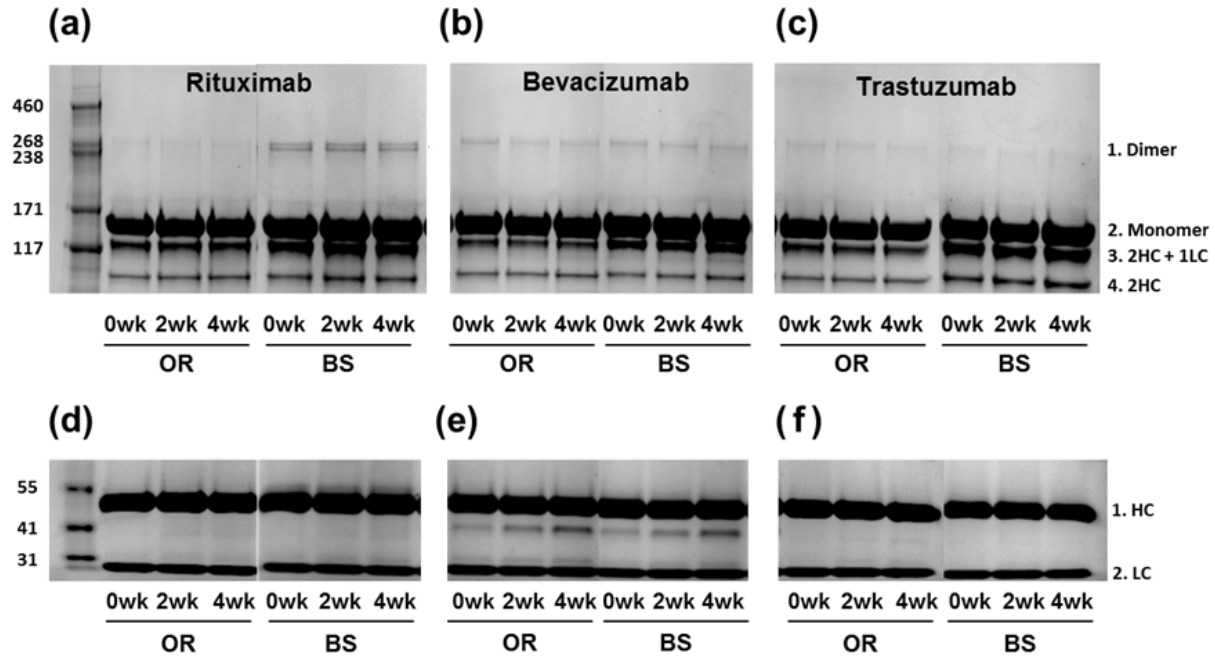

Figure 4-8 *Non-reducing SDS-PAGE gel of (a) the rituximab pair, (b) the bevacizumab pair and (c) the trastuzumab pair and reducing SDS-PAGE gel of (d) the rituximab pair, (e) the bevacizumab pair and (f) the trastuzumab pair at 0,2 and 4 weeks thermal stress. HC: heavy chain, LC: light chain*

4.5 **Discussion**

In this study, forced degradation was used to compare the biosimilarity of OR and BS pairs in terms of the presence of initial structural differences and how those aspects change when subject to thermal stress. Three different pairs, including rituximab, bevacizumab and trastuzumab, were used for the entire analysis. Although each pair of drug products were manufactured with identical cell lines (Chinese Hamster Ovary cells) and formulations [391], they were still subjected to the inherent variability of manufacturing processes. All samples were diluted to 1 mg/ml with 0.9% NaCl, the appropriate condition for intravenous infusion when administered. [384,392,393] Then,

structural analyses were performed with various techniques to identify and track how initial differences between the OR and BS pairs changed upon incubation

Our study revealed that both the OR and BS for all drug products are structurally stable after 4 weeks of thermal stress. No differences in terms of secondary and tertiary structures measured by CD and IF were detectable over the course of incubation. This reflects how structurally stable mAbs are below their melting temperature. Previous studies have demonstrated that thermal unfolding of antibodies occurs over 55 ºC, with CD spectra shapes changing when incubated above this temperature [394–396]. In addition, a recent study subjecting Remicade and Remsima to both high humidity and thermal stress at 40ºC showed highly similar secondary structure data by CD over the entire course of incubation. However, unlike our result, a decrease in maximum fluorescence intensity was observed with high homology between two products by IF [318].

Aggregation and fragmentation were measured by SEC. The AUC of the monomer peak remained similar over the course of incubation, with a rate of monomer loss measured within 1 % for all three pairs for 4 weeks. No significant increases in aggregation levels were detected by SEC and SDS-PAGE. The trastuzumab pairs showed the lowest levels of initial aggregation, which is likely attributed to the fact that, as opposed to the other mAb pairs which are already in solution, trastuzumab is a lyophilized product that is mixed with water prior to injection. Interestingly, the relative levels of aggregation and fragmentation remained similar over the course of incubation, reflecting the ability of the formulation to prevent aggregation for each mAb pair even when diluted (Rituximab contains polysorbate 80 while bevacizumab and trastuzumab

contain polysorbate 20.) Buffer systems without surfactant have been used as another stress condition to truly test if the formulation was responsible for the prevention of aggregate formation. [397–400] However, it should be noted that buffers without surfactant differ from a real-world situation. A recent briefing document for FDA biosimilar approval indicated that Remicade and Remsima showed comparable levels of the monomer peak with no discernable changes detected when incubated (containing polysorbate 80) at 40ºC for 3 months. [96] In addition, a long-term stability study of diluted rituximab at 40ºC was performed for 6 months, where similar levels of aggregates, increased fragmentation and unchanged structural contents were reported, which aligns with our results. [401] In general, SDS-PAGE showed better resolution than SEC regarding the detection of fragments; SEC chromatograms only showed one fragment peak, whereas SDS-PAGE showed 5 fragment peaks including 2HC+1LC, 2HC and 1HC.

CIU-IM-MS analysis provided a gas phase folding stability profile for the OR and BS pairs both before and after incubation. The trastuzumab pair showed the most notable change in unfolding via different CIU50 values when comparing unstressed and 4-week stressed. Again, this may be attributed to trastuzumab's lyophilized formulation, unlike the other mAb pairs that are shipped as liquid formulations. Based on our results, the CIU50 approach is capable of monitoring subtle changes in mAbs between the OR and BS pairs as well as between stressed and unstressed mAbs. Recently, Kerr et. al used CIU-IM-MS data to compare the structural stability of originators rituximab, bevacizumab and trastuzumab when subject to incubation at 25 ± 2ºC for 6 months. In this study, bevacizumab showed the most differences in unfolding after incubation, indicated by the presence of an additional transition in the CIU plots. [402] This difference from our findings

can be attributed to the different methods used to quantify changes in structural stability – Kerr et al based structural stability on the 25+ charge state and a scaled deviation score value that was further supported by root-mean-squared deviation (RMSD), while our data is based on the 24+ charge state CIU50 following sigmoidal fitting. The CIU value is relatively independent of signal intensity and, in some cases, provides a better diagnostic for comparing stability shifts in samples, whereas RMSD tells us information about where those differences are most intense in the CIU. [350]

CEX analysis showed the most initial differences between the OR and BS pairs, which included an especially high level of basic variants in all three BS drugs. The basic variants, typically characterized by differences in C-terminal lys presence, tends to be benign in terms of their effect on mAb safety or efficacy. [190] However, deamidation of asparagine residues located on the CDR regions can reduce antigen binding affinity . [318,403–405] Further fraction collection and follow-up MS analysis is needed to identify the exact deamidation site of each acidic peak variant. Interestingly, the CEX peak identities became less distinctive over the course of incubation while area under the curve remained similar (RSD less than 5%). A similar tendency was also observed in a previous study when IgG1 subjects to thermal stress at 25 ºC for 12 months with mild chemical oxidation by tBHP. CEX peaks became indistinctive due to the formation of a basic shoulder derived from methionine sulfoxide that retains longer on the CEX column. [406] In addition, an increase of acidic variants was commonly observed upon thermal stress [186,403,407–410] where the OR and BS also showed an increased level of acidic variants upon incubation.

Intact MS analysis showed initial difference between the OR and BS regarding the global mAb structure. While intact MS can provide a fast analysis of the major glycoforms and some PTMs, such as C-terminal lysine, it is hard to assign other chemical modifications with small mass differences such as deamidation (+1) and oxidation (+16) by intact MS. [163] Overall, glycans were well matched between the OR and BS. A difference in peak numbers, derived from different numbers of C-terminal lysine which were also well corresponded to CEX data, showed distinctive basic charge variant peaks that OR drugs did not contain.

Taken together, our research highlights the comparison of higher order structure and charge variants between the OR and the BS when subject to thermal stress conditions. Because of the highly similar properties between the OR and the BS, their behaviors were similar when subject to thermal incubation. We demonstrated the capability of CIU-IM-MS to detect subtle differences between the OR and the BS. Future studies are needed to identify changes of individual amino acid modifications and their effect on biological activity, which would provide valuable data on the actual effect of thermal stress.

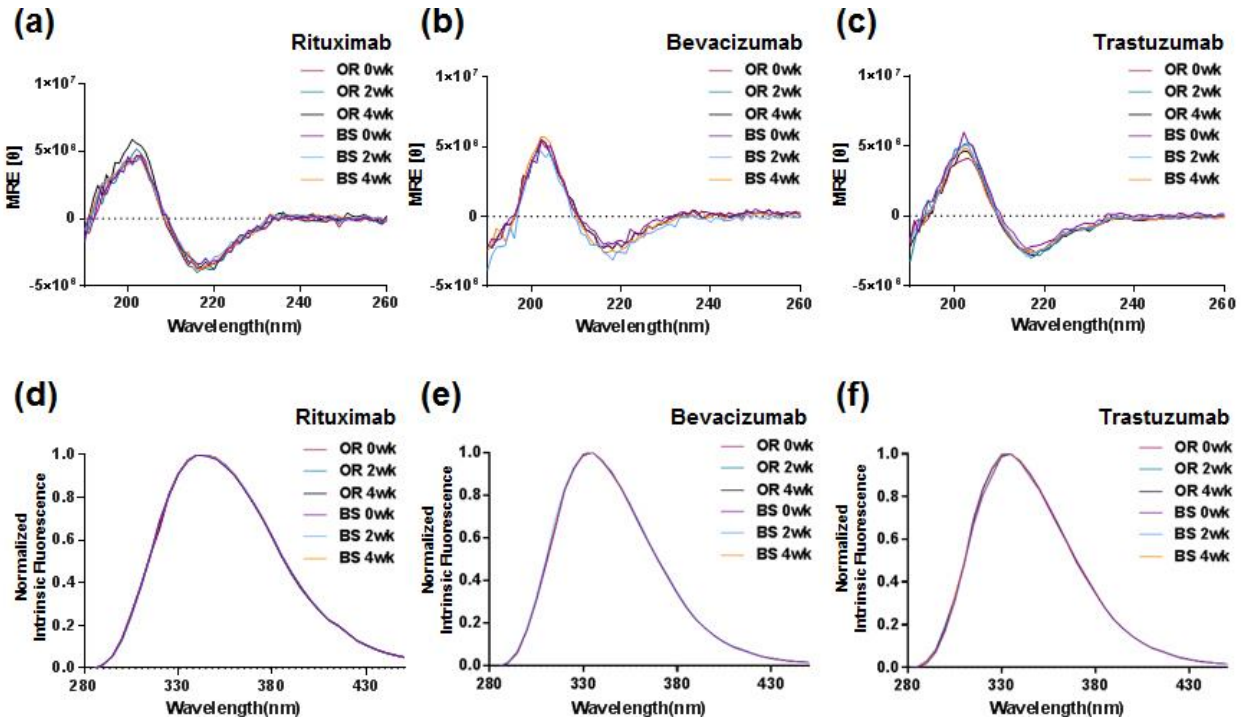

Figure 4-9 *Representative far UV circular dichroism spectra of (a) the rituximab pair, (b) the bevacizumab pair and (c) the trastuzumab pair at 0 and 4 weeks. Representative intrinsic fluorescence spectra of (d) the rituximab pair, (e) the bevacizumab pair and (f) the trastuzumab pair at 0 and 4 weeks.*

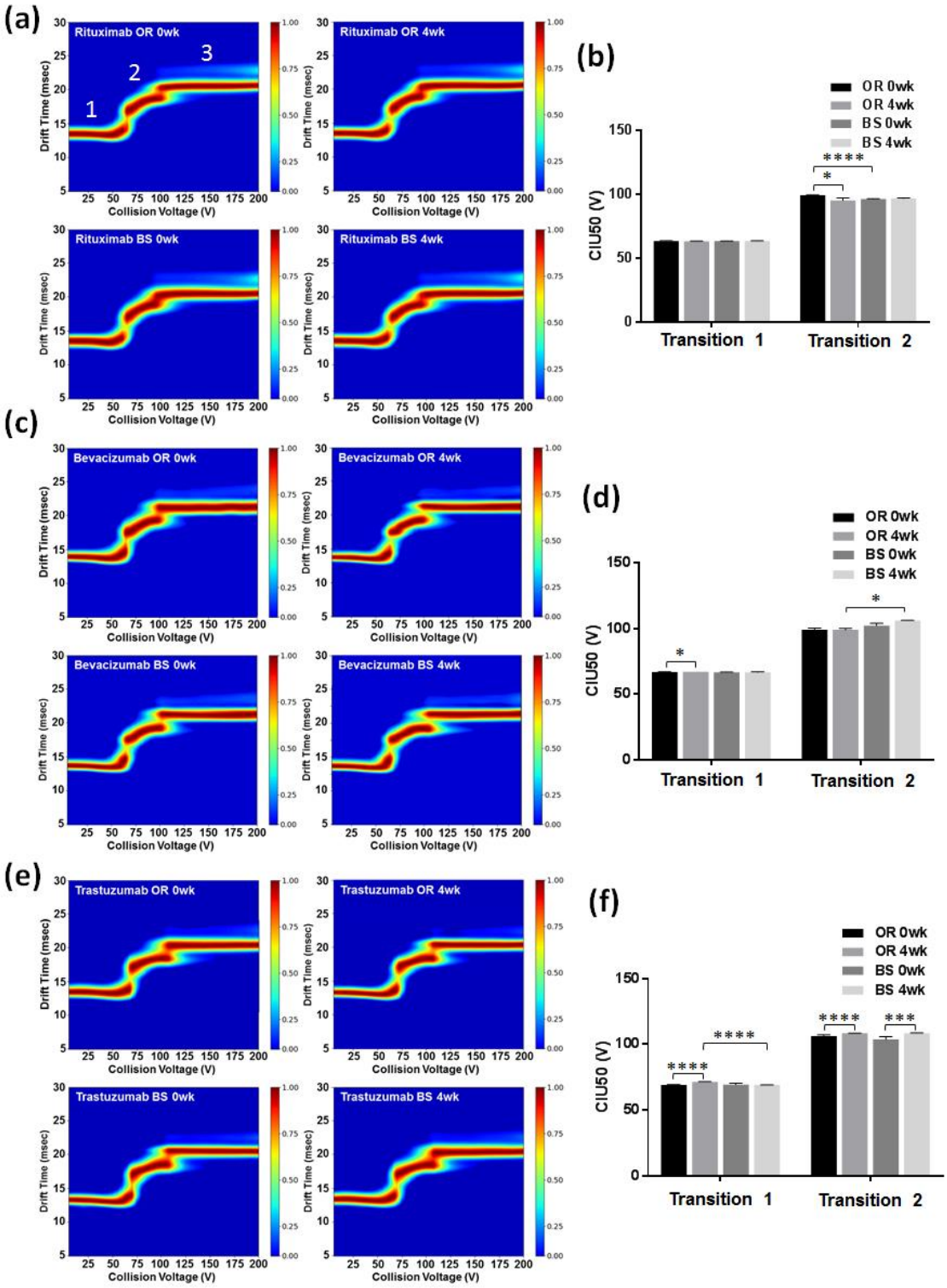

Figure 4-10 *Representative CIU fingerprints of (a) the rituximab pair (c) the bevacizumab pair and (e) the trastuzumab pair and CIU50 values of (b) the rituximab pair (d) the bevacizumab pair and (f) the trastuzumab pair at 0 and 4 weeks. (N = 3; mean ± SD, Student's t-test, *p<0.05, ***p<0.001, ****p<0.0001)*

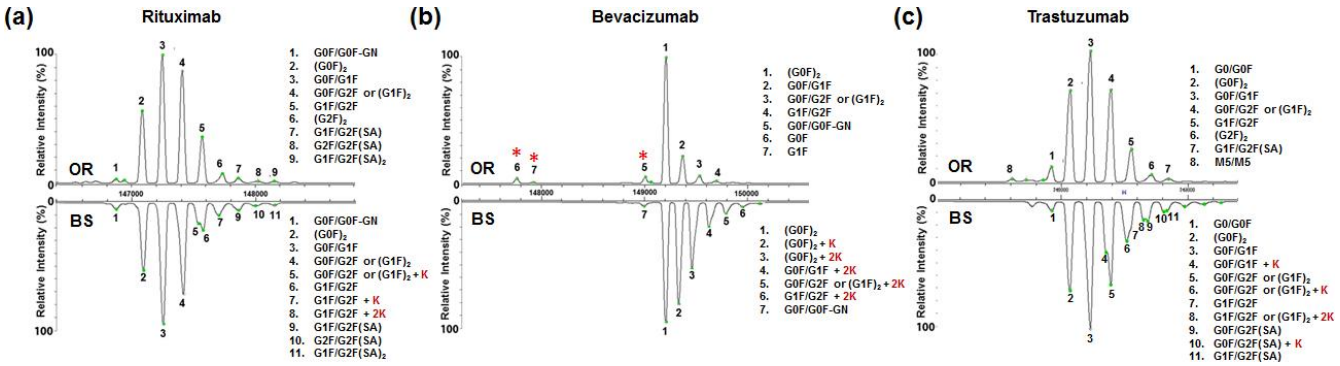

Figure 4-11 *Comparison of deconvoluted mass spectra with annotated glycoforms and C-terminal Lys of (a) the rituximab pair, (b) the bevacizumab pair and (c) the trastuzumab pair at 4-week thermal stress.*

Table 4-2 *Secondary structure composition of the rituximab, bevacizumab and trastuzumab pairs over the course of incubation at 40ºC.*

Sample		Incubation	α-helix	β-sheet	β-turn	Random coil
Rituximab	OR	0wk	2.3 ± 0.6	45.2 ± 2.1	20.2 ± 0.5	32.3 ± 1.1
		2wk	2.5 ± 0.3	45.1 ± 0.9	20.2 ± 0.2	32.3 ± 0.4
		4wk	2.7 ± 0.2	45.1 ± 1.4	20.1 ± 0.4	32.1 ± 1.0
	BS	0wk	2.2 ± 0.5	45.4 ± 1.7	20.2 ± 0.4	32.2 ± 0.4
		2wk	1.9 ± 0.6	45.7 ± 1.9	19.8 ± 0.6	32.6 ± 1.4
		4wk	2.5 ± 0.2	44.6 ± 0.2	20.3 ± 0.1	32.5 ± 0.3
Bevacizumab	OR	0wk	2.6 ± 0.2	43.5 ± 0.4	20.2 ± 0.1	33.7 ± 0.3
		2wk	2.4 ± 0.4	43.9 ± 1.6	20 ± 0.4	33.8 ± 0.8
		4wk	2.5 ± 0.1	43.5 ± 0.1	20.3 ± 0.1	33.7 ±0.1
	BS	0wk	2.4 ± 0.1	43.6 ± 0.1	20.2 ± 0.1	33.8 ± 0.1
		2wk	2.5 ± 0.2	43.5 ± 1.0	20.3 ± 0.4	33.7 ± 0.1
		4wk	2.2 ± 0.2	44.6 ± 0.3	19.9 ± 0.4	33.3 ± 0.3
Trastuzumab	OR	0wk	2.4 ± 0.2	44.9 ± 1.3	20.3 ± 0.4	32.3 ± 0.8
		2wk	2.5 ± 0.3	45.6 ± 0.9	20.1 ± 0.3	31.8 ± 0.6
		4wk	3.1 ± 0.5	42.8 ± 2.2	20.6 ± 0.5	33.5 ± 1.2
	BS	0wk	2.9 ± 0.1	43.2 ± 0.6	20.8 ± 0.3	33.1 ± 0.4
		2wk	3.0 ± 0.2	42.8 ± 1.1	21.0 ± 0.3	33.3 ± 0.7
		4wk	2.9 ± 0.1	43.4 ± 0.2	20.9 ± 0.1	32.8 ± 0.1

Chapter 5: Conclusions and Prospective

The work presented in this thesis compares originator (innovator) and biosimilar biologics using various analytical techniques to validate biosimilarity. The utility of state-of-the-art-techniques, orthogonal methods and stressed conditions provide valuable data on how to test for biosimilarity regarding the structural and functional aspects of these biologic molecules.

The use of biosimilars provide a great option for patients by increasing their access to life-saving treatments at lower costs. In chapter 2, we focused on structural comparison between the originator and the biosimilar filgrastim which had a relatively simple structure and small numbers of PTMs relative to those found in our studied mAb drugs. We observed identical primary structures and very similar higher order structures. While previous studies from other biosimilar developers have reported analytical comparability between the originator and biosimilar using various analytical techniques, we were the first to show its comparative unfolding pattern by IM-MS. The 2D-NMR analysis performed to compare biosimilar filgrastim to the originator Neupogen had been submitted to the US FDA to prove the structural similarity of these two products which implications that allowed the company to avoid performing a costly clinical comparability study. The similarity between the oxidation levels at Met residues located in close proximity to the G-CSF receptor binding sites have been used to infer similar biological activity between the originator and biosimilar. However, investigating the actual similarity for target binding between the two products could further confirm their similarity.

In chapter 3, we analyzed the structural comparability between originator and a biosimilar rituximab a specific focus on glycosylation differences and their impact on biological activity. Both showed almost identical primary and higher order structures with minor differences in PTM levels, which include pyroGlu formation, C-terminal Lys clipping and glycoform distributions. A study by our laboratory has shown that afucosylation differences between the originator and the biosimilar can result in different FcγIIIa receptor binding affinities, potentially resulting in differences in clinical efficacy of the two products. This is especially important for drugs like rituximab that treat diseases which are Fc-mediated efficacy like IBD and cancer. [53,376] Based on this observation, rituximab was chosen as a model drug to correlate afucosylation levels with the drug's biological activity - ADCC. The biosimilar showed higher afucosylation levels which manifested into both a higher FcγIIIa receptor binding affinity and ADCC activity. Importantly, we saw different detection sensitivities for glycoform distributions which were highly analytical method dependent, which further underlines the value of the use of orthogonal analytical techniques and the high glycoform resolving power of LC-MS/MS methodology. In addition, MAM was proven to provide extensive data on several quality attributes such as the primary sequence, amino acid modification and glycan distribution by a single method. These MAM approaches will be a crucial part of biosimilar development.

Finally, we showed several initial structural differences and similarities present in the three different mAb originator-biosimilar pairs and then compared them after exposure to thermal stress conditions, which can be found in Chapter 4. The idea was that subtle initial differences present between the originator and biosimilar could be amplified when

the proteins are subjected to forced degradation conditions, while their behaviors in response to the stress conditions would be similar. The most distinct differences between the originators and the biosimilars are detected in major glycoform and charge variant distributions that are commonly defined by the manufacturing process. After applying thermal stress, we saw differences in unfolding patterns by CIU-IM-MS that were seemingly derived from the difference in initial dosage forms, one as a solution and the other a lyophilized cake. Additional studies on the biological activity of each mAb after thermal stress would provide valuable data on confirming true stability and biosimilarity. Additional experiments to assess PTMs at the amino acid level are also necessary in order to understand the source of charge variants. While the work presented in Chapter 4 is mainly related to higher order structures, it presents a non-traditional way of demonstrating biosimilarity.

The main concerns regarding biosimilars that have been raised are differences of immunogenicity and efficacy between an originator and a biosimilar in certain specific disease indications. These two aspects of innovator and biosimilar differences are especially importiant clinically when considering biosimilar interchangeability. If the biosimilar is designated as interchangeable, the switch of prescription from an originator to a biosimilar (or vice versa) could be performed by a pharmacist without the knowledge of either the patient or physician. While there are currently no interchangeable biosimilars approved in US, the FDA has recently released its final guidance for the demonstration of biosimilar interchangeability. [411] Boehringer Ingelheim has started a switching study with the intent for its adalimumab biosimilar to be designated as interchangeable. Recent studies comparing the infliximab originator and two biosimilars revealed variation in

afucosylation levels, which resulted in a significant difference in the relative FcγRIIIa receptor binding affinity while following a similar trend for ADCC. [53,328] The results of the NOR-SWITCH study on switching from originator to biosimilar treatment showed that the biosimilar showed the rate difference of -14.4% with Crohn's disease patients (close to the pre-defined 15% non-inferiority margin). [412] This result has raised a question about whether the biosimilar is less effective in Crohn's disease. In this regard, our research investigating the differences in afucosylation and ADCC between an originator and a biosimilar could provide insights for acceptable specifications for interchangable biosimilar products. By establishing specifications around afucosylation levels, the differences in patient responses upon switching could be minimized. Thus, future studies need to be completed to establish how much afucosylation and ADCC variation is necessary to be considered clinically meaningful. Auxiliary to glycan differences, an allelic V-F polymorphism in FCGR3 gene at residue 158 result in individual patient's different response to mAb treatment (V/V – strong response). [413] Therefore, understanding the collective impact of glycosylation differences and genetic polymorphism on treatment efficacy could unlock new possibilities in personalized medicine approaches.

Bibliography

[1] Chiavenna SM, Jaworski JP, Vendrell A. State of the art in anti-cancer mAbs. J Biomed Sci 2017;24:1–12.

[2] Rodney J. Y. H, Milo G. Hematopoietic Growth and Coagulation Factors. Biotechnol. Biopharm. Transform. Proteins Genes into Drugs. 2nd ed., Hoboken, New Jersey: John Wiley & Sons, Inc; 2013, p. 211–50.

[3] Rosman Z, Shoenfeld Y, Zandman-Goddard G. Biologic therapy for autoimmune diseases: An update. BMC Med 2013;11:1–12.

[4] Marston HD, Paules CI, Fauci AS. Monoclonal Antibodies for Emerging Infectious Diseases — Borrowing from History. Perspective 2018;378:1469–72. doi:10.1056/NEJMp1002530.

[5] Statistica. No Title 2018.

[6] Chames P, Van Regenmortel M, Weiss E, Baty D. Therapeutic antibodies: Successes, limitations and hopes for the future. Br J Pharmacol 2009;157:220–33. doi:10.1111/j.1476-5381.2009.00190.x.

[7] Neves H, Kwok HF. Recent advances in the field of anti-cancer immunotherapy. BBA Clin 2015;3:280–8. doi:10.1016/j.bbacli.2015.04.001.

[8] Iwamoto N, Shimada T. Recent advances in mass spectrometry-based approaches for proteomics and biologics: Great contribution for developing therapeutic antibodies. Pharmacol Ther 2018;185:147–54. doi:10.1016/j.pharmthera.2017.12.007.

[9] Declerck PJ. Biologicals and biosimilars: a review of the science and its implications. Generics Biosimilars Initiat J 2012;1:13–6. doi:10.5639/gabij.2012.0101.005.

[10] Reynolds T, de Zafra C, Kim A, Gelzleichter TR. Overview of Biopharmaceuticals and Comparison with Small-molecule Drug Development. Nonclinical Dev. Nov. Biol. Biosimilars, Vaccines Spec. Biol., 2013, p. 3–33. doi:10.1016/B978-0-12-394810-6.00001-0.

[11] Morrow T, Felcone LH. Defining the difference: What Makes Biologics Unique. Biotechnol Healthc 2004;1:24–9. doi:10.1177/2050640615590302.

[12] CDER/CBER, FDA. Scientific Considerations in Demonstrating Biosimilarity to a Reference Product Guidance for Industry Scientific Considerations in Demonstrating Biosimilarity to a Reference Product. vol. April. 2015.

[13] European Medicine Agency. Guideline on similar biological medicinal products. 2015.

[14] CDER. List of Licensed Biological Products. 2018.

[15] European Medicines Agency. European public assessment reports on authorised biosimilar medicines 2018. http://www.ema.europa.eu/ema/index.jsp?curl=pages%2Fmedicines%2Flanding%2Fepar_search.jsp&mid=WC0b01ac058001d124&searchTab=searchByAuthType&alreadyLoaded=true&isNewQuery=true&status=Authorised&keyword=Enter+keywords&searchType=name&taxonomyPath=&treeNumbe (accessed June 28, 2018).

[16] U.S. Food and Drug Administration. Good ANDA Submission Practices Guidance for Industry. 2018.

[17] European Medicines Agency. European Medicines Agency procedural advice for users of the centralised procedure for generic/hybrid applications. 2017.

[18] Tsuruta LR, Lopes dos Santos M, Moro AM. Biosimilars advancements: Moving on to the future. Biotechnol Prog 2015;31:1139–49. doi:10.1002/btpr.2066.

[19] Socinski MA, Curigliano G, Jacobs I, Gumbiner B, MacDonald J, Thomas D. Clinical considerations for the development of biosimilars in oncology. MAbs 2015;7:286–93. doi:10.1080/19420862.2015.1008346.

[20] Weise M, Kurki P, Wolff-Holz E, Bielsky MC, Schneider CK. Biosimilars: The science of extrapolation. Blood 2014;124:3191–6. doi:10.1182/blood-2014-06-583617.

[21] Feagan BG, Choquette D, Ghosh S, Gladman DD, Ho V, Meibohm B, et al. The challenge of indication extrapolation for infliximab biosimilars. Biologicals 2014;42:177–83. doi:10.1016/j.biologicals.2014.05.005.

[22] Biosimilars approved in Europe. Online, GaBi 2016. http://www.gabionline.net/Biosimilars/General/Biosimilars-approved-in-Europe.

[23] Blackstone E, Fuhr JP. Innovation and Competition. Biotechnol Healthc 2012:24–7.

[24] CDER. List of Licensed Biological Products. 2019.

[25] European Medicines Agency. Guideline on Similar Biological Medicinal Products Containing Biotechnology-Derived Proteins As Active Substance: Quality Issues (revision 1). 2014.

[26] U.S. Food and Drug Administration. Scientific Considerations in Demonstrating Biosimilarity to a Reference Product Guidance for Industry. 2015.

[27] U.S. Food and Drug Administration. Clinical Pharmacology Data to Support a Demonstration of Biosimilarity to a Reference Product Guidance for Industry. 2016.

[28] European Medicines Agency. Guideline on Similar Biological Medicinal Products Containing Biotechnology-Derived Proteins As Active Substance: Quality Issues. vol. 44. 2012. doi:10.1136/bmj.333.7574.873-a.

[29] Lai T, Yang Y, Ng SK. Advances in Mammalian Cell Line Development Technologies. Pharmaceuticals 2013;6:579–603. doi:10.3390/ph6050579.

[30] Boeger H, Bushnell DA, Davis R, Griesenbeck J, Lorch Y, Strattan JS, et al. Structural basis of eukaryotic gene transcription. FEBS Lett 2005;579:899–903.

[31] Ghaderi D, Zhang M, Hurtado-Ziola N, Varki A. Production platforms for biotherapeutic glycoproteins. Occurrence, impact, and challenges of non-human sialylation. Biotechnol Genet Eng Rev 2012;28:147–75. doi:10.5661/bger-28-147.

[32] Conner J, Wuchterl D, Lopez M, Minshall B, Prusti R, Boclair D, et al. Chapter 26 – The Biomanufacturing of Biotechnology Products. Biotechnol. Entrep., 2014, p. 351–85. doi:10.1016/B978-0-12-404730-3.00026-9.

[33] Patel PK, King CR, Feldman SR. Biologics and biosimilars. J Dermatolog Treat 2015;26:299–302. doi:10.3109/09546634.2015.1054782.

[34] Schiestl M, Stangler T, Torella C, Čepeljnik T, Toll H, Grau R. Acceptable changes in quality attributes of glycosylated biopharmaceuticals. Nat Biotechnol 2011;29:310–2. doi:10.1038/nbt.1839.

[35] Damen CWN, Chen W, Chakraborty AB, van Oosterhout M, Mazzeo JR, Gebler JC, et al. Electrospray Ionization Quadrupole Ion-Mobility Time-of-Flight Mass Spectrometry as a Tool to Distinguish the Lot-to-Lot Heterogeneity in N-Glycosylation Profile of the Therapeutic Monoclonal Antibody Trastuzumab. J Am Soc Mass Spectrom 2009;20:2021–33. doi:10.1016/j.jasms.2009.07.017.

[36] European Medicines Agency. Guideline on process validation for the manufacture of biotechnology-derived active substances and data to be provided in the regulatory submissionTitle. 2016.

[37] U.S. Food and Drug Administration. Analytical Procedures and Methods Validation for Drugs and Biologics Guidance for Industry. 2015.

[38] U.S. Food and Drug Administration. Chemistry, Manufacturing, and Controls Changes to an Approved Application: Certain Biological Products Draft Guidance for Industry. 2017.

[39] U.S. Food and Drug Administration. Guidance for Industry Q5E Comparability of Biotechnological/Biological Products Subject to Changes in Their Manufacturing Process. 2005.

[40] European Medicines Agency. Guideline on Comparability of Biotechnology-derived Medicinal Products after a Change in the Manufacturing Process. 2007.

[41] International Conference on Harmonisation (ICH). ICH Harmonised Tripartite Guideline Pharmaceutical Development Q8(R2). 2009.

[42] Vandekerckhove K, Seidl A, Gutka H, Kumar M, Gratzl G, Keire D, et al. Rational Selection , Criticality Assessment , and Tiering of Quality Attributes and Test Methods for Analytical Similarity Evaluation of Biosimilars 2018:1–9. doi:10.1208/s12248-018-0230-9.

[43] Chow S-C, Liu L. Analytical Similarity Assessment. In: Endrenyi L, Declerck PJ, Chow S-C, editors. Biosimilar Drug Prod. Dev., Boca Raton: Taylor & Francis Group; 2017, p. 83–108.

[44] Kirchhoff CF, Wang XZM, Conlon HD, Anderson S, Ryan AM, Bose A. Biosimilars: Key regulatory considerations and similarity assessment tools. Biotechnol Bioeng 2017;114:2696–705. doi:10.1002/bit.26438.

[45] Olson EJ, Coleman DA. FDA Draft Guidance for Industry: Statistical Approaches to

Evaluate Analytical Similarity Docket No. FDA-2017-D-5525: Comments from Genentech a Member of the Roche Group. 2017.

[46] Brenna Z. Sandoz Raises Questions With FDA Draft Guidance on Statistical Approaches for Biosimilars. Regul Focus 2017. https://www.raps.org/regulatory-focus™/news-articles/2017/10/sandoz-raises-questions-with-fda-draft-guidance-on-statistical-approaches-for-biosimilars.

[47] U.S. Food and Drug Administration. FDA Withdraws Draft Guidance for Industry: Statistical Approaches to Evaluate Analytical Similarity 2018. https://www.fda.gov/Drugs/DrugSafety/ucm611398.htm.

[48] American Association of Pharmaceutical Scientists. Comments on Draft Guidance: Statistical Approaches to Evaluate Analytical Similarity Docket No. FDA-2017-D-5525. 2017.

[49] European Medicines Agency. Meeting Report : Workshop on the draft reflection paper on statistical methodology for the comparative assessment of quality attributes in drug development. 2018.

[50] Beck A, Sanglier-Cianférani S, Van Dorsselaer A. Biosimilar, biobetter, and next generation antibody characterization by mass spectrometry. Anal Chem 2012;84:4637–46. doi:10.1021/ac3002885.

[51] Cai X-Y, Wake A, Gouty D. Analytical and bioanalytical assay challenges to support comparability studies for biosimilar drug development. Bioanalysis 2013;5:517–20. doi:10.4155/bio.13.1.

[52] Alexander PA, He Y, Chen Y, Orban J, Bryan PN. A minimal sequence code for switching protein structure and function. Proc Natl Acad Sci 2009;106:21149–54. doi:10.1073/pnas.0906408106.

[53] Pisupati K, Tian Y, Okbazghi S, Benet A, Ackermann R, Ford M, et al. A Multidimensional Analytical Comparison of Remicade and the Biosimilar Remsima. Anal Chem 2017;89:4838–46. doi:10.1021/acs.analchem.6b04436.

[54] Hong J, Lee Y, Lee C, Eo S, Kim S, Lee N, et al. Physicochemical and biological characterization of SB2, a biosimilar of Remicade® (infliximab). MAbs 2017;9:364–82. doi:10.1080/19420862.2016.1264550.

[55] Jung SK, Lee KH, Jeon JW, Lee JW, Kwon BO, Kim YJ, et al. Physicochemical characterization of Remsima®. MAbs 2014;6:1163–77. doi:10.4161/mabs.32221.

[56] Beck A, Debaene F, Diemer H, Wagner-Rousset E, Colas O, Dorsselaer A Van, et al. Cutting-edge mass spectrometry characterization of originator, biosimilar and biobetter antibodies. J Mass Spectrom 2015;50:285–97. doi:10.1002/jms.3554.

[57] Xie H, Chakraborty A, Ahn J, Yu YQ, Dakshinamoorthy DP, Gilar M, et al. Rapid comparison of a candidate biosimilar to an innovator monoclonal antibody with advanced liquid chromatography and mass spectrometry technologies. MAbs 2010. doi:10.4161/mabs.11986.

[58] Wang H, Tang HY, Tan GC, Speicher DW. Data analysis strategy for maximizing high-

confidence protein identifications in complex proteomes such as human tumor secretomes and human serum. J Proteome Res 2011;10:4993–5005. doi:10.1021/pr200464c.

[59] Gahoual R, Burr A, Busnel JM, Kuhn L, Hammann P, Beck A, et al. Rapid and multi-level characterization of trastuzumab using sheathless capillary electrophoresis-tandem mass spectrometry. MAbs 2013;5:479–90. doi:10.4161/mabs.23995.

[60] Gahoual R, Biacchi M, Chicher J, Kuhn L, Hammann P, Beck A, et al. Monoclonal antibodies biosimilarity assessment using transient isotachophoresis capillary zone electrophoresis-tandem mass spectrometry. MAbs 2014;6:1464–73. doi:10.4161/mabs.36305.

[61] The United States Pharmacopeial Convention. 2018 U.S. Pharmacopoeia-National Formulary [USP 40-NF35], <1052> Biotechnology-derived Articles-Amino Acid Analysis. 2018.

[62] Soga T, Heiger DN. Amino acid analysis by capillary electrophoresis electrospray ionization mass spectrometry. Anal Chem 2000;72:1236–41. doi:10.1021/ac990976y.

[63] Soga T, Kakazu Y, Robert M, Tomita M, Nishioka T. Qualitative and quantitative analysis of amino acids by capillary electrophoresis-electrospray ionization-tandem mass spectrometry. Electrophoresis 2004;25:1964–72. doi:10.1002/elps.200305791.

[64] CDER/CBER, FDA. Quality Considerations in Demonstrating Biosimilarity of a Therapeutic Protein Product to a Reference Product. 2015.

[65] Bandyopadhyay S, Mahajan M, Mehta T, Singh AK, Gupta AK, Parikh A, et al. Physicochemical and functional characterization of a biosimilar adalimumab ZRC-3197. Biosimilars 2014;5:1–18. doi:10.2147/BS.S75573.

[66] Liu J, Eris T, Li C, Cao S, Kuhns S. Assessing Analytical Similarity of Proposed Amgen Biosimilar ABP 501 to Adalimumab. BioDrugs 2016;30:321–38. doi:10.1007/s40259-016-0184-3.

[67] Pelton JT, McLean LR. Spectroscopic methods for analysis of protein secondary structure. Anal Biochem 2000;277:167–76. doi:10.1006/abio.1999.4320 M4 - Citavi.

[68] Visser J, Feuerstein I, Stangler T, Schmiederer T, Fritsch C, Schiestl M. Physicochemical and functional comparability between the proposed biosimilar rituximab GP2013 and originator rituximab. BioDrugs 2013;27:495–507. doi:10.1007/s40259-013-0036-3.

[69] Magnenat L, Palmese A, Fremaux C, D'Amici F, Terlizzese M, Rossi M, et al. Demonstration of physicochemical and functional similarity between the proposed biosimilar adalimumab MSB11022 and Humira®. MAbs 2017;9:127–39. doi:10.1080/19420862.2016.1259046.

[70] Deechongkit S, Aoki KH, Park SS, Kerwin BA. Biophysical comparability of the same protein from different manufacturers: A case study using Epoetin alfa from Epogen® and Eprex®. J Pharm Sci 2006;95:1931–43. doi:10.1002/jps.20649.

[71] Barth A. Infrared spectroscopy of proteins. Biochim Biophys Acta - Bioenerg 2007;1767:1073–101. doi:10.1016/j.bbabio.2007.06.004.

[72] Jackson M, Mantsch HH. The Use and Misuse of FTIR Spectroscopy in the Determination of Protein Structure. Crit Rev Biochem Mol Biol 1995;30:95–120. doi:10.3109/10409239509085140.

[73] Kelly SM, Jess TJ, Price NC. How to study proteins by circular dichroism. Biochim Biophys Acta - Proteins Proteomics 2005;1751:119–39. doi:10.1016/j.bbapap.2005.06.005.

[74] Greenfield NJ. Using circular dichroism spectra to estimate protein secondary structure. Nat Protoc 2006;1:2876–90. doi:10.1038/nprot.2006.202.Using.

[75] Yang H, Yang S, Kong J, Dong A, Yu S. Obtaining information about protein secondary structures in aqueous solution using Fourier transform IR spectroscopy. Nat Protoc 2015;10:382–96. doi:10.1038/nprot.2015.024.

[76] Berkowitz SA, Engen JR, Mazzeo JR, Jones GB. Analytical tools for characterizing biopharmaceuticals and the implications for biosimilars. Nat Rev Drug Discov 2012;11:527–40. doi:10.1038/nrd3746.

[77] Sorgel F, Schwebig A, Holzmann J, Prasch S, Singh P, Kinzig M. Comparability of biosimilar filgrastim with originator filgrastim: Protein characterization, pharmacodynamics, and pharmacokinetics. BioDrugs 2015;29:123–31. doi:10.1007/s40259-015-0124-7.

[78] U.S. Food and Drug Administration. FDA Briefing Document Oncologic Drugs Advisory Committee Meeting BLA 125553 EP2006, a proposed biosimilar to Neupogen (filgrastim). 2015.

[79] U.S. Food and Drug Administration. FDA Briefing Document Arthritis Advisory Committee Meeting BLA 761042 GP2015, a Proposed Biosimilar to Enbrel (etanercept). 2016.

[80] Weiss WF, Gabrielson JP, Al-Azzam W, Chen G, Davis DL, Das TK, et al. Technical Decision Making With Higher Order Structure Data: Perspectives on Higher Order Structure Characterization From the Biopharmaceutical Industry. J Pharm Sci 2016;105:3465–70. doi:10.1016/j.xphs.2016.09.003.

[81] Kelly SMMM, Price NCCC. The use of circular dichroism in the investigation of protein structure and function. Curr Protein Pept Sci 2000;1:349–84. doi:10.2174/1389203003381315.

[82] Prasad PN. Fundamentals of Light–Matter Interactions. Introd. to Biophotonics, 2004, p. 92–128. doi:10.1002/0471465380.ch4.

[83] Bruylants G, Wouters J, Michaux C. Differential Scanning Calorimetry in Life Science: Thermodynamics, Stability, Molecular Recognition and Application in Drug Design. Curr Med Chem 2005;12:2011–20. doi:10.2174/0929867054546564.

[84] Clas S, Dalton C, Hancock B. Differential scanning calorimetry: applications in drug development. Pharm Sci Technolo Today 1999;2:311–20. doi:http://dx.doi.org/10.1016/S1461-5347(99)00181-9.

[85] Johnson CM. Differential scanning calorimetry as a tool for protein folding and stability. Arch Biochem Biophys 2013;531:100–9. doi:10.1016/j.abb.2012.09.008.

[86] Japelj B, Ilc G, Marušič J, Senčar J, Kuzman D, Plavec J. Biosimilar structural comparability assessment by NMR: From small proteins to monoclonal antibodies. Sci Rep 2016;6:1–12. doi:10.1038/srep32201.

[87] Vaisar T, Pennathur S, Green PS, Gharib S a, Hoofnagle AN, Cheung MC, et al. Shotgun proteomics implicates protease inhibition and complement activation in the antiinflammatory properties of HDL. J Clin Invest 2007;117:746–56. doi:10.1172/JCI26206DS1.

[88] Aubin Y, Gingras G, Sauvé S. Assessment of the three-dimensional structure of recombinant protein therapeutics by NMR fingerprinting: Demonstration on recombinant human granulocyte macrophage-colony stimulation factor. Anal Chem 2008;80:2623–7. doi:10.1021/ac7026222.

[89] Hodgson DJ, Aubin Y. Assessment of the structure of pegylated-recombinant protein therapeutics by the NMR fingerprint assay. J Pharm Biomed Anal 2017;138:351–6. doi:10.1016/j.jpba.2017.01.058.

[90] Arbogast LW, Brinson RG, Marino JP. Mapping Monoclonal Antibody Structure by 2D 13C NMR at Natural Abundance. Anal Chem 2015;87:3556–61. doi:10.1021/ac504804m.

[91] Berkowitz SA. Analytical Characterization Structural Assessment of Biosimilarity. In: Endrenyi L, Declerck P, Chow S-C, editors. Biosimilar Drug Prod. Dev., 2017, p. 15–82.

[92] Wang X, Li Q, Davies M. Development of antibody arrays for monoclonal antibody higher order structure analysis. Front Pharmacol 2013;4 AUG:1–8. doi:10.3389/fphar.2013.00103.

[93] Song Y, Yu D, Mayani M, Mussa N, Li ZJ. Monoclonal antibody higher order structure analysis by high throughput protein conformational array. MAbs 2018;10:397–405. doi:10.1080/19420862.2017.1421880.

[94] Shon D -H, Enomoto A, Yamauchi K, Kaminogawa S. Antibodies raised against peptide fragments of bovine αs1-casein cross-react with the native protein, but recognize sites distinct from the determinants on the protein. Eur J Immunol 1991;21:1475–80. doi:10.1002/eji.1830210622.

[95] Jung SK, Lee KH, Jeon JW, Lee JW, Kwon BO, Kim YJ, et al. Physicochemical characterization of Remsima?? MAbs 2014;6:1163–77. doi:10.4161/mabs.32221.

[96] U.S. Food and Drug Administration. FDA Briefing Document Arthritis Advisory Committee Meeting BLA 125544 CT-P13 , a proposed biosimilar to Remicade. 2016.

[97] Fang J, Doneanu C, Alley WR, Yu YQ, Beck A, Chen W. Advanced assessment of the physicochemical characteristics of Remicade® and Inflectra® by sensitive LC/MS techniques. MAbs 2016;8:1021–34. doi:10.1080/19420862.2016.1193661.

[98] Masson GR, Jenkins ML, Burke JE. An overview of hydrogen deuterium exchange mass spectrometry (HDX-MS) in drug discovery. Expert Opin Drug Discov 2017;12:981–94. doi:10.1080/17460441.2017.1363734.

[99] Tian Y, Han L, Buckner AC, Ruotolo BT. Collision Induced Unfolding of Intact Antibodies: Rapid Characterization of Disulfide Bonding Patterns, Glycosylation, and Structures. Anal

Chem 2015;87:11509–15. doi:10.1021/acs.analchem.5b03291.

[100] Guo J, Kumar S, Prashad A, Starkey J, Singh SK. Assessment of physical stability of an antibody drug conjugate by higher order structure analysis: Impact of thiol-maleimide chemistry. Pharm Res 2014;31:1710–23. doi:10.1007/s11095-013-1274-2.

[101] Beck A, Wagner-Rousset E, Ayoub D, Van Dorsselaer A, Sanglier-Cianférani S. Characterization of therapeutic antibodies and related products. Anal Chem 2013;85:715–36. doi:10.1021/ac3032355.

[102] Tian Y, Ruotolo BT. Collision induced unfolding detects subtle differences in intact antibody glycoforms and associated fragments. Int J Mass Spectrom 2018;425:1–9. doi:10.1016/j.ijms.2017.12.005.

[103] Eschweiler JD, Rabuck-Gibbons JN, Tian Y, Ruotolo BT. CIUSuite: A Quantitative Analysis Package for Collision Induced Unfolding Measurements of Gas-Phase Protein Ions. Anal Chem 2015;87:11516–22. doi:10.1021/acs.analchem.5b03292.

[104] Han L, Ruotolo BT. Traveling-wave ion mobility-mass spectrometry reveals additional mechanistic details in the stabilization of protein complex ions through tuned salt additives. Int J Ion Mobil Spectrom 2013;16:41–50. doi:10.1007/s12127-013-0121-9.

[105] Walsh G, Jefferis R. Post-translational modifications in the context of therapeutic proteins. Nat Biotechnol 2006;24:1241–52. doi:10.1038/nbt1252.

[106] Gervais D. Protein deamidation in biopharmaceutical manufacture: Understanding, control and impact. J Chem Technol Biotechnol 2016;91:569–75. doi:10.1002/jctb.4850.

[107] Chung S, Tian J, Tan Z, Chen J, Lee J, Borys M, et al. Industrial bioprocessing perspectives on managing therapeutic protein charge variant profiles. Biotechnol Bioeng 2018;115:1646–65. doi:10.1002/bit.26587.

[108] Jefferis R. Characterization of Biosimilar Biologics The Link between Structure and Functions. In: Endrenyi L, Declerck PJ, Chow S-C, editors. Biosimilar Drug Prod. Dev., Boca Raton: CRC Press, Taylor & Frances group; 2017, p. 109–50.

[109] Walsh CT, Garneau-Tsodikova S, Gatto GJ. Protein posttranslational modifications: The chemistry of proteome diversifications. Angew Chemie - Int Ed 2005;44:7342–72. doi:10.1002/anie.200501023.

[110] Kuriakose A, Chirmule N, Nair P. Immunogenicity of Biotherapeutics: Causes and Association with Posttranslational Modifications. J Immunol Res 2016. doi:10.1155/2016/1298473.

[111] Mullard A. Bracing for the biosimilar wave. Nat Rev Drug Discov 2017;16:152–4. doi:10.1038/nrd.2017.36.

[112] Tebbey PW, Varga A, Naill M, Clewell J, Venema J. Consistency of quality attributes for the glycosylated monoclonal antibody Humira® (adalimumab). MAbs 2015;7:805–11. doi:10.1080/19420862.2015.1073429.

[113] Gerngross TU. Advances in the production of human therapeutic proteins in yeasts and filamentous fungi. Nat Biotechnol 2004;22:1409–14. doi:10.1038/nbt1028.

[114] Li H, Sethuraman N, Stadheim TA, Zha D, Prinz B, Ballew N, et al. Optimization of humanized IgGs in glycoengineered Pichia pastoris. Nat Biotechnol 2006;24:210–5. doi:10.1038/nbt1178.

[115] Rothman RJ, Perussia B, Herlyn D, Warren L. Antibody-dependent cytotoxicity mediated by natural killer cells is enhanced by castanospermine-induced alterations of IgG glycosylation. Mol Immunol 1989;26:1113–23. doi:10.1016/0161-5890(89)90055-2.

[116] Yamane-Ohnuki N, Kinoshita S, Inoue-Urakubo M, Kusunoki M, Iida S, Nakano R, et al. Establishment of FUT8 knockout Chinese hamster ovary cells: An ideal host cell line for producing completely defucosylated antibodies with enhanced antibody-dependent cellular cytotoxicity. Biotechnol Bioeng 2004;87:614–22. doi:10.1002/bit.20151.

[117] Okazaki A, Shoji-Hosaka E, Nakamura K, Wakitani M, Uchida K, Kakita S, et al. Fucose Depletion from Human IgG1 Oligosaccharide Enhances Binding Enthalpy and Association Rate between IgG1 and FcγRIIIa. J Mol Biol 2004;336:1239–49. doi:10.1016/j.jmb.2004.01.007.

[118] Natsume A, Wakitani M, Yamane-Ohnuki N, Shoji-Hosaka E, Niwa R, Uchida K, et al. Fucose removal from complex-type oligosaccharide enhances the antibody-dependent cellular cytotoxicity of single-gene-encoded bispecific antibody comprising of two single-chain antibodies linked to the antibody constant region. J Biochem 2006;140:359–68. doi:10.1093/jb/mvj157.

[119] Mori K, Kuni-Kamochi R, Yamane-Ohnuki N, Wakitani M, Yamano K, Imai H, et al. Engineering Chinese hamster ovary cells to maximize effector function of produced antibodies using FUT8 siRNA. Biotechnol Bioeng 2004;88:901–8. doi:10.1002/bit.20326.

[120] Kanda Y, Imai-Nishiya H, Kuni-Kamochi R, Mori K, Inoue M, Kitajima-Miyama K, et al. Establishment of a GDP-mannose 4,6-dehydratase (GMD) knockout host cell line: A new strategy for generating completely non-fucosylated recombinant therapeutics. J Biotechnol 2007;130:300–10. doi:10.1016/j.jbiotec.2007.04.025.

[121] Ito A, Ishida T, Yano H, Inagaki A, Suzuki S, Sato F, et al. Defucosylated anti-CCR4 monoclonal antibody exercises potent ADCC-mediated antitumor effect in the novel tumor-bearing humanized NOD/Shi-scid, IL-2Rγnull mouse model. Cancer Immunol Immunother 2009;58:1195–206. doi:10.1007/s00262-008-0632-0.

[122] Jones AJS, Papac DI, Chin EH, Keck R, Baughman SA, Lin YS, et al. Selective clearance of glycoforms of a complex glycoprotein pharmaceutical caused by terminal N-acetylglucosamine is similar in humans and cynomolgus monkeys. Glycobiology 2007;17:529–40. doi:10.1093/glycob/cwm017.

[123] Keck R, Nayak N, Lerner L, Raju S, Ma S, Schreitmueller T, et al. Characterization of a complex glycoprotein whose variable metabolic clearance in humans is dependent on terminal N-acetylglucosamine content. Biologicals 2008;36:49–60. doi:10.1016/j.biologicals.2007.05.004.

[124] Hodoniczky J, Yuan ZZ, James DC. Control of recombinant monoclonal antibody effector functions by Fc N-glycan remodeling in vitro. Biotechnol Prog 2005;21:1644–52. doi:10.1021/bp050228w.

[125] Boyd PN, Lines AC, Patel AK. The effect of the removal of sialic acid, galactose and total

carbohydrate on the functional activity of Campath-1H. Mol Immunol 1995;32:1311–8. doi:10.1016/0161-5890(95)00118-2.

[126] Peipp M, Dechant M, Valerius T. Effector mechanisms of therapeutic antibodies against ErbB receptors. Curr Opin Immunol 2008;20:436–43. doi:10.1016/j.coi.2008.05.012.

[127] Karsten CM, Pandey MK, Figge J, Kilchenstein R, Taylor PR, Rosas M, et al. Anti-inflammatory activity of IgG1 mediated by Fc galactosylation and association of FcγRIIB and dectin-1. Nat Med 2012;18:1401–6. doi:10.1038/nm.2862.

[128] Wright A, Morrison SL. Effect of altered CH2-associated carbohydrate structure on the functional properties and in vivo fate of chimeric mouse-human immunoglobulin G1. J Exp Med 1994;180:1087–96. doi:10.1084/jem.180.3.1087.

[129] Wright A, Sato Y, Okada T, Chang KH, Endo T, Morrison SL. In vivo trafficking and catabolism of IgG1 antibodies with Fc associated carbohydrates of differing structure. Glycobiology 2000;10:1347–55. doi:10.1093/glycob/10.12.1347.

[130] Kanda Y, Yamane-Ohnuki N, Sakai N, Yamano K, Nakano R, Inoue M, et al. Comparison of cell lines for stable production of fucose-negative antibodies with enhanced ADCC. Biotechnol Bioeng 2006;94:680–8. doi:10.1002/bit.20880.

[131] Zhou Q, Shankara S, Roy A, Qiu H, Estes S, McVie-Wylie A, et al. Development of a simple and rapid method for producing non-fucosylated oligomannose containing antibodies with increased effector function. Biotechnol Bioeng 2008;99:652–65. doi:10.1002/bit.21598.

[132] Nimmerjahn F, Ravetch J V. Anti-Inflammatory Actions of Intravenous Immunoglobulin. Annu Rev Immunol 2008;26:513–33. doi:10.1146/annurev.immunol.26.021607.090232.

[133] Liu L, Gomathinayagam S, Hamuro L, Prueksaritanont T, Wang W, Stadheim TA, et al. The impact of glycosylation on the pharmacokinetics of a TNFR2:Fc fusion protein expressed in glycoengineered pichia pastoris. Pharm Res 2013;30:803–12. doi:10.1007/s11095-012-0921-3.

[134] Anthony RM, Ravetch J V. A novel role for the IgG Fc glycan: The anti-inflammatory activity of sialylated IgG Fcs. J Clin Immunol 2010;30:S9-14. doi:10.1007/s10875-010-9405-6.

[135] Anthony RM, Kobayashi T, Wermeling F, Ravetch J V. Intravenous gammaglobulin suppresses inflammation through a novel T H 2 pathway. Nature 2011;475:110–4. doi:10.1038/nature10134.

[136] Kaneko Y, Nimmerjahn F, Ravetch J V. Anti-inflammatory activity of immunoglobulin G resulting from Fc sialylation. Science (80-) 2006;313:670–3. doi:10.1126/science.1129594.

[137] Samuelsson A, Towers TL, Ravetch J V. Anti-inflammatory activity of IVIG mediated through the inhibitory Fc receptor. Science (80-) 2001;291:484–6. doi:10.1126/science.291.5503.484.

[138] Sondermann P, Pincetic A, Maamary J, Lammens K, Ravetch J V. General mechanism for modulating immunoglobulin effector function. Proc Natl Acad Sci 2013;110:9868–72.

doi:10.1073/pnas.1307864110.

[139] Zupke C, Brady LJ, Slade PG, Clark P, Caspary RG, Livingston B, et al. Real-time product attribute control to manufacture antibodies with defined N-linked glycan levels. Biotechnol Prog 2015;31:1433–41. doi:10.1002/btpr.2136.

[140] Henninot A, Terrier A, Charton J, Urbain R, Fontayne A, Deprez B, et al. Characterization of monoclonal antibodies by a fast and easy liquid chromatography-mass spectrometry time-of-flight analysis on culture supernatant. Anal Biochem 2015;491:52–4. doi:10.1016/j.ab.2015.08.006.

[141] Zhang P, Woen S, Wang T, Liau B, Zhao S, Chen C, et al. Challenges of glycosylation analysis and control: An integrated approach to producing optimal and consistent therapeutic drugs. Drug Discov Today 2016;21:740–65. doi:10.1016/j.drudis.2016.01.006.

[142] Tsai P-L, Chen S-F. A Brief Review of Bioinformatics Tools for Glycosylation Analysis by Mass Spectrometry. Bioinforma TooLs GLYcosYLatIon Anal BY MS 2017;6:S0064–S0064. doi:10.5702/massspectrometry.S0064.

[143] Tajiri M, Yoshida S, Wada Y. Differential analysis of site-specific glycans on plasma and cellular fibronectins: Application of a hydrophilic affinity method for glycopeptide enrichment. Glycobiology 2005;15:1332–40. doi:10.1093/glycob/cwj019.

[144] Wohlgemuth J, Karas M, Eichhorn T, Hendriks R, Andrecht S. Quantitative site-specific analysis of protein glycosylation by LC-MS using different glycopeptide-enrichment strategies. Anal Biochem 2009;395:178–88. doi:10.1016/j.ab.2009.08.023.

[145] Morimoto K, Nishikaze T, Yoshizawa AC, Kajihara S, Aoshima K, Oda Y, et al. GlycanAnalysis Plug-in: a database search tool for N-glycan structures using mass spectrometry. Bioinformatics 2015;31:2217–9. doi:10.1093/bioinformatics/btv110.

[146] Bern M, Kil YJ, Becker C. Byonic: Advanced peptide and protein identification software. Curr Protoc Bioinforma 2012. doi:10.1002/0471250953.bi1320s40.

[147] Woodin CL, Maxon M, Desaire H. Software for automated interpretation of mass spectrometry data from glycans and glycopeptides. Analyst 2013;138:2793–803. doi:10.1039/c2an36042j.

[148] Kolarich D, Jensen PH, Altmann F, Packer NH. Determination of site-specific glycan heterogeneity on glycoproteins. Nat Protoc 2012;7:1285–98. doi:10.1038/nprot.2012.062.

[149] Irungu J, Go EP, Dalpathado DS, Desaire H. Simplification of mass spectral analysis of acidic glycopeptides using GlycoPep ID. Anal Chem 2007;79:3065–74. doi:10.1021/ac062100e.

[150] U.S. Food and Drug Administration. FDA Briefing Document Arthritis Advisory Committee Meeting BLA 761024 ABP-501, a Proposed Biosimilar to Humira (adalimumab). 2016.

[151] U.S. Food and Drug Administration. FDA Briefing Document Oncologic Drugs Advisory Committee Meeting BLA 761074 MYL-1401O, a proposed biosimilar to Herceptin (trastuzumab). 2017.

[152] Kobata A. Exo- and endoglycosidases revisited. Proc Japan Acad Ser B 2013;89:97–

117. doi:10.2183/pjab.89.97.

[153] Wada Y, Dell A, Haslam SM, Rangè Re Tissot B, Canis KV, Azadi P, et al. Comparison of Methods for Profiling O-Glycosylation. Mol Cell Proteomics 2010;9:719–27. doi:10.1074/mcp.M900450-MCP200.

[154] Cao L, Diedrich JK, Ma Y, Wang N, Pauthner M, Park SKR, et al. Global site-specific analysis of glycoprotein N-glycan processing. Nat Protoc 2018;13:1196–212. doi:10.1038/nprot.2018.024.

[155] Lauber MA, Yu YQ, Brousmiche DW, Hua Z, Koza SM, Magnelli P, et al. Rapid preparation of released N -glycans for HILIC analysis using a labeling reagent that facilitates sensitive fluorescence and ESI-MS detection. Anal Chem 2015;87:5401–9. doi:10.1021/acs.analchem.5b00758.

[156] Szekrényes Á, Park SAS, Cosgrave E, Jones A, Haxo T, Kimzey M, et al. Multi-site N-Glycan mapping study 2: UHPLC. Electrophoresis 2018;39:998–1005. doi:10.1002/elps.201700463.

[157] Yang S, Zhang L, Thomas S, Hu Y, Li S, Cipollo J, et al. Modification of Sialic Acids on Solid Phase: Accurate Characterization of Protein Sialylation. Anal Chem 2017;89:6330–5. doi:10.1021/acs.analchem.7b01048.

[158] Rohrer JS, Townsend RR. Separation of partially desialylated branched oligosaccharide isomers containing α(2←3)- and α(2←6)-linked Neu5Ac. Glycobiology 1995;5:391–5. doi:10.1093/glycob/5.4.391.

[159] Reid townsend R, Hardy MR, Lee YC. Separation of oligosaccharides using high-performance anion-exchange chromatography with pulsed amperometric detection. Methods Enzymol 1989;179:65–76. doi:10.1016/0076-6879(89)79114-X.

[160] Rohrer JS, Thayer J, Weitzhandler M, Avdalovic N. Analysis of the N-acetylneuraminic acid and N-glycolylneuraminic acid contents of glycoproteins by high-pH anion-exchange chromatography with pulsed amperometric detection (HPAEC/PAD). Glycobiology 1998;8:35–43. doi:10.1093/glycob/8.1.35.

[161] Corradini C, Cavazza A, Bignardi C. High-Performance Anion-Exchange Chromatography Coupled with Pulsed Electrochemical Detection as a Powerful Tool to Evaluate Carbohydrates of Food Interest: Principles and Applications. Int J Carbohydr Chem 2012;2012:1–13. doi:10.1155/2012/487564.

[162] Hao Z, Zhang T, Xuan Y, Wang H, Qian J, Lin S, et al. Chapter 10. Intact Antibody Characterization Using Orbitrap Mass Spectrometry. ACS Symp Ser 2015;1202:289–315. doi:10.1021/bk-2015-1202.ch010.

[163] Xie H, Chakraborty A, Ahn J, Yu YQ, Dakshinamoorthy DP, Gilar M, et al. Rapid comparison of a candidate biosimilar to an innovator monoclonal antibody with advanced liquid chromatography and mass spectrometry technologies. MAbs 2010;2:379–94. doi:10.4161/mabs.11986.

[164] Li W, Kerwin JL, Schiel J, Formolo T, Davis D, Mahan A, et al. Structural elucidation of post-translational modifications in monoclonal antibodies. ACS Symp Ser 2015;1201:119–83. doi:10.1021/bk-2015-1201.ch003.

[165] Nathan JJ, Ramchandani M, Kaur P. Manufacturing of Biologics. In: Yamauchi PS, editor. Biol. Syst. Agents Dermatology, Gewerbestrasse: Springer International Publishing; 2018, p. 101–10.

[166] Mulinacci F, Poirier E, Capelle MAH, Gurny R, Arvinte T. Influence of methionine oxidation on the aggregation of recombinant human growth hormone. Eur J Pharm Biopharm 2013;85:42–52. doi:10.1016/j.ejpb.2013.03.015.

[167] Hu D, Qin Z, Xue B, Fink AL, Uversky VN. Effect of methionine oxidation on the structural properties, conformational stability, and aggregation of immunoglobulin light chain LEN. Biochemistry 2008;47:8665–77. doi:10.1021/bi800806d.

[168] Van Beers MMC, Sauerborn M, Gilli F, Brinks V, Schellekens H, Jiskoot W. Oxidized and aggregated recombinant human interferon beta is immunogenic in human interferon beta transgenic mice. Pharm Res 2011;28:2393–402. doi:10.1007/s11095-011-0451-4.

[169] Mirzaei H, Regnier F. Protein:protein aggregation induced by protein oxidation. J Chromatogr B Anal Technol Biomed Life Sci 2008;873:8–14. doi:10.1016/j.jchromb.2008.04.025.

[170] Filipe V, Jiskoot W, Basmeleh AH, Halim A, Schellekens H, Brinks V. Immunogenicity of different stressed IgG monoclonal antibody formulations in immune tolerant transgenic mice. MAbs 2012;4:740–52. doi:10.4161/mabs.22066.

[171] Sohal RS. Role of oxidative stress and protein oxidation in the aging process. Free Radic Biol Med 2002;33:37–44. doi:10.1016/S0891-5849(02)00856-0.

[172] Davies MJ. Protein oxidation and peroxidation. Biochem J 2016;473:805–25. doi:10.1042/BJ20151227.

[173] Kuo TT, Aveson VG. Neonatal Fc receptor and IgG-based therapeutics. MAbs 2011;3:422–30. doi:10.4161/mabs.3.5.16983.

[174] Mo J, Yan Q, So CK, Soden T, Lewis MJ, Hu P. Understanding the Impact of Methionine Oxidation on the Biological Functions of IgG1 Antibodies Using Hydrogen/Deuterium Exchange Mass Spectrometry. Anal Chem 2016;88:9495–502. doi:10.1021/acs.analchem.6b01958.

[175] Bertolotti-Ciarlet A, Wang W, Lownes R, Pristatsky P, Fang Y, McKelvey T, et al. Impact of methionine oxidation on the binding of human IgG1 to Fc Rn and Fc gamma receptors. Mol Immunol 2009;46:1878–82. doi:10.1016/j.molimm.2009.02.002.

[176] Liu D, Ren D, Huang H, Dankberg J, Rosenfeld R, Cocco MJ, et al. Structure and stability changes of human IgG1 Fc as a consequence of methionine oxidation. Biochemistry 2008;47:5088–100. doi:10.1021/bi702238b.

[177] Pan H, Chen K, Chu L, Kinderman F, Apostol I, Huang G. Methionine oxidation in human IgG2 Fc decreases binding affinities to protein A and FcRn. Protein Sci 2009;18:424–33. doi:10.1002/pro.45.

[178] Niazi SK. Stability and formulation considerations. Biosimilars Interchang. Biol. Tactical Elem., Boca Raton: Taylor & Francis Group; 2016, p. 83–122.

[179] Robinson NE. Protein deamidation. Proc Natl Acad Sci 2002;99:5283–8.

doi:10.1073/pnas.082102799.

[180] Jenkins N. Modifications of therapeutic proteins: Challenges and prospects. Cytotechnology, vol. 53, 2007, p. 121–5. doi:10.1007/s10616-007-9075-2.

[181] Phillips JJ, Buchanan A, Andrews J, Chodorge M, Sridharan S, Mitchell L, et al. Rate of Asparagine Deamidation in a Monoclonal Antibody Correlating with Hydrogen Exchange Rate at Adjacent Downstream Residues. Anal Chem 2017;89:2361–8. doi:10.1021/acs.analchem.6b04158.

[182] Huang L, Lu J, Wroblewski VJ, Beals JM, Riggin RM. In vivo deamidation characterization of monoclonal antibody by LC/MS/MS. Anal Chem 2005;77:1432–9. doi:10.1021/ac0494174.

[183] Harris RJ, Kabakoff B, Macchi FD, Shen FJ, Kwong M, Andya JD, et al. Identification of multiple sources of charge heterogeneity in a recombinant antibody. J Chromatogr B Biomed Sci Appl 2001;752:233–45. doi:10.1016/S0378-4347(00)00548-X.

[184] Doyle HA, Zhou J, Wolff MJ, Harvey BP, Roman RM, Gee RJ, et al. Isoaspartyl post-translational modification triggers anti-tumor T and B lymphocyte immunity. J Biol Chem 2006;281:32676–83. doi:10.1074/jbc.M604847200.

[185] Wang W, Meeler AR, Bergerud LT, Hesselberg M, Byrne M, Wu Z. Quantification and characterization of antibody deamidation by peptide mapping with mass spectrometry. Int J Mass Spectrom 2012;312:107–13. doi:10.1016/j.ijms.2011.06.006.

[186] Chelius D, Render DS, Bondarenko P V. Identification and characterization of deamidation sites in the conserved regions of human immunoglobulin gamma antibodies. Anal Chem 2005;77:6004–11. doi:10.1021/ac050672d.

[187] Timm V, Gruber P, Wasiliu M, Lindhofer H, Chelius D. Identification and characterization of oxidation and deamidation sites in monoclonal rat/mouse hybrid antibodies. J Chromatogr B Anal Technol Biomed Life Sci 2010;878:777–84. doi:10.1016/j.jchromb.2010.01.036.

[188] Holzmann J, Hausberger A, Rupprechter A, Toll H. Top-down MS for rapid methionine oxidation site assignment in filgrastim. Anal Bioanal Chem 2013;405:6667–74. doi:10.1007/s00216-013-7138-0.

[189] Liu H, Caza-Bulseco G, Faldu D, Chumsae C, Sun J. Heterogeneity of monoclonal antibodies. J Pharm Sci 2008;97:2426–47. doi:10.1002/jps.21180.

[190] Khawli LA, Goswami S, Hutchinson R, Kwong ZW, Yang J, Wang X, et al. Charge variants in IgG1: Isolation, characterization, in vitro binding properties and pharmacokinetics in rats. MAbs 2010;2:613–24. doi:10.4161/mabs.2.6.13333.

[191] Yu L, Vizel A, Huff MB, Young M, Remmele RL, He B. Investigation of N-terminal glutamate cyclization of recombinant monoclonal antibody in formulation development. J Pharm Biomed Anal 2006;42:455–63. doi:10.1016/j.jpba.2006.05.008.

[192] Lyubarskaya Y, Houde D, Woodard J, Murphy D, Mhatre R. Analysis of recombinant monoclonal antibody isoforms by electrospray ionization mass spectrometry as a strategy for streamlining characterization of recombinant monoclonal antibody charge

heterogeneity. Anal Biochem 2006;348:24–39. doi:10.1016/j.ab.2005.10.003.

[193] Liu YD, Goetze AM, Bass RB, Flynn GC. N-terminal glutamate to pyroglutamate conversion in vivo for human IgG2 antibodies. J Biol Chem 2011;286:11211–7. doi:10.1074/jbc.M110.185041.

[194] U.S. Food and Drug Administration. FDA Briefing Document Oncologic Drugs Advisory Committee BLA 761028 ABP215, a proposed biosimilar to Avastin (bevacizumab). 2017.

[195] Kahle J, Watzig H. Determination of protein charge variants with (imaged) capillary isoelectric focusing and capillary zone electrophoresis. Electrophoresis 2018;0:1–20.

[196] Fekete S, Beck A, Fekete J, Guillarme D. Method development for the separation of monoclonal antibody charge variants in cation exchange chromatography, Part II: PH gradient approach. J Pharm Biomed Anal 2015;102:282–9. doi:10.1016/j.jpba.2014.09.032.

[197] Yamamoto S, Ishihara T. Resolution and retention of proteins near Isoelectric points in ion-exchange chromatography. Molecular recognition in electrostatic interaction chromatography. Sep Sci Technol 2000;35:1707–17. doi:10.1081/SS-100102489.

[198] Ahamed T, Nfor BK, Verhaert PDEM, van Dedem GWK, van der Wielen LAM, Eppink MHM, et al. pH-gradient ion-exchange chromatography: An analytical tool for design and optimization of protein separations. J Chromatogr A 2007;1164:181–8. doi:10.1016/j.chroma.2007.07.010.

[199] Fekete S, Gassner A-LL, Rudaz S, Schappler J, Guillarme D. Analytical strategies for the characterization of therapeutic monoclonal antibodies. TrAC - Trends Anal Chem 2013;42:74–83. doi:10.1016/j.trac.2012.09.012.

[200] Moorhouse KG, Nashabeh W, Deveney J, Bjork NS, Mulkerrin MG, Ryskamp T. Validation of an HPLC method for the analysis of the charge heterogeneity of the recombinant monoclonal antibody IDEC-C2B8 after papain digestion. J Pharm Biomed Anal 1997;16:593–603. doi:10.1016/S0731-7085(97)00178-7.

[201] Flores-Ortiz LF, Campos-García VR, Perdomo-Abúndez FC, Pérez NO, Medina-Rivero E. Physicochemical properties of Rituximab. J Liq Chromatogr Relat Technol 2014;37:1438–52. doi:10.1080/10826076.2013.794738.

[202] Voeten RLC, Ventouri IK, Haselberg R, Somsen GW. Capillary Electrophoresis: Trends and Recent Advances. Anal Chem 2018:1464–81. doi:10.1021/acs.analchem.8b00015.

[203] Dai J, Lamp J, Xia Q, Zhang Y. Capillary Isoelectric Focusing-Mass Spectrometry Method for the Separation and Online Characterization of Intact Monoclonal Antibody Charge Variants. Anal Chem 2018;90:2246–54. doi:10.1021/acs.analchem.7b04608.

[204] Krenkova J, Foret F. On-line CE/ESI/MS interfacing: Recent developments and applications in proteomics. Proteomics 2012;12:2978–90. doi:10.1002/pmic.201200140.

[205] Mokaddem M, Gareil P, Varenne A. Online CIEF-ESI-MS in glycerol-water media with a view to hydrophobic protein applications. Electrophoresis 2009;30:4040–8. doi:10.1002/elps.200900091.

[206] Gahoual R, Beck A, Leize-Wagner E, François Y-N. Cutting-edge capillary

electrophoresis characterization of monoclonal antibodies and related products. J Chromatogr B 2016;1032:61–78. doi:10.1016/j.jchromb.2016.05.028.

[207] Hjertén S, Zhu M de. Adaptation of the equipment for high-performance electrophoresis to isoelectric focusing. J Chromatogr A 1985;346:265–70. doi:10.1016/S0021-9673(00)90512-0.

[208] Li N, Kessler K, Bass L, Zeng D. Evaluation of the iCE280 Analyzer as a potential high-throughput tool for formulation development. J Pharm Biomed Anal 2007;43:963–72. doi:10.1016/j.jpba.2006.09.024.

[209] Anderson CL, Wang Y, Rustandi RR. Applications of imaged capillary isoelectric focussing technique in development of biopharmaceutical glycoprotein-based products. Electrophoresis 2012;33:1538–44. doi:10.1002/elps.201100611.

[210] Michels DA, Salas-Solano O, Felten C. Imaged capillary isoelectric focusing for charge-variant analysis of biopharmaceuticals. Bioprocess Int 2011;9:48–54.

[211] He Y, Mo J, He X, Ruesch M. Rapid Analysis of Charge Heterogeneity of Monoclonal Antibodies by Capillary Zone Electrophoresis and Imaged Capillary Isoelectric Focusing. In: Garcia CD, editor. Capill. Electrophor. Microchip Capill. Electrophor. Princ. Appl. Limitations, Hoboken: John Wiley & Sons, Inc; 2013, p. 293–308. doi:10.1002/9781118530009.

[212] Salas-Solano O, Felten C. Capillary electrophoresis and bioanalysis. In: Ahuja S, editor. Sep. Sci. Technol., vol. 9, London: Elsevier; 2008, p. 401–24. doi:10.1080/00372367408056075.

[213] Espinosa- de la Garza CE, Perdomo-Abúndez FC, Padilla-Calderón J, Uribe-Wiechers JM, Pérez NO, Flores-Ortiz LF, et al. Analysis of recombinant monoclonal antibodies by capillary zone electrophoresis. Electrophoresis 2013;34:1133–40. doi:10.1002/elps.201200575.

[214] He Y, Isele C, Hou W, Ruesch M. Rapid analysis of charge variants of monoclonal antibodies with capillary zone electrophoresis in dynamically coated fused-silica capillary. J Sep Sci 2011;34:548–55. doi:10.1002/jssc.201000719.

[215] Turner A, Schiel JE. Qualification of NISTmAb charge heterogeneity control assays. Anal Bioanal Chem 2018;410:2079–93. doi:10.1007/s00216-017-0816-6.

[216] Vanhonacker K, Op de Beeck J. µPAC™ Microchip Chromatography: Better By Design. Bioprocess Int 2017.

[217] Siew A. Impurity testing of biologic drug products. BioPharm Int 2018.

[218] U.S. Food and Drug Administration. Guidance for industry Q6B specifications: Test procedures and acceptance criteria for biotechnological/biological products. 1999:1–24. doi:10.1093/elt/40.2.121.

[219] Cook KM, Hogg PJ. Post-Translational Control of Protein Function by Disulfide Bond Cleavage. Antioxid Redox Signal 2013;18:1987–2015. doi:10.1089/ars.2012.4807.

[220] Azimi I, Wong JWH, Hogg PJ. Control of Mature Protein Function by Allosteric Disulfide Bonds. Antioxid Redox Signal 2011;14:113–26. doi:10.1089/ars.2010.3620.

[221] Holder PG, Rabuka D. Technologies for Antibody-Drug Conjugation. In: Liu C, Morrow Jr. KJ, editors. Biosimilars Monoclon. Antibodies A Pract. Guid. to Manuf. Preclin. Clin. Dev., Hoboken: John Wiley & Sons, Inc; 2017, p. 591–640.

[222] Zhang W, Czupryn MJ. Free sulfhydryl in recombinant monoclonal antibodies. Biotechnol Prog 2002;18:509–13. doi:10.1021/bp025511z.

[223] Dillon TM, Bondarenko P V., Rehder DS, Pipes GD, Kleemann GR, Ricci MS. Optimization of a reversed-phase high-performance liquid chromatography/mass spectrometry method for characterizing recombinant antibody heterogeneity and stability. J Chromatogr A 2006;1120:112–20. doi:10.1016/j.chroma.2006.01.016.

[224] Trexler-Schmidt M, Sargis S, Chiu J, Sze-Khoo S, Mun M, Kao YH, et al. Identification and prevention of antibody disulfide bond reduction during cell culture manufacturing. Biotechnol Bioeng 2010;106:452–61. doi:10.1002/bit.22699.

[225] Hutterer KM, Hong RW, Lull J, Zhao X, Wang T, Pei R, et al. Monoclonal antibody disulfide reduction during manufacturing Untangling process effects from product effects. MAbs 2013;5:608–13. doi:10.4161/mabs.24725.

[226] Lamanna WC, Mayer RE, Rupprechter A, Fuchs M, Higel F, Fritsch C, et al. The structure-function relationship of disulfide bonds in etanercept. Sci Rep 2017;7:1–8. doi:10.1038/s41598-017-04320-5.

[227] Cho IH, Lee N, Song D, Jung SY, Bou-Assaf G, Sosic Z, et al. Evaluation of the structural, physicochemical, and biological characteristics of SB4, a biosimilar of etanercept. MAbs 2016;8:1136–55. doi:10.1080/19420862.2016.1193659.

[228] Wu S-L, Jiang H, Lu Q, Dai S, Hancock WS, Karger BL. Mass Spectrometric Determination of Disulfide Linkages in Recombinant Therapeutic Proteins Using On-line LC-MS with Electron Transfer Dissociation (ETD). Anal Chem 2009;81:112–22. doi:10.1021/ac801560k.

[229] Bean MF, Carr SA. Characterization of disulfide bond position in proteins and sequence analysis of cystine-bridged peptides by tandem mass spectrometry. Anal Biochem 1992;201:216–26. doi:10.1016/0003-2697(92)90331-Z.

[230] Jiang W, Liu S, Zhong Z. Product Analysis of Biosimilar Antibodies. In: Liu C, Morrow, Jr. KJ, editors. Biosimilars Monoclon. Antibodies A Pract. Guid. to Manuf. Preclin. Clin. Dev. 1st ed., Hoboken, New Jersey: John Wiley & Sons, Inc; 2017, p. 427–58.

[231] Chen X, Zhou Y, Peng X, Yoon J. Fluorescent and colorimetric probes for detection of thiols. Chem Soc Rev 2010;39:2120–35. doi:10.1039/b925092a.

[232] Walton DJ, Shilton BH. Site specificity of protein glycation. Amino Acids 1991;1:199–203. doi:10.1007/BF00806917.

[233] Garlick RL, Mazer JS. The principal site of nonenzymatic glycosylation of human serum albumin in vivo. J Biol Chem 1983;258:6142–6.

[234] Quan C, Alcala E, Petkovska I, Matthews D, Canova-Davis E, Taticek R, et al. A study in glycation of a therapeutic recombinant humanized monoclonal antibody: Where it is, how it got there, and how it affects charge-based behavior. Anal Biochem 2008;373:179–91.

doi:10.1016/j.ab.2007.09.027.

[235] Quan CP, Wu S, Dasovich N, Hsu C, Patapoff T, Canova-Davis E. Susceptibility of rhDNase I to glycation in the dry-powder state. Anal Chem 1999;71:4445–54. doi:10.1021/ac9900580.

[236] Gadgil HS, Bondarenko P V., Pipes G, Rehder D, Mcauley A, Perico N, et al. The LC/MS analysis of glycation of IgG molecules in sucrose containing formulations. J Pharm Sci 2007;96:2607–21. doi:10.1002/jps.20966.

[237] Gramer MJ. Product Quality Considerations for Mammalian Cell Culture Process Development and Manufacturing. In: Zhou W, Kantardjieff A, editors. Mamm. Cell Cult. Biol. Manuf., Berlin: Springer-Verlag; 2014, p. 123–66.

[238] Tsekovska RG, Boyanova MS, Mironova RS, Ivanov IG. Effect of arginine on glycation and stability of recombinant human interferon-gamma. Biotechnol Biotechnol Equip 2009;23:1063–7. doi:10.1080/13102818.2009.10817613.

[239] Kantardjieff A, Zhou W. Mammalian cell cultures for biologics manufacturing. Adv Biochem Eng Biotechnol 2014;139:1–9. doi:10.1007/10_2013_255.

[240] Wei B, Berning K, Quan C, Zhang YT. Glycation of antibodies: Modification, methods and potential effects on biological functions. MAbs 2017;9:586–94. doi:10.1080/19420862.2017.1300214.

[241] Kennedy DM, Skillen a W, Self CH. Glycation of monoclonal antibodies impairs their ability to bind antigen. Clin Exp Immunol 1994;98:245–51. doi:10.1111/j.1365-2249.1994.tb06133.x.

[242] Chen M, Lu Y, Ma Q, Guo L, Feng YQ. Boronate affinity monolith for highly selective enrichment of glycopeptides and glycoproteins. Analyst 2009;134:2158–64. doi:10.1039/b909581k.

[243] Li Y, Pfüller U, Linné Larsson E, Jungvid H, Galaev IY, Mattiasson B. Separation of mistletoe lectins based on the degree of glycosylation using boronate affinity chromatography. J Chromatogr A 2001;925:115–21. doi:10.1016/S0021-9673(01)00967-0.

[244] Kislinger T, Humeny A, Peich CC, Becker CM, Pischetsrieder M. Analysis of protein glycation products by MALDI-TOF/MS. Ann. N. Y. Acad. Sci., vol. 1043, 2005, p. 249–59. doi:10.1196/annals.1333.030.

[245] Lapolla A, Fedele D, Reitano R, Aricò NC, Seraglia R, Traldi P, et al. Enzymatic digestion and mass spectrometry in the study of advanced glycation end products/peptides. J Am Soc Mass Spectrom 2004;15:496–509. doi:10.1016/j.jasms.2003.11.014.

[246] Sandoz. GP2015 Biosimilar (Etanercept) - Analytical Demonstration of Similarity. 2016.

[247] Den Engelsman J, Garidel P, Smulders R, Koll H, Smith B, Bassarab S, et al. Strategies for the assessment of protein aggregates in pharmaceutical biotech product development. Pharm Res 2011;28:920–33. doi:10.1007/s11095-010-0297-1.

[248] Vugmeyster Y. Pharmacokinetics and toxicology of therapeutic proteins: Advances and challenges. World J Biol Chem 2012;3:73. doi:10.4331/wjbc.v3.i4.73.

[249] Roberts CJ. Protein aggregation and its impact on product quality. Curr Opin Biotechnol 2014;30:211–7. doi:10.1016/j.copbio.2014.08.001.

[250] Meager A, Dolman C, Dilger P, Bird C, Giovannoni G, Schellekens H, et al. An Assessment of Biological Potency and Molecular Characteristics of Different Innovator and Noninnovator Interferon-Beta Products. J Interf Cytokine Res 2011;31:383–92. doi:10.1089/jir.2010.0113.

[251] Hochuli E. Interferon immunogenicity: technical evaluation of interferon-alpha 2a. J Interferon Cytokine Res 1997;17 Suppl 1:S15-21.

[252] Fradkin AH, Carpenter JF, Randolph TW. Immunogenicity of aggregates of recombinant human growth hormone in mouse models. J Pharm Sci 2009;98:3247–64. doi:10.1002/jps.21834.

[253] Pathak JA, Sologuren RR, Narwal R. Do clustering monoclonal antibody solutions really have a concentration dependence of viscosity? Biophys J 2013;104:913–23. doi:10.1016/j.bpj.2013.01.007.

[254] Moussa EM, Panchal JP, Moorthy BS, Blum JS, Joubert MK, Narhi LO, et al. Immunogenicity of Therapeutic Protein Aggregates. J Pharm Sci 2016;105:417–30. doi:10.1016/j.xphs.2015.11.002.

[255] Barth HG, Boyes BE, Jackson C. Size Exclusion Chromatography and Related Separation Techniques. Anal Chem 1998;70:251–78. doi:10.1021/a1980015t.

[256] Wen J, Arakawa T, Philo JS. Size-exclusion chromatography with on-line light-scattering, absorbance, and refractive index detectors for studying proteins and their interactions. Anal Biochem 1996;240:155–66. doi:10.1006/abio.1996.0345.

[257] Mahler HC, Friess W, Grauschopf U, Kiese S. Protein aggregation: Pathways, induction factors and analysis. J Pharm Sci 2009;98:2909–34. doi:10.1002/jps.21566.

[258] Liu J, Andya JD, Shire SJ. A critical review of analytical ultracentrifugation and field flow fractionation methods for measuring protein aggregation. AAPS J 2006;8:E580–9. doi:10.1208/aapsj080367.

[259] Wagner M, Holzschuh S, Traeger A, Fahr A, Schubert US. Asymmetric flow field-flow fractionation in the field of nanomedicine. Anal Chem 2014;86:5201–10. doi:10.1021/ac501664t.

[260] Rebolj K, Pahovnik D, Žagar E. Characterization of a protein conjugate using an asymmetrical-flow field-flow fractionation and a size-exclusion chromatography with multi-detection system. Anal Chem 2012;84:7374–83. doi:10.1021/ac3010378.

[261] Cole JL, Lary JW, Moody T, Laue TM. Analytical Ultracentrifugation: Sedimentation Velocity and Sedimentation Equilibrium. Methods Cell Biol 2008;84:143–79. doi:10.1016/S0091-679X(07)84006-4.Analytical.

[262] Lebowitz J, Lewis MS, Schuck P. Modern analytical ultracentrifugation in protein science: A tutorial review. Protein Sci 2009;11:2067–79. doi:10.1110/ps.0207702.

[263] Filipe V, Hawe A, Jiskoot W. Critical evaluation of nanoparticle tracking analysis (NTA) by NanoSight for the measurement of nanoparticles and protein aggregates. Pharm Res

2010;27:796–810. doi:10.1007/s11095-010-0073-2.

[264] Patapoff TW, Tani TH, Cromwell MEM. A low-volume, short-path length dynamic light scattering sample cell for highly turbid suspensions. Anal Biochem 1999;270:338–40. doi:10.1006/abio.1999.4108.

[265] Hassan P a, Rana S, Verma G. Making sense of brownian motion: colloid characterization by dynamic light scattering. Langmuir 2015;31:3–12. doi:10.1021/la501789z.

[266] Gallego-Urrea JA, Tuoriniemi J, Hassellöv M. Applications of particle-tracking analysis to the determination of size distributions and concentrations of nanoparticles in environmental, biological and food samples. TrAC - Trends Anal Chem 2011;30:473–83. doi:10.1016/j.trac.2011.01.005.

[267] Qi W, Kenyon S, Taddei M, Cheung J, Gutka H. Enhanced biosimilar product characterization: A case study using raman spectroscopy combined with dynamic light scattering. Bioprocess Int 2016;14.

[268] European Medicines Agency. Guideline on similar biological medicinal products containing monoclonal antibodies – non-clinical and clinical issues. 2012.

[269] Pollard TD. A Guide to Simple and Informative Binding Assays. Mol Biol Cell 2010;21:4061–7. doi:10.1091/mbc.e10-08-0683.

[270] Velayudhan J, Chen Y, Rohrbach A, Pastula C, Maher G, Thomas H, et al. Demonstration of Functional Similarity of Proposed Biosimilar ABP 501 to Adalimumab. BioDrugs 2016;30:339–51. doi:10.1007/s40259-016-0185-2.

[271] Idusogie EE, Presta LG, Gazzano-Santoro H, Totpal K, Wong PY, Ultsch M, et al. Mapping of the C1q Binding Site on Rituxan, a Chimeric Antibody with a Human IgG1 Fc. J Immunol 2000;164:4178 LP – 4184.

[272] Tak For Yu Z, Guan H, Ki Cheung M, McHugh WM, Cornell TT, Shanley TP, et al. Rapid, automated, parallel quantitative immunoassays using highly integrated microfluidics and AlphaLISA. Sci Rep 2015;5:11339. doi:10.1038/srep11339.

[273] Prasad A, Lautenschlager C, Hurt S, Titus D, Parent S. A Comparison of AlphaLISA and TR-FRET Homogeneous Immunoassays in Serum-Containing Samples. 2009.

[274] Eglen RM, Reisine T, Roby P, Rouleau N, Illy C, Bossé R, et al. The use of AlphaScreen technology in HTS: current status. Curr Chem Genomics 2008;1:2–10. doi:10.2174/1875397300801010002.

[275] Seo N, Polozova A, Zhang M, Yates Z, Cao S, Li H, et al. Analytical and functional similarity of Amgen biosimilar ABP 215 to bevacizumab. MAbs 2018;10:678–91. doi:10.1080/19420862.2018.1452580.

[276] Wu Q, Lee HY, Wong PY, Jiang G, Gazzano-Santoro H. Development and applications of AlphaScreen-based FcRn binding assay to characterize monoclonal antibodies. J Immunol Methods 2015;420:31–7. doi:10.1016/J.JIM.2015.03.012.

[277] Characterizing biosimilar molecules: Utilizing SPR as an orthogonal technique for demonstrating potency. 2017.

[278] Homola J, Piliarik M. Surface plasmon resonance (SPR) sensors. Surf. plasmon Reson. based sensors, Springer; 2006, p. 45–67.

[279] Malmqvist M, Karlsson R. Biomolecular interaction analysis: affinity biosensor technologies for functional analysis of proteins. Curr Opin Chem Biol 1997;1:378–83. doi:10.1016/S1367-5931(97)80077-4.

[280] Richalet-Sécordel PM, Rauffer-Bruyère N, Christensen LLH, Ofenloch-Haehnle B, Seidel C, Van Regenmortel MHV. Concentration Measurement of Unpurified Proteins Using Biosensor Technology under Conditions of Partial Mass Transport Limitation. Anal Biochem 1997;249:165–73. doi:10.1006/abio.1997.2183.

[281] Christensen LLH. Theoretical Analysis of Protein Concentration Determination Using Biosensor Technology under Conditions of Partial Mass Transport Limitation. Anal Biochem 1997;249:153–64. doi:10.1006/ABIO.1997.2182.

[282] Sigmundsson K, Másson G, Rice R, Beauchemin N, Öbrink B. Determination of Active Concentrations and Association and Dissociation Rate Constants of Interacting Biomolecules: An Analytical Solution to the Theory for Kinetic and Mass Transport Limitations in Biosensor Technology and Its Experimental Verification†. Biochemistry 2002;41:8263–76. doi:10.1021/BI020099H.

[283] Yu Y, Mitchell S, Lynaugh H, Brown M, Nobrega RP, Zhi X, et al. Understanding ForteBio's Sensors for High-Throughput Kinetic and Epitope Screening for Purified Antibodies and Yeast Culture Supernatant. J Biomol Screen 2016;21:88–95. doi:10.1177/1087057115609564.

[284] Lad L, Clancy S, Kovalenko M, Liu C, Hui T, Smith V, et al. High-Throughput Kinetic Screening of Hybridomas to Identify High-Affinity Antibodies Using Bio-Layer Interferometry. J Biomol Screen 2015;20:498–507. doi:10.1177/1087057114560123.

[285] Tobias R, Kumaraswamy S. Biomolecular Binding Kinetics Assays on the Octet Platform. 2017.

[286] Cooper MA. Optical biosensors in drug discovery. Nat Rev Drug Discov 2002;1:515–28. doi:10.1038/nrd838.

[287] Kumaraswamy S, Tobias R. Label-free kinetic analysis of an antibody-antigen interaction using biolayer interferometry. Protein-Protein Interact. Methods Appl. Second Ed., 2015, p. 165–82. doi:10.1007/978-1-4939-2425-7_10.

[288] Hofmann HP, Kronthaler U, Fritsch C, Grau R, Müller SO, Mayer R, et al. Characterization and non-clinical assessment of the proposed etanercept biosimilar GP2015 with originator etanercept (Enbrel®). Expert Opin Biol Ther 2016;16:1185–95. doi:10.1080/14712598.2016.1217329.

[289] Wang W, Singh S, Zeng DL, King K, Nema S. Antibody structure, instability, and formulation. J Pharm Sci 2007;96:1–26.

[290] Crombet-Ramos T, Rak J, Pérez R, Viloria-Petit A. Antiproliferative, antiangiogenic and proapoptotic activity of h-R3: A humanized anti-EGFR antibody. Int J Cancer 2002;101:567–75. doi:10.1002/ijc.10647.

[291] Jiang X-R, Song A, Bergelson S, Arroll T, Parekh B, May K, et al. Advances in the assessment and control of the effector functions of therapeutic antibodies. Nat Rev Drug Discov 2011;10:101.

[292] Parekh BS, Berger E, Sibley S, Cahya S, Xiao L, LaCerte MA, et al. Development and validation of an antibody-dependent cell-mediated cytotoxicity-reporter gene assay. MAbs 2012;4:310–8. doi:10.4161/mabs.19873.

[293] Schnueriger A, Grau R, Sondermann P, Schreitmueller T, Marti S, Zocher M. Development of a quantitative, cell-line based assay to measure ADCC activity mediated by therapeutic antibodies. Mol Immunol 2011;48:1512–7.

[294] Cartron G, Dacheux L, Salles G, Solal-Celigny P, Bardos P, Colombat P, et al. Therapeutic activity of humanized anti-CD20 monoclonal antibody and polymorphism in IgG Fc receptor FcγRIIIa gene. Blood 2002;99:754–8.

[295] Kronthaler U, Fritsch C, Hainzl O, Seidl A, da Silva A. Comparative functional and pharmacological characterization of Sandoz proposed biosimilar adalimumab (GP2017): rationale for extrapolation across indications. Expert Opin Biol Ther 2018;18:921–30.

[296] Srgel F, Lerch H, Lauber T. Physicochemical and biologic comparability of a biosimilar granulocyte colony-stimulating factor with its reference product. BioDrugs 2010;24:347–57. doi:10.2165/11585100-000000000-00000.

[297] Wadhwa M, Knezevic I, Kang H-N, Thorpe R. Immunogenicity assessment of biotherapeutic products: an overview of assays and their utility. Biologicals 2015;43:298–306.

[298] Nowak C, K. Cheung J, M. Dellatore S, Katiyar A, Bhat R, Sun J, et al. Forced degradation of recombinant monoclonal antibodies: A practical guide. MAbs 2017. doi:10.1080/19420862.2017.1368602.

[299] European Biopharmaceutical enterprises. Forced Degradation Studies for Therapeutic Proteins. 5019.

[300] Blessy M, Patel RD, Prajapati PN, Agrawal YK. Development of forced degradation and stability indicating studies of drugs - A review. J Pharm Anal 2014. doi:10.1016/j.jpha.2013.09.003.

[301] U.S. Food and Drug Administration. FDA Advisory Committee Briefing Document CT-P10, a Proposed Biosimilar to Rituxan. 2018.

[302] Vanz ALS, Renard G, Palma MS, Chies JM, Dalmora SL, Basso LA, et al. Human granulocyte colony stimulating factor (hG-CSF): Cloning, overexpression, purification and characterization. Microb Cell Fact 2008. doi:10.1186/1475-2859-7-13.

[303] Dexter TM. Granulocyte colony stimulating factor: from laboratory bench to clinical use. Eur J Cancer 1994.

[304] Amgen. Highlights of prescribing information, Neupogen (Filgrastim) injection for subcutaneous or intravenous use. 2018.

[305] CDER/CBER, FDA. Scientific Considerations in Demonstrating Biosimilarity to a Reference Product Guidance for Industry. 2015.

[306] Price WN, Rai AK. Are Trade Secrets Delaying Biosimilars? Science (80-) 2015;348:188–90. doi:10.1126/science.aab1684.

[307] Woodcock J, Griffin J, Behrman R, Cherney B, Crescenzi T, Fraser B, et al. The FDA's assessment of follow-on protein products: a historical perspective. Nat Rev Drug Discov 2007;6:437–42. doi:10.1038/nrd2307.

[308] Kozlowski S, Woodcock J, Midthun K, Behrman Sherman R. Developing the Nation's Biosimilars Program. N Engl J Med 2011;365:385–8. doi:10.1056/NEJMp1107285.

[309] Hausberger A, Lamanna WC, Hartinger M, Seidl A, Toll H, Holzmann J. Identification of Low-Level Product-Related Variants in Filgrastim Products Presently Available in Highly Regulated Markets. BioDrugs 2016;30:233–42. doi:10.1007/s40259-016-0169-2.

[310] Skrlin A, Krnic EK, Gosak D, Prester B, Mrsa V, Vuletic M, et al. Correlation of liquid chromatographic and biological assay for potency assessment of filgrastim and related impurities. J Pharm Biomed Anal 2010;53:262–8. doi:10.1016/j.jpba.2010.02.006.

[311] Skrlin A, Radic I, Vuletic M, Schwinke D, Runac D, Kusalic T, et al. Comparison of the physicochemical properties of a biosimilar filgrastim with those of reference filgrastim. Biologicals 2010;38:557–66. doi:10.1016/j.biologicals.2010.05.002.

[312] Wei Z, Shacter E, Schenerman M, Dougherty J, McLeod LD. The role of higher-order structure in defining biopharmaceutical quality. Bioprocess Int 2011.

[313] Ratanji KD, Derrick JP, Dearman RJ, Kimber I. Immunogenicity of therapeutic proteins: Influence of aggregation. J Immunotoxicol 2013;11:99–109. doi:10.3109/1547691X.2013.821564.

[314] Feldman MF, Wacker M, Hernandez M, Hitchen PG, Marolda CL, Kowarik M, et al. Engineering N-linked protein glycosylation with diverse O antigen lipopolysaccharide structures in Escherichia coli. Proc Natl Acad Sci 2005. doi:10.1073/pnas.0500044102.

[315] Lu HS, Fausset PR, Narhi LO, Horan T, Shinagawa K, Shimamoto G, et al. Chemical modification and site-directed mutagenesis of methionine residues in recombinant human granulocyte colony-stimulating factor: effect on stability and biological activity. Arch Biochem Biophys 1999;362:1–11. doi:10.1006/abbi.1998.1022.

[316] Shekhawat R, Shah CK, Patel A, Srinivasan S, Kapoor P, Patel S, et al. Structural similarity, characterization of Poly Ethylene Glycol linkage and identification of product related variants in biosimilar pegfilgrastim. PLoS One 2019. doi:10.1371/journal.pone.0212622.

[317] Lu HS, Fausset PR, Narhi LO, Horan T, Shinagawa K, Shimamoto G, et al. Chemical modification and site-directed mutagenesis of methionine residues in recombinant human granulocyte colony-stimulating factor. Effect on stability and biological activity. Arch Biochem Biophys 1999. doi:10.1006/abbi.1998.1022.

[318] Pisupati K, Benet A, Tian Y, Okbazghi S, Kang J, Ford M, et al. Biosimilarity under stress: A forced degradation study of Remicade® and Remsima™. MAbs 2017. doi:10.1080/19420862.2017.1347741.

[319] Clore GM, Gronenborn AM. Determining the structures of large proteins and protein

complexes by NMR. Trends Biotechnol 1998. doi:10.1016/S0167-7799(97)01135-9.

[320] Ghasriani H, Hodgson DJ, Brinson RG, McEwen I, Buhse LF, Kozlowski S, et al. Precision and robustness of 2D-NMR for structure assessment of filgrastim biosimilars. Nat Biotechnol 2016;34:139–41. doi:10.1038/nbt.3474.

[321] Brinson RG, Ghasriani H, Hodgson DJ, Adams KM, McEwen I, Freedberg DI, et al. Application of 2D-NMR with room temperature NMR probes for the assessment of the higher order structure of filgrastim. J Pharm Biomed Anal 2017;141:229–33. doi:10.1016/j.jpba.2017.03.063.

[322] Ohki S ya, Kainosho M. Stable isotope labeling methods for protein NMR spectroscopy. Prog Nucl Magn Reson Spectrosc 2008. doi:10.1016/j.pnmrs.2008.01.003.

[323] Rogers RS, Abernathy M, Richardson DD, Rouse JC, Sperry JB, Swann P, et al. A View on the Importance of “Multi-Attribute Method” for Measuring Purity of Biopharmaceuticals and Improving Overall Control Strategy. AAPS J 2018. doi:10.1208/s12248-017-0168-3.

[324] European Medicines Agency. European public assessment reports on centrally authorised biosimilar medicines n.d. http://www.ema.europa.eu/ema/index.jsp?curl=pages%2Fmedicines%2Flanding%2Fepar_search.jsp&mid=WC0b01ac058001d124&searchTab=searchByAuthType&alreadyLoaded=true&isNewQuery=true&status=Authorised&keyword=Enter+keywords&searchType=name&taxonomyPath=&treeNumbe.

[325] U.S. Food and Drug Administration. Biosimilar product information n.d. https://www.fda.gov/Drugs/DevelopmentApprovalProcess/HowDrugsareDevelopedandApproved/ApprovalApplications/TherapeuticBiologicApplications/Biosimilars/ucm580432.htm.

[326] Calvo B, Zuniga L. Therapeutic Monoclonal Antibodies: Strategies and Challenges for Biosimilars Development. Curr Med Chem 2012;19:4445–50. doi:10.2174/092986712803251485.

[327] Mellstedt H. Clinical considerations for biosimilar antibodies. Eur J Cancer, Suppl 2013;11:1–11. doi:10.1016/S1359-6349(13)70001-6.

[328] Lee C, Jeong M, Lee JAJ, Seo S, Cho SC, Zhang W, et al. Glycosylation profile and biological activity of Remicade® compared with Flixabi® and Remsima®. MAbs 2017;9:968–77. doi:10.1080/19420862.2017.1337620.

[329] Beck A, Diemer H, Ayoub D, Debaene F, Wagner-Rousset E, Carapito C, et al. Analytical characterization of biosimilar antibodies and Fc-fusion proteins. TrAC - Trends Anal Chem 2013;48:81–95. doi:10.1016/j.trac.2013.02.014.

[330] U.S. Food and Drug Administration. Product Approval Information - Licensing Action - Rituxan 1997. https://www.accessdata.fda.gov/drugsatfda_docs/appletter/1997/ritugen112697L.htm.

[331] Weiner GJ. Rituximab: Mechanism of action. Semin Hematol 2010;47:115–23. doi:10.1053/j.seminhematol.2010.01.011.

[332] Cerny T, Borisch B, Introna M, Johnson P, Rose AL. Mechanism of action of rituximab.

Anticancer Drugs 2002;13 Suppl 2:S3–10. doi:10.1097/00001813-200211002-00002.

[333] Smith MR. Rituximab (monoclonal anti-CD20 antibody): Mechanisms of action and resistance. Oncogene 2003;22:7359–68. doi:10.1038/sj.onc.1206939.

[334] Dotan E, Aggarwal C, Smith MR. Impact of Rituximab (Rituxan) on the Treatment of B-Cell Non-Hodgkin's Lymphoma. P T 2010;35:Table 3.

[335] Huhn D, von Schilling C, Wilhelm M, Ho a D, Hallek M, Kuse R, et al. Rituximab therapy of patients with B-cell chronic lymphocytic leukemia. Blood 2001;98:1326–31. doi:10.1182/blood.V98.5.1326.

[336] Mok CC. Rituximab for the treatment of rheumatoid arthritis: an update. Drug Des Devel Ther 2014;8:87–100. doi:10.2147/DDDT.S41645.

[337] Frampton JE, Scott LJ. Rituximab: In rheumatoid arthritis. BioDrugs 2007;21:333–41. doi:10.2165/00063030-200721050-00005.

[338] Dall'Ozzo S, Tartas S, Paintaud G, Cartron G, Colombat P, Bardos P, et al. Rituximab-dependent cytotoxicity by natural killer cells: Influence of FCGR3A polymorphism on the concentration-effect relationship. Cancer Res 2004;64:4664–9. doi:10.1158/0008-5472.CAN-03-2862.

[339] Bowles JA, Wang SY, Link BK, Allan B, Beuerlein G, Campbell MA, et al. Anti-CD20 monoclonal antibody with enhanced affinity for CD16 activates NK cells at lower concentrations and more effectively than rituximab. Blood 2006;108:2648–54. doi:10.1182/blood-2006-04-020057.

[340] Liu L. Antibody glycosylation and its impact on the pharmacokinetics and pharmacodynamics of monoclonal antibodies and Fc-fusion proteins. J Pharm Sci 2015;104:1866–84. doi:10.1002/jps.24444.

[341] Niwa R, Hatanaka S, Shoji-hosaka E, Sakurada M, Kobayashi Y, Uehara A, et al. Enhancement of the Antibody-Dependent Cellular Cytotoxicity of Low-Fucose IgG1 Is Independent of Fc □ RIIIa Functional Polymorphism. Clin Cancer Res 2004;10:6248–55. doi:10.1158/1078-0432.CCR-04-0850.

[342] Iida S, Kuni-Kamochi R, Mori K, Misaka H, Inoue M, Okazaki A, et al. Two mechanisms of the enhanced antibody-dependent cellular cytotoxicity (ADCC) efficacy of non-fucosylated therapeutic antibodies in human blood. BMC Cancer 2009;9. doi:10.1186/1471-2407-9-58.

[343] Greenwald M, Tesser J, Sewell KL. Biosimilars Have Arrived: Rituximab. Arthritis 2018;2018. doi:10.1155/2018/3762864.

[344] European Medicines Agency. EPAR summary for the public: Truxima. 2017.

[345] European Medicines Agency. EPAR summary for the public: Rixathon. 2017.

[346] Althoff E. Sandoz decides not to pursue US biosimilar rituximab; will focus on robust biosimilar portfolio for unmet access and sustainability needs n.d. https://www.novartis.com/news/media-releases/sandoz-decides-not-pursue-us-biosimilar-rituximab-will-focus-robust-biosimilar-portfolio-unmet-access-and-sustainability-needs.

[347] Biosimilars of rituximab n.d. http://www.gabionline.net/Biosimilars/General/Biosimilars-of-rituximab.

[348] Welch AR. Russia's Biosimilar Market At A Glance 2017. https://www.biosimilardevelopment.com/doc/russia-s-biosimilar-market-at-a-glance-0001.

[349] Haynes SE, Polasky DA, Dixit SM, Majmudar JD, Neeson K, Ruotolo BT, et al. Variable-Velocity Traveling-Wave Ion Mobility Separation Enhancing Peak Capacity for Data-Independent Acquisition Proteomics. Anal Chem 2017. doi:10.1021/acs.analchem.7b00112.

[350] Polasky DA, Dixit SM, Fantin SM, Ruotolo BT. CIUSuite 2: Next-Generation Software for the Analysis of Gas-Phase Protein Unfolding Data. Anal Chem 2019. doi:10.1021/acs.analchem.8b05762.

[351] Wang L, Pan H, Smith DL. Hydrogen exchange-mass spectrometry: optimization of digestion conditions. Mol Cell Proteomics 2002;1:132–8. doi:10.1074/mcp.M100009-MCP200.

[352] Bai Y, Milne JS, Mayne L, Englander SW. Primary structure effects on peptide group hydrogen exchange. Proteins Struct Funct Bioinforma 1993;17:75–86. doi:10.1002/prot.340170110.

[353] Alsenaidy MA, Okbazghi SZ, Kim JH, Joshi SB, Russell Middaugh C, Tolbert TJ, et al. Physical stability comparisons of IgG1-Fc variants: Effects of N-glycosylation site occupancy and Asp/gln residues at site asn 297. J Pharm Sci 2014;103:1613–27. doi:10.1002/jps.23975.

[354] Okbazghi SZ, More AS, White DR, Duan S, Shah IS, Joshi SB, et al. Production, Characterization, and Biological Evaluation of Well-Defined IgG1 Fc Glycoforms as a Model System for Biosimilarity Analysis. J Pharm Sci 2016;105:559–74. doi:10.1016/j.xphs.2015.11.003.

[355] Christopher M. Protein Folding and Misfolding. Nature 2003;426:884–90. doi:10.1007/978-3-642-22230-6.

[356] Upton R, Migas LG, Pacholarz KJ, Beniston RG, Estdale S, Firth D, et al. Hybrid mass spectrometry methods reveal lot-to-lot differences and delineate the effects of glycosylation on the tertiary structure of Herceptin®. Chem Sci 2019;10:2811–20. doi:10.1039/c8sc05029e.

[357] Watanabe Y, Vasiljevic S, Allen JD, Seabright GE, Duyvesteyn HME, Doores KJ, et al. Signature of Antibody Domain Exchange by Native Mass Spectrometry and Collision-Induced Unfolding. Anal Chem 2018;90:7325–31. doi:10.1021/acs.analchem.8b00573.

[358] Hamuro Y, Coales SJ, Southern MR, Nemeth-Cawley JF, Stranz DD, Griffin PR. Rapid analysis of protein structure and dynamics by hydrogen/deuterium exchange mass spectrometry. J Biomol Tech 2003;14:171–82.

[359] Wei H, Mo J, Tao L, Russell RJ, Tymiak AA, Chen G, et al. Hydrogen/deuterium exchange mass spectrometry for probing higher order structure of protein therapeutics: Methodology and applications. Drug Discov Today 2014;19:95–102. doi:10.1016/j.drudis.2013.07.019.

[360] Vlasak J, Ionescu R. Heterogeneity of Monoclonal Antibodies Revealed by Charge-Sensitive Methods. Curr Pharm Biotechnol 2008;9:468–81. doi:10.2174/138920108786786402.

[361] Reusch D, Tejada ML. Fc glycans of therapeutic antibodies as critical quality attributes. Glycobiology 2015;25:1325–34. doi:10.1093/glycob/cwv065.

[362] Do T, Ho F, Heidecker B, Witte K, Chang L, Lerner L. A rapid method for determining dynamic binding capacity of resins for the purification of proteins. Protein Expr Purif 2008;60:147–50. doi:10.1016/j.pep.2008.04.009.

[363] Lee KH, Lee J, Bae JS, Kim YJ, Kang HA, Kim SH, et al. Analytical similarity assessment of rituximab biosimilar CT-P10 to reference medicinal product. MAbs 2018;10:380–96. doi:10.1080/19420862.2018.1433976.

[364] Rivers J, McDonald L, Edwards IJ, Beynon RJ. Asparagine deamidation and the role of higher order protein structure. J Proteome Res 2008;7:921–7. doi:10.1021/pr070425l.

[365] Alsenaidy MA, Jain NK, Kim JH, Middaugh CR, Volkin DB. Protein comparability assessments and potential applicability of high throughput biophysical methods and data visualization tools to compare physical stability profiles. Front Pharmacol 2014. doi:10.3389/fphar.2014.00039.

[366] Shah DD, Singh SM, Mallela KMG. Effect of Chemical Oxidation on the Higher Order Structure, Stability, Aggregation, and Biological Function of Interferon Alpha-2a: Role of Local Structural Changes Detected by 2D NMR. Pharm Res 2018;35:1–17. doi:10.1007/s11095-018-2518-y.

[367] Houde D. Investigating the conformation and conformational dynamics of protein biopharmaceuticals with hydrogen/deuterium exchange mass spectrometry. 2010.

[368] Houde D, Arndt J, Domeier W, Berkowitz S, Engen JR. Characterization of IgG1 Conformation and conformational dynamics by hydrogen/deuterium exchange mass spectrometry. Anal Chem 2009;81:2644–51. doi:10.1021/ac802575y.

[369] More AS, Toprani VM, Okbazghi SZ, Kim JH, Joshi SB, Middaugh CR, et al. Correlating the Impact of Well-Defined Oligosaccharide Structures on Physical Stability Profiles of IgG1-Fc Glycoforms. J Pharm Sci 2016;105:588–601. doi:10.1016/j.xphs.2015.10.014.

[370] Antes B, Amon S, Rizzi A, Wiederkum S, Kainer M, Szolar O, et al. Analysis of lysine clipping of a humanized Lewis-Y specific IgG antibody and its relation to Fc-mediated effector function. J Chromatogr B Anal Technol Biomed Life Sci 2007;852:250–6. doi:10.1016/j.jchromb.2007.01.024.

[371] U.S. Food and Drug Administration. FDA Briefing Document Oncology Drugs Advisory Committee Meeting BLA 125545 Epoetin Hospira, a Proposed Biosimilar to Epogen/Procrit (Epoetin Alfa). 2017.

[372] Niwa R, Natsume A, Uehara A, Wakitani M, Iida S, Uchida K, et al. IgG subclass-independent improvement of antibody-dependent cellular cytotoxicity by fucose removal from Asn297-linked oligosaccharides. J Immunol Methods 2005;306:151–60. doi:10.1016/j.jim.2005.08.009.

[373] Shields RL, Lai J, Keck R, O'Connell LY, Hong K, Gloria Meng Y, et al. Lack of fucose on human IgG1 N-linked oligosaccharide improves binding to human FcγRIII and antibody-dependent cellular toxicity. J Biol Chem 2002;277:26733–40. doi:10.1074/jbc.M202069200.

[374] Peipp M, Van Bueren JJL, Schneider-Merck T, Bleeker WWK, Dechant M, Beyer T, et al. Antibody fucosylation differentially impacts cytotoxicity mediated by NK and PMN effector cells. Blood 2008;112:2390–9. doi:10.1182/blood-2008-03-144600.

[375] Junttila TT, Parsons K, Olsson C, Lu Y, Xin Y, Theriault J, et al. Superior in vivo efficacy of afucosylated trastuzumab in the treatment of HER2-amplified breast cancer. Cancer Res 2010;70:4481–9. doi:10.1158/0008-5472.CAN-09-3704.

[376] Kang J, Pisupati K, Benet A, Ruotolo BT, Schwendeman SP, Schwendeman A. Infliximab Biosimilars in the Age of Personalized Medicine. Trends Biotechnol 2018;36:987–92. doi:10.1016/j.tibtech.2018.05.002.

[377] U.S. Food and Drug Administration. Biosimilar product information n.d. https://www.fda.gov/drugs/developmentapprovalprocess/howdrugsaredevelopedandapproved/approvalapplications/therapeuticbiologicapplications/biosimilars/ucm580432.htm.

[378] Vulto AG, Jaquez OA. The process defines the product: what really matters in biosimilar design and production? Rheumatology (Oxford) 2017;56:iv14–29. doi:10.1093/rheumatology/kex278.

[379] Lee N, Lee JAJ, Yang H, Baek S, Kim S, Kim S, et al. Evaluation of similar quality attribute characteristics in SB5 and reference product of adalimumab. MAbs 2019. doi:10.1080/19420862.2018.1530920.

[380] Schiestl M, Stangler T, Torella C, Čepeljnik T, Toll H, Grau R. Acceptable changes in quality attributes of glycosylated biopharmaceuticals. Nat Biotechnol 2011. doi:10.1038/nbt.1839.

[381] Amgen. AMJEVITA (adalimumab-atto) injection for subcutaneous use label 2016:1–61. https://www.accessdata.fda.gov/drugsatfda_docs/label/2016/761024lbl.pdf.

[382] Ingelheim B. CYLTEZO (adalimumab-adbm) injection, for subcutaneous use label 2017:1–38. https://www.accessdata.fda.gov/drugsatfda_docs/label/2017/761058lbl.pdf.

[383] Abbvie. HUMIRA (adalimumab) injection for subcutaneous use label 2017:1–94. https://www.accessdata.fda.gov/drugsatfda_docs/label/2017/125057s399lbl.pdf.

[384] Genetech. HERCEPTIN intravenous infusion label 2010:1–33. https://www.accessdata.fda.gov/drugsatfda_docs/label/2010/103792s5250lbl.pdf.

[385] Mylan. OGIVRI (trastuzumab-dkst) for injection, for intravenous use label 2017:1–39. https://www.accessdata.fda.gov/drugsatfda_docs/label/2017/761074s000lbl.pdf.

[386] Lakowicz JR. Principles of fluorescence spectroscopy. Third edit. Springer; 2006. doi:10.1007/978-0-387-46312-4.

[387] Hong P, Koza S, Bouvier ESP. A review size-exclusion chromatography for the analysis of protein biotherapeutics and their aggregates. J Liq Chromatogr Relat Technol 2012. doi:10.1080/10826076.2012.743724.

[388] Kanojia G, Have R Ten, Bakker A, Wagner K, Frijlink HW, Kersten GFA, et al. The production of a stable Infliximab powder: The evaluation of spray and freeze-drying for production. PLoS One 2016. doi:10.1371/journal.pone.0163109.

[389] Isoda Y, Yagi H, Satoh T, Shibata-Koyama M, Masuda K, Satoh M, et al. Importance of the side chain at position 296 of antibody Fc in interactions with FcγRIIIa and other Fcγ receptors. PLoS One 2015. doi:10.1371/journal.pone.0140120.

[390] Sun S, Akkapeddi P, Marques MC, Martínez-Sáez N, Torres VM, Cordeiro C, et al. One-pot stapling of interchain disulfides of antibodies using an isobutylene motif. Org Biomol Chem 2019. doi:10.1039/c8ob02877j.

[391] Dumont J, Euwart D, Mei B, Estes S, Kshirsagar R. Human cell lines for biopharmaceutical manufacturing: history, status, and future perspectives. Crit Rev Biotechnol 2016. doi:10.3109/07388551.2015.1084266.

[392] Genentech. Rituxan (rituximab) Injection for Intravenous Use 2010:1–35. https://www.accessdata.fda.gov/drugsatfda_docs/label/2010/103705s5311lbl.pdf.

[393] Genentech. Avastin (bevacizumab) solution for intravenous infusion 2009:1–22. https://www.accessdata.fda.gov/drugsatfda_docs/label/2009/125085s0169lbl.pdf.

[394] Sousa F, Sarmento B, Neves-Petersen MT. Biophysical study of bevacizumab structure and bioactivity under thermal and pH-stresses. Eur J Pharm Sci 2017. doi:10.1016/j.ejps.2017.05.019.

[395] King AC, Woods M, Liu W, Lu Z, Gill D, Krebs MRH. High-throughput measurement, correlation analysis, and machine-learning predictions for pH and thermal stabilities of Pfizer-generated antibodies. Protein Sci 2011. doi:10.1002/pro.680.

[396] A. Alsaddique J, M. Pabari R, Ramtoola Z. Effect of Thermal and Shear Stressors on the Physical Properties, Structural Integrity and Biological Activity of the Anti-TNF-alpha Monoclonal Antibody, Infliximab. Curr Pharm Biotechnol 2016. doi:10.2174/1389201017666160519111815.

[397] Telikepalli SN, Kumru OS, Kalonia C, Esfandiary R, Joshi SB, Middaugh CR, et al. Structural characterization of IgG1 mAb aggregates and particles generated under various stress conditions. J Pharm Sci 2014. doi:10.1002/jps.23839.

[398] Joubert MK, Luo Q, Nashed-Samuel Y, Wypych J, Narhi LO. Classification and characterization of therapeutic antibody aggregates. J Biol Chem 2011. doi:10.1074/jbc.M110.160457.

[399] Rombach-Riegraf V, Karle AC, Wolf B, Sordé L, Koepke S, Gottlieb S, et al. Aggregation of human recombinant monoclonal antibodies influences the capacity of dendritic cells to stimulate adaptive T-cell responses in vitro. PLoS One 2014. doi:10.1371/journal.pone.0086322.

[400] Zhang A, Singh SK, Shirts MR, Kumar S, Fernandez EJ. Distinct aggregation mechanisms of monoclonal antibody under thermal and freeze-thaw stresses revealed by hydrogen exchange. Pharm Res 2012. doi:10.1007/s11095-011-0538-y.

[401] Paul M, Vieillard V, Jaccoulet E, Astier A. Long-term stability of diluted solutions of the

monoclonal antibody rituximab. Int J Pharm 2012. doi:10.1016/j.ijpharm.2012.06.063.

[402] Kerr RA, Keire DA, Ye H. The impact of standard accelerated stability conditions on antibody higher order structure as assessed by mass spectrometry. MAbs 2019. doi:10.1080/19420862.2019.1599632.

[403] Schmid I, Bonnington L, Gerl M, Bomans K, Thaller AL, Wagner K, et al. Assessment of susceptible chemical modification sites of trastuzumab and endogenous human immunoglobulins at physiological conditions. Commun Biol 2018. doi:10.1038/s42003-018-0032-8.

[404] Haberger M, Bomans K, Diepold K, Hook M, Gassner J, Schlothauer T, et al. Assessment of chemical modifications of sites in the CDRs of recombinant antibodies: Susceptibility vs. functionality of critical quality attributes. MAbs 2014. doi:10.4161/mabs.27876.

[405] Yan B, Steen S, Hambly D, Valliere-Douglass J, Vanden Bos T, Smallwood S, et al. Succinimide formation at Asn 55 in the complementarity determining region of a recombinant monoclonal antibody IgG1 heavy chain. J Pharm Sci 2009. doi:10.1002/jps.21655.

[406] Chumsae C, Gaza-Bulseco G, Sun J, Liu H. Comparison of methionine oxidation in thermal stability and chemically stressed samples of a fully human monoclonal antibody. J Chromatogr B Anal Technol Biomed Life Sci 2007;850:285–94. doi:10.1016/j.jchromb.2006.11.050.

[407] Kim J, Jones L, Taylor L, Kannan G, Jackson F, Lau H, et al. Characterization of a unique IgG1 mAb CEX profile by limited Lys-C proteolysis/CEX separation coupled with mass spectrometry and structural analysis. J Chromatogr B Anal Technol Biomed Life Sci 2010. doi:10.1016/j.jchromb.2010.05.032.

[408] Kim DG, Kim HJ, Kim HJ. Effects of carboxypeptidase B treatment and elevated temperature on recombinant monoclonal antibody charge variants in cation-exchange chromatography analysis. Arch Pharm Res 2016. doi:10.1007/s12272-016-0818-5.

[409] Griaud F, Denefeld B, Lang M, Hensinger H, Haberl P, Berg M. Unbiased in-depth characterization of CEX fractions from a stressed monoclonal antibody by mass spectrometry. MAbs 2017. doi:10.1080/19420862.2017.1313367.

[410] Haberger M, Bomans K, Diepold K, Hook M, Gassner J, Schlothauer T, et al. Assessment of chemical modifications of sites in the CDRs of recombinant antibodies. MAbs 2014. doi:10.4161/mabs.27876.

[411] CDER/CBER. Considerations in Demonstrating Interchangeability With a Reference Product. 2019.

[412] Jørgensen KK, Olsen IC, Goll GL, Lorentzen M, Bolstad N, Haavardsholm EA, et al. Switching from originator infliximab to biosimilar CT-P13 compared with maintained treatment with originator infliximab (NOR-SWITCH): a 52-week, randomised, double-blind, non-inferiority trial. Lancet 2017;389:2304–16. doi:10.1016/S0140-6736(17)30068-5.

[413] Lehrnbecher T, Foster CB, Zhu S, Leitman SF, Goldin LR, Huppi K, et al. Variant

genotypes of the low-affinity Fcγ receptors in two control populations and a review of low-affinity Fcγ receptor polymorphisms in control and disease populations. Blood 1999.